The Dissertation Committee for Hung Phuc Nguyen Certifies that this is the approved version of the following dissertation:

DETERMINING HOW NOISE AND TASK REDUNDANCY INFLUENCE MOTOR CONTROL OF PLANAR REACHING

Committee:

Jonathan B. Dingwell, Supervisor

Carolyn C. Seepersad, Co-Supervisor

Joseph Cusumano

Richard R. Neptune

Raul G. Longoria

DETERMINING HOW NOISE AND TASK REDUNDANCY INFLUENCE MOTOR CONTROL OF PLANAR REACHING

By

HUNG PHUC NGUYEN, B.S.M.E; M.S.E

Dissertation

Presented to the Faculty of the Graduate School of

The University of Texas at Austin

in Partial Fulfillment

of the Requirements

for the Degree of

Doctor of Philosophy

The University of Texas at Austin

December 2013

Dedication

I want to dedicate this to Athena, for without her support, it would not have been possible. You are an inspiration and I find strength from you everyday.

Acknowledgements

I want to thank my family for their supports throughout my studies. Without their supports and loves, this work would not have been possible. I want to thank you my advisor, Dr. Dingwell, for helping me grow as a student and as a researcher. I want to thank my lab members at the Biodynamics Laboratory at the University of Texas - Austin for their critiques and encouragements throughout my dissertation. Lastly, I want to thank you my students in my General Engineering course for challenging me everyday to become a better educator.

DETERMINING HOW NOISE AND TASK REDUNDANCY INFLUENCE MOTOR CONTROL OF PLANAR REACHING

Hung Phuc Nguyen, PhD

The University of Texas at Austin, 2013

Supervisor: Jonathan Dingwell

Co-Supervisor: Carolyn Seepersad

Motor noise and redundancy are vexing issues in motor control; yet their understanding provides great insights on underlying control mechanisms that govern movement. They provide glimpses into how the nervous system organizes and regulates movement within the motor control system. Understand of motor control could spur new advances in motor control could lead to better development of rehabilitation process and technology to counteract debilitating affects of neuromuscular disorders and motor readjustment with prostheses. However, before such process and technology could be developed and adapted for clinical use, a deeper understanding of motor control is needed to unravel the neural roadmap that regulates and generates movement. New theory of motor control could precipitate the development of more robust control mechanisms for robotic-human interaction. This work aims at expanding a more rigorous analytical and mathematical framework to understand how these control mechanisms reconcile redundancy and stochastic noise in human motor control.

Table of Contents

List of Tables

List of Figures

Chapter 1: Overview

According to the World Health Report (2002), stroke is the leading cause of serious, long term disability in the United States. With residual disability experienced by stroke survivors (e.g. hemiparesis), neuro-rehabilitation is critical in reducing the need for dependent care and minimizing the long-term effects of stroke by promoting independence in activities of daily living (ADL). Since 1980, robotic-assisted rehabilitation has been promoted as a cheaper and more effective alternative to traditional rehabilitation; however, studies have shown that robotic-assisted rehabilitation does not provide significant advantages over traditional approach (i.e. human assistant physical therapy) (Picelli, Melotti et al. 2012; Vaney, Gattlen et al. 2012; Wu, Yang et al. 2012; Moreno, Barroso et al. 2013). A better understanding of the underlying motor control mechanisms that govern movement could precipitate the developments of new clinical processes and rehabilitation devices that could provide more direct and effective therapeutic treatment and motor recovery by targeting rehabilitation of high level of motor control. However, before such processes and technology could be developed and adapted for clinical use, a deeper understand of motor control is needed to unravel the neural roadmap that regulates and generates movement.

The vast majority of the tasks we perform everyday involved some degree of redundancy because of the larger numbers of articulating joints in the body and the even larger numbers of muscles that coordinate the movement of those joints (Bernstein 1976). Humans can perform these highly redundant tasks with high accuracy and repeatability partly because redundancy provides flexibility and maneuverability during the performance of these tasks. Within the human motor control system, there are many levels of redundancy. Motor redundancy can occur at the neural (Tolhurst, Movshon et al. 1983), muscle (Sohn, McKay et al. 2013), joint (Scholz, Schoner et al. 2000), and even at the task level(Dingwell, Smallwood et al. 2013). As long as the dimension of the task is the less than the dimension of the execution space, redundancy exists. The

nervous system possesses a robust control system that adapts and optimizes performance from one movement to the next to resolve the redundancy and minimizes the influence of noise within the motor control system. This control framework not only resolves redundancy that existed at every level of the human motor system but also creates a system that is highly adaptable to noise (Harris and Wolpert 1998; Hamilton, Jones et al. 2004). Currently there is no unified control framework that adequately addresses the optimality of redundancy and stochastic noise during motor performance. Numerous theories have been proposed to understand and determine how or what the central nervous system controls during redundant task. Our understanding of how the nervous system resolves redundancy and noise during a task greatly advances our scientific knowledge in the area of human rehabilitation and human-robotic interaction.

Motor noise and redundancy have been vexing issues in motor control; thus their understandings provide great insights on underlying control mechanisms that govern movement. They provide glimpses into how the nervous system organizes and regulates movement within the motor control system. New advances in motor control could lead to better development of rehabilitation process and technology to counteract debilitating affects of neuromuscular disorders and motor readjustment with prostheses. New theory of motor control could translate into development of more robust control mechanisms for robotic-human interaction.

This work aims at expanding a rigorous analytical and mathematical framework to understand these control mechanisms by reconciling redundancy and stochastic noise in human motor control. This was done by investigating the effect on noise and control on motor outputs and expanding a novel approach to motor control. The findings from these studies will provide a strong foundational knowledge on motor control and reveal the potential of robotic rehabilitation by understanding the fundamental of motor control.

Chapter 2: Introduction and Specific Aims

When we extend our hand to reach for our daily cup of coffee in the morning, there is a neuronal chain of commands that originates from the Central Nervous System (CNS) that relays our thoughts to the muscle fibers. Those commands are converted into physical mechanical forces that ultimately generate the reaching movement. Yet, every time we reach for the cup of coffee, we do it slightly different. The inherent motor noise at the neural level and the redundant joint space ensure that our movements are variable every time we reach for our morning elixir. Such task has become habitual that we perform it without directly planning or contemplating its outcome. While this task might seem trivial, the underlying control mechanisms that allow people to resolve redundancy and noise during a task is still enigmatic.

Reaching is a simple task we perform many times throughout the day with high accuracy and minimal effort. While the task is very elementary, it requires a high level of control to overcome many fundamental challenges during the movement. When we extend our hand to reach for an object, there is an infinite set of trajectories and speeds at which we can choose to move; yet humans seem to move and accomplish the task with ease and minimal delay. For example, during skilled task like free throwing shooting, there are multiple redundant systems that a player has to resolve to successfully hit the target. The goal of free throw shooting is to put the basketball through the hoop; however, there are infinite sets of trajectory that will accomplish the task. Some players choose a flatter trajectory while others prefer an arched trajectory. In a simplistic mathematical model, there are infinite sets of release angle and velocity that will allow the ball to fall though the hoop. However, these release angles and velocities are the results of the mechanical forces generated by the player. Those forces emanate from the joint actuators of the upper and lower extremity; yet different combinations from those forces can yield the correct release angle and velocity to accomplish the task.

The mechanical forces needed to shoot the basketball are driven by the muscle fibers that are plagued with signal-dependent noise. However, years of practice have afforded great free throw shooters the ability to control the joint actuator firing intensity and pattern to generate the right release angle and velocity that will put the basketball through the hoop. How does our internal motor control system quickly resolved motor redundancy to achieve the desired combination? The nervous system relies on proprioceptive and visual feedback to drive muscle actuators to compensate for deviations during reaching. Yet, it is still unclear how those neural commands are structured and sent to the actuators that generate these movements.

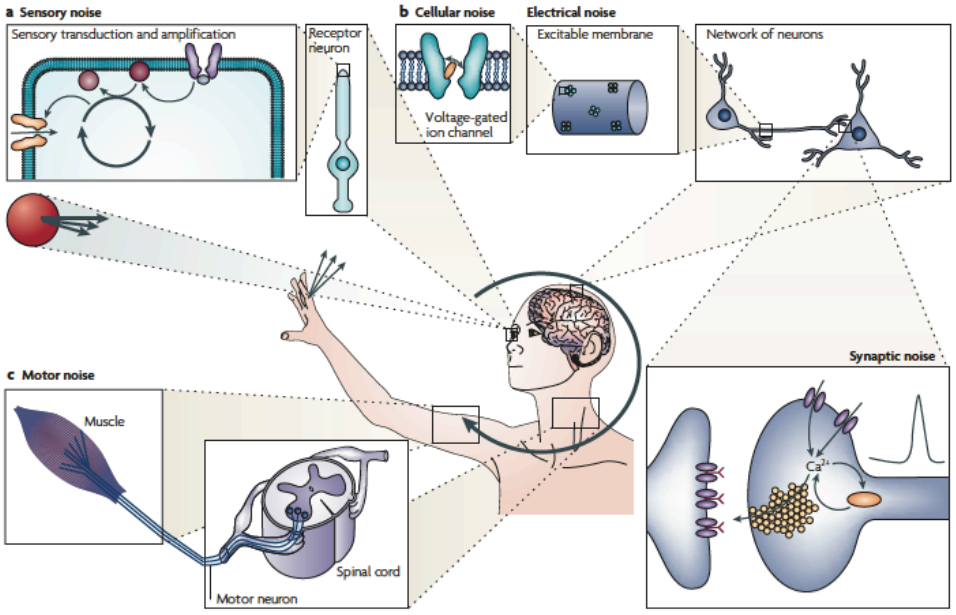

Figure 1: Overview of the stages at which noise is present in the nervous system. Noise permeates every level of movement from synaptic noise to motor noise (Faisal, Selen et al. 2008).

Human motor control system is saturated with noise (Harris and Wolpert 1998; Faisal, Selen et al. 2008). Noise is present at every level of the nervous system and it has positive and negative affects on human movement. The behavioral outputs and information processing are affected by sensory noise, motor noise and even synaptic noise (Figure 1). Noise may provide a mechanism to explore the task space; thus it might

aid in finding the best solution to achieve the desired results. Conversely, noise can also corrupt control (Takahashi, Nemet et al. 2003). Yet, the nervous system can mitigate the effects of noise and use it to improve task performance. For example, co-contraction of different arm muscles had been shown to be an effective strategy to increase movement accuracy during a pointing task (Gribble, Mullin et al. 2003), yet co-contraction also increased muscle force and signal-dependent neuromuscular noise. The increase in signal-dependent noise was alleviated by the increase in the joint stiffness (i.e. impedance) (Selen, Franklin et al. 2009). Therefore, noise could be exploited by the nervous system to improve task performance.

Experimental studies (Scholz and Schoner 1999; Cohen and Sternad 2008) demonstrated that the central nervous system possesses a remarkably robust system that could perform skilled tasks with high precision despite noisy signals in motor sensory. However, it is still unclear how the nervous system accounted for the effects of motor noise during redundant tasks. Are there strategies that people adopt to generate accurate and repeatable movements in the presence of kinematic and task redundancy (Scott 2004; Todorov 2004) and inherent noise in movement (Faisal, Selen et al. 2008).

Optimality principles have been widely used to explain how movements are planned and generated. These competing principles provide means to explain how noise and redundancy are resolved during movement. Hogan and Flash argued that reaching movements were planned and organized by minimizing the Jerk (derivative of acceleration) during movement (Flash and Hogan 1985). One prominent feature of minimum Jerk movement is a bell-shaped velocity curve at the end effector. In this particular class of reaching movement, rather than resolving for the redundancy in the joint or control for noise, the nervous system simple selects the path that minimizes the Jerk of the movement. Similarly, for repetitive reaching task, the nervous system could select the movement trajectory that minimizes the total energy expenditure (Alexander 1997; Galna and Sparrow 2006; Nishii and Taniai 2009) or minimizes the torque change (Uno, Kawato et al. 1989; Kawato, Maeda et al. 1990) or minimizes the variance of end

point variance (Harris and Wolpert 1998). However, these optimization strategies rely on finding the *best* trajectory to resolve the redundancy in the task. It does not provide any mechanism to account for trial-to-trial variability, which is critical in understanding variability and redundancy. Several new approaches had been proposed to understand the underlying control mechanisms that govern movement in redundant space. These new theories rely both on experimental and mathematical model to explain how the nervous system might regulate movement during redundant reaching task.

EXPERIMENTAL APPROACHES

Several experimental approaches had been proposed to understand the underlying motor control principles. Rather than relying on finding the "best" trajectory to resolve redundancy and noise, these experimental approaches rely on how the data are organized to infer control during the task.

Uncontrolled Manifold (UCM)

The Uncontrolled Manifold (UCM) was developed to estimate the stability of movement by calculating the variability from trial-to-trial during task performance. The term "uncontrolled" is sometimes a misnomer since control always exists during a task; however, the strength at which the variables are controlled could vary. UCM assumed that if the variable was *stable* during the task, this indicated that the nervous system was *controlling* the variable during the task. The stability measures were estimated by calculating the variability of the task from trial-to-trial. This was calculated by defining a configuration space that may span all the joints angles that contributed to the movement of the task. For a redundant task, there was an infinite set of solution that could satisfy the objective of the task. A set of hypothesized controlled variable was then defined; these controlled variables were defined as a function of the joint angles. For each hypothesized controlled variable, the joint space was divided into two orthogonal subspaces: one subspace which contained all the joint configurations that did not affect the control variables (uncontrolled subspace) and an orthogonal subspace that affected

the motion of the controlled variables (controlled subspace). If the variability of the uncontrolled subspace of the controlled variable is larger than the variability of the uncontrolled subspace; then the nervous is controlling this variable during the task.

For example, if you need to use two fingers to press on a key to yield a constant force (Figure 2) or $F(f_1, f_2) = \text{constant}$. There are many ways in which the forces could be applied to generate the same output force. The forces from the two fingers are projected onto a manifold and the distribution of these forces along manifold could be used to infer control. For example, the distribution in Figure 2b indicates that subject was strongly controlling for the output forces from the two fingers. This is indicated by the large variance along the manifold and small variance in the direction perpendicular to the manifold. The data distribution shown in Figure 2c would indicate weak or no control in the resultant force from the two fingers. The variables that demonstrated larger variance along the redundant space than the orthogonal space is deemed "controlled" during the task (Figure 2b). The variance along the manifold is defined as compensated variance (V_{comp}) because f_2 and f_1 work together to compensate for each other to maintain the same goal while the variance along the orthogonal subspace is defined as uncompensated (V_{un}).

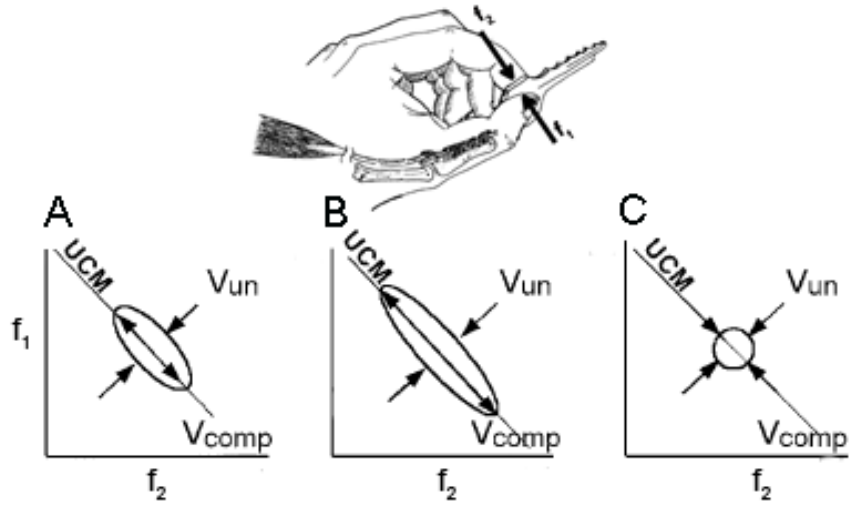

Figure 2: Different possible distributions of variance along the uncontrolled manifold. The variance along the manifold is called the uncompensated variance (V_{comp}) and the variance along the orthogonal subspace is called the uncompensated variance (V_{un}). The line along the manifold indicates where the task variables $E_1 + E_2$ = constant. Motor control is identified by looking at the ratio of the compensated and uncompensated variance ($R_V = V_{comp}/V_{un}$).

Similarly, during a sit-to-stand task (Scholz and Schoner 1999) the redundant joint space variables were also mapped to several hypothesized control outputs (Figure 3). The variance distributions on the manifold were then used to infer control. During the task, the ankle (θ_{Ankle}), thigh (θ_{Thigh}), trunk (θ_{Trunk}) and neck (θ_{Neck}) were experimentally recorded. Since the task was redundant, subject could manipulate different combination of the joint angles to accomplish objective of the task. Therefore, several hypothesized control variables were tested to determine which variables were controlled during the task. For example, the center of mass of the body (CM_{Body}) and the head (CM_{Head}) were chosen as controlled variables. The joint angles were then mapped onto the task trajectory. The variances along these trajectories were calculated and the uncontrolled hypothesis was tested. If the variance along the uncontrolled manifold was larger then the variance perpendicular to the manifold, then the hypothesis was accepted and the variables was deemed "controlled" during the experiment.

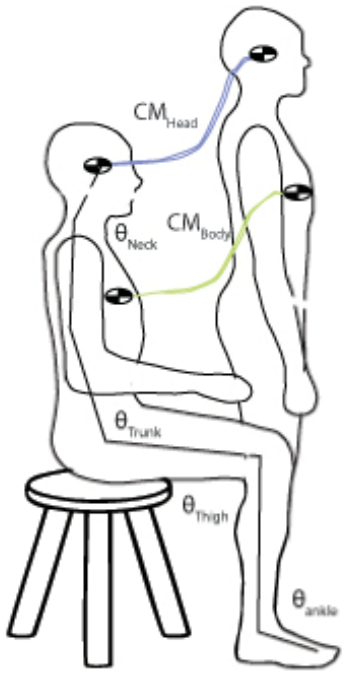

Figure 3: Diagram of the sit-to-stand task with selected joint space and their trajectories. The joint angles $(\theta_{ankle}, \theta_{Thigh}, \theta_{Trunk}, \theta_{Neck})$ define the body variables of the system. The body variables were mapped onto the "controlled" trajectory.

UCM argues that if we examine the decomposition of the body variables onto some properties of interest in the body (e.g. center of mass, hand trajectory, etc.), the ratios of the variance along and perpendicular to the manifold provide some indication of which variables were controlled during task performance. The uncontrolled portion of the manifold, direction of larger variance, allows the body to exploit the kinematic redundancy inherent in the task (Scholz, Schoner et al. 2000; Latash, Scholz et al. 2002). UCM assumes that such a manifold exist over the movement trajectory and estimates it based on the average movement over a set of trials. However, this assumption disregards the external properties that define the task. This type of analysis have been experimental applied to task such as: pointing task (Domkin, Laczko et al. 2002; Domkin, Laczko et al. 2005; Campolo, Widjaja et al. 2013), multi-finger force production task (Latash, Scholz et al. 2001; Scholz, Kang et al. 2003; Wu, Pazin et al. 2013), during sit-to-stand task (Scholz and Schoner 1999), pistol shooting task (Scholz, Schoner et al. 2000). This

analysis had also been used to study the variability of preadolescents walking with Down Syndrome(Black, Smith et al. 2007).

Tolerance-Noise-Covariation (TNC)

The Tolerance-Noise-Covariance method is another experimental approach that attempted to define the task goal independent of the measured data to understand how subjects explored or organized task variables during performance (Muller, Frank et al. 2007; Cohen and Sternad 2008; Muller and Sternad 2009; Sternad, Abe et al. 2011). TNC is a framework that examines the relationship between the variability in the execution space and variability in the task's goal. It is based on the analysis of the location, size and shape of each set of trial in the execution space rather than the body variable space. TNC evaluates the task performance based on the tolerance (location), covariation and noise (dispersion) of the data.

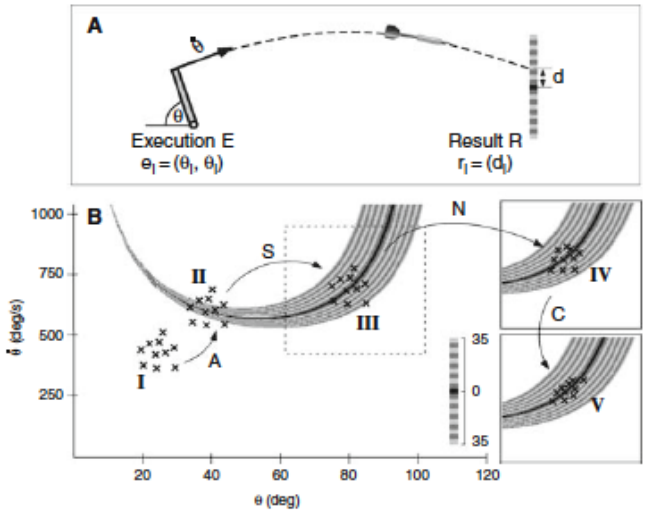

Figure 4: (A) A simplified dart throwing task (B) The execution space with the solution manifold for the task. Solid line indicated perfect execution of the task and shaded lines denote regions around the bullseye (target). I, II, III, IV, V show hypothetical data distributions during the dark throwing task. (Muller and Sternad 2009).

In contrast to UCM, TNC relates the goal of the task to the body-level variables; however, it is still relying on the average recorded data to infer control. For example,

Figure 4 shows the diagram of a simplified dart-throwing task. Restricting the task to a one-dimensional plane, the throw (R) is fully defined by the initial release angle (θ) and initial throwing velocity ($\dot{\theta}$). In the task space (Figure 4b), the outputs show several hypothetical situations where subjects started out completely missing the target (I); however, with more practice subjects were able to find the target (II) and eventually finding the combination of release angle and velocity that were less sensitive to error in the release angle and velocity. This would allow them to perform the task with high accuracy and repeatability. TNC argues that by examining how subjects' variability changes during the performance of skilled task (IV, V); it is possible to understand the underlying process that governs motor learning and control.

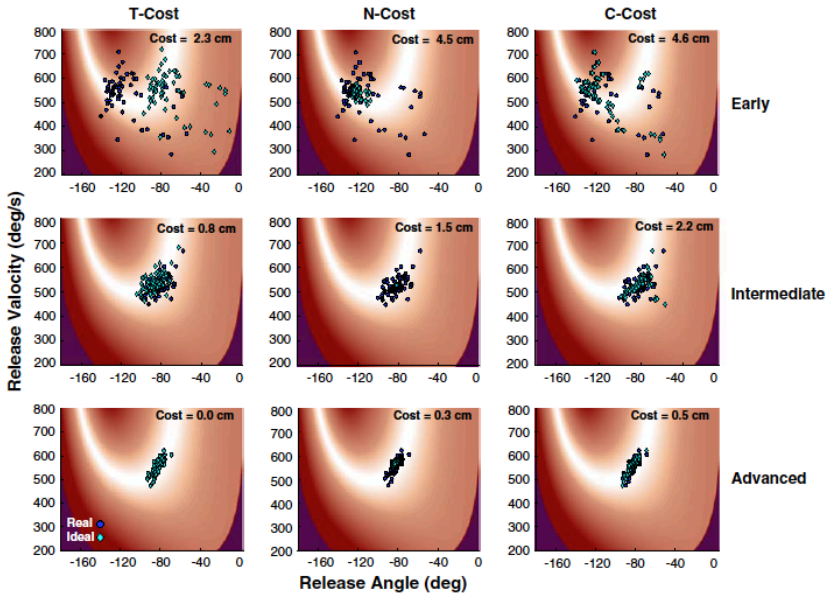

Figure 5: Example of the cost of the Tolerance – Noise – and Covariation during an experimental execution of a virtual skittle task (Cohen and Sternad 2008). With more practice time, subjects were able to achieve success at a high rate by manipulate or improving the different cost variables during task performance.

The T-cost is the cost of the performing the task. This is a measurement of the how the body variables affect the goal of the task. The C-cost is the covariation; it is the cost for not exploiting the redundancy that is inherent in the task. The N-cost is the cost

of task performance due to noise in the execution variables. TNC postulates that these three costs are directly related to the goal of the task. This type of analysis was applied to performance on skittle task (Cohen and Sternad 2008), throwing task(Cohen and Sternad 2012). In the skittle task, subjects were asked to swing a virtual ball to hit a virtual target by controlling the initial release angle and velocity. The task goal was to hit the target. In this experiment, people tended to reduce T-cost, then aligned their movement along it (reducing C-cost) and finally reducing the overall variability (N-cost) (Figure 5). Therefore by examining the distribution of these cost variables, TNC argues that it is possible to observe how people exploit the redundancy to improve task performance.

The TNC costs for the skittle task were calculated by comparing the experimental data set results with and reconstructed *best* data set results by optimizing the cost variable one at a time. The reconstructed results were then compared with real data set to determine the cost (error) of the task performance. For example, to calculate the T-Cost, which measures the cost of not being located at the *best* position on the task space, the mean of the average trial data set were moved to different positions in the task space that would yield the best results while preserving the dispersion along each axis (i.e. Noise and Covariation remain the same). The position that yields the best results would then be compared with experimental data. The N-Cost was calculated by measuring the radial distance from the data set to an "optimal" data set where the variability was the smallest. The optimal data set was achieved by projecting all the points in the data set to the mean. The C-Cost was calculated by comparing the data set with an optimal data set where the mean and distribution were maintained but individual pairings were recombined to achieve the best performance.

Limitations of Experimental Approaches

There are some drawbacks to these experimental methods that make them inefficient tools to resolve redundancy in the task in the present of variability. UCM relies on the ratios of variances computed across all trials to infer control while TNC relies on the final data distribution to hypothesize what subjects were manipulating

during a task. However, approaches that rely solely on analyzing the average behavior do not give any details on the trial-to-trial dynamics that are essential in understanding how the nervous system exploits the redundancy from movement to movement (Gates and Dingwell 2008; Dingwell and Cusumano 2010). Furthermore, UCM relies on the structure of the variance to infer control; but the variance can be structured in a way that is independent of the task (Valero-Cuevas, Venkadesan et al. 2009). The structure of the variance could arise from the biomechanical or muscular-skeletal coupling that caused by simple inertia effect (Dingwell, John et al. 2010) or the influence of soft tissue. Furthermore, signal dependent noise can generate structure in the variance independent of the task controller.

In UCM, the average recorded movement paths were used to define each proposed manifold. However, using the average recorded movement as the task goal sometimes lead to ambiguous interpretation of the observed results. For example, a study by Yang (Yang, Scholz et al. 2007) that applied the UCM approach to learning a reaching task in a viscous curl field. The force field was manipulated proportional to the velocity profile. Subjects were asked to make a reaching movement to the target and compensate for the force. The variance of the planar scapular, shoulder, elbow and wrist joint movement were decomposed into two orthogonal components: one representing the combination of joint angles that achieved the average hand path and one composed of the combination of joint angles did not achieve task success. One of the bases for using UCM approach requires that the nervous system is aware of the average behavior. The results did show that subjects were more variance along the uncontrolled manifold. However, the study also showed that after the initial exposure to the force field, subjects were still making curved hand path when the force field was turned off. However, subject might not be using the kinematic redundancy in the task to adapt to the force field and make straight line reaching movement, but they merely anticipated the presence of the viscous force field. The UCM approach assumes that stability could be correlated with variability exhibited during the task. However, the variances only indicated that the

average magnitude of the variation that occurred across many cycles and did not reveal how the nervous system responded to perturbation from one cycle to the next (Dingwell and Cusumano 2000; Dingwell, Kang et al. 2007).

These motor control theories are derived based on experimental observations; therefore they often lack an analytical foundation to conduct extensive tests to determine the sensitivity or robustness of the system. These approaches are limited by the tasks and how the control variables are defined (Valero-Cuevas, Venkadesan et al. 2009; Cusumano and Dingwell 2013; Dingwell, Smallwood et al. 2013). Furthermore, small variations in these variances do not necessary translate to control by the nervous system. For example, in learning to play the violin from a novice to an expert (Konczak, Vander Velden et al. 2009); people progressively minimized the variability of the distal joint angles; while allowing the variability of the proximal joint angles to fluctuate. This variability appeared to display a structural progression toward steady behavior; but it was not sufficient to conclude that these variables were 'controlled' during the task. These variabilities did not capture the motor control process that involved decoding sensory cues, analyzing feedback information, and compensating for biological and physical uncertainty. These elements need to be incorporated into a mathematical framework that correlates trial-to-trial dynamical system to understand how each element affects the overall behavior. This process allows us to understand how motor noise affects the variability of the joint angles. It is difficult to identify the cause and effect in such complex tasks without an analytical framework to analyze the dynamics interactions within the system.

COMPUTATIONAL APPROACHES

We need to develop not only a model of the task, but also a model of the controller to understand how the nervous system resolves redundancy and compensate for motor noise. Such model will allow us to directly manipulate the variable in the execution space and task space. Furthermore, it provides us a tool to analyze the

sensitivity of the system when it is exposed to different task goals (Loeb, Levine et al. 1990).

Optimality principles have been used to understand how the central nervous system solves the redundancy and noise problem (Kuo 1995; Todorov and Jordan 2002; Scott 2004; Todorov 2004; Todorov 2005; Todorov, Li et al. 2005; Bays and Wolpert 2007; Braun and Wolpert 2007; Guigon, Baraduc et al. 2008). However, these optimality principles do not clarify how the nervous system overcomes variability observed in movement. Does the nervous system simply minimize the variability in the task or is it exploiting the variability to improve task performance (Todorov and Jordan 1998; Cusumano and Cesari 2006; Dingwell, John et al. 2010) while minimizing control effort.

Minimum Intervention Principle (MIP)

For a redundant task, experimental results have demonstrated that subjects tend to be more variable along the direction that does affect the task goal and less variable along the direction that affects the task goal (Scholz and Schoner 1999; Cusumano and Cesari 2006; Dingwell, Smallwood et al. 2013). However, unlike UCM, similar behavior could also be observed when the control variables are not defined *a priori*. In UCM, the controlled variables were chosen and tested with the *uncontrolled hypothesis*; however, using MIP approach the task could be defined based on the task space rather than the joint space.

For example, Figure 6a shows a simple redundant task where the target was defined by $\left(X_1 + X_2 = \text{constant}\right)$. Figure 6b shows the data distribution generated by using an optimal feedback controller. The control law strongly corrected for perturbation in the *task-relevant* direction, but weakly controlled for deviation in the redundant direction or *task-irrelevant* direction. This is recognized as a *Minimal Intervention Principle* (MIP) of stochastic optimal feedback control. This property emerged from a simple principle that deviations that do not affect the task goal are weakly control to minimize the control effort. This is similar to the observations seen in UCM analysis;

however, in UCM analysis, the control variables were randomly chosen until the data satisfy the *uncontrolled hypothesis*.

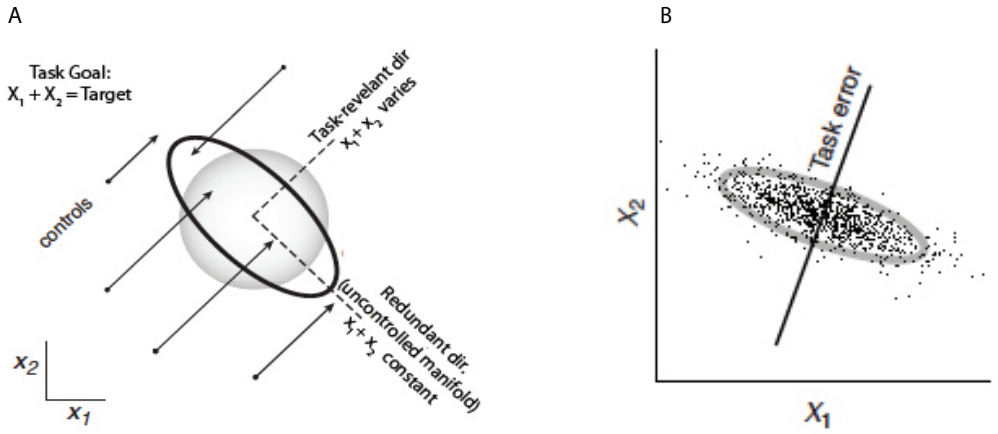

Figure 6: A simple redundant task where the task goal was defined by X_1 and X_2 $\left(X_1 + X_2 = \text{constant}\right)$. Using optimal control feedback, it was possible to observe similar behavior exhibited when analyzing the system using UCM. (Todorov and Jordan 2002).

Stochastic Optimal Control (SOC)

Stochastic optimal control has emerged as the primary principle for explaining variability during motor coordination for redundant tasks (Todorov and Jordan 2002). This principle provides an analytical framework to find optimality between redundancy and stochastic noise (internal and external) that arises during the task. This variability exists because the nervous system exploits redundancy during the task to generate the *best* possible solution. During redundant tasks, there is less variability in directions that are *relevant* to the task goal while there is more variability in directions that are *irrelevant* to the task goal (Figure 6). The stochastic optimal control captures the minimum intervention mechanism clearly exhibited by subjects when performing a redundant task.

However, stochastic optimal control may not be sufficient to explain the stochastic nature of motor behavior. An alternative framework proposed by Guigon (Guigon, Baraduc et al. 2008) based on a deterministic controller coupled with an optimal

state estimator. The Terminal Optimal Feedback Controller (TOFC) not only minimizes the inherent noise during movement, but it also accounts for the kinematic redundancy that exists in most daily tasks. The added state estimator allows the controller to find the optimal trajectory along the path to the target via points along the path rather than relying on weighted parameters in optimal controller to find the best trajectory. However, the question remains as to how the system is overcoming variability or using the inherent variability to improve task performance. While these optimal controllers do provide insight on how people might resolve redundancy and account for task variability, they fail to account for the dynamic fluctuation from trial-to-trial during the execution of a redundant task.

Goal Equivalent Manifold (GEM)

The Goal Equivalent Manifold (GEM) approach uses a mathematical framework within the stochastic optimal control to understand the movement-to-movement fluctuation as well making distinct separation between the task-space (task-space variables) and the execution space (i.e. body-state variables). It provides an analytical tool to resolve the redundancy and inherent variability from movement to movement. In contrast to UCM, the goal manifold is defined independent of any hypothetical control variables; therefore, there are no *a priori* assumptions about what is being controlled during the task. Such separation would allow for more free analysis of the dynamical behavior during the task. However, the GEM analysis also provides a means to capture the behavior exhibited under UCM approach as long as the variables analyzed are being controlled during the task. Thus GEM approach is both more general and precise than UCM approach.

Experimental studies have shown that the human nervous system exploits redundancy in learning a new task (Scheidt, Reinkensmeyer et al. 2000; Scheidt, Dingwell et al. 2001; Todorov and Jordan 2002; Todorov 2004; Cusumano and Cesari 2006; John and Cusumano 2007; Scheidt and Ghez 2007; Cohen and Sternad 2008). However, in some studies, the control variables were not well defined; thus convoluting

the relationship between the control variables and the goal of the task. To untangle this relationship, the task has to be defined independently from the control variables. While the GEM defines the goal of the task similar to TNC, the analytical method embraced by the GEM approach provides a more mathematical concrete and adaptable platform to investigate how motor variability and redundancy are controlled. However, the commonality among all these approaches is the idea that during a redundant task subjects were more variable in the task-irrelevant dimension while they were less variable in the task-relevant dimension.

The Goal Equivalent Manifold (GEM) approach was first introduced by Cusumano et. al (Cusumano and Cesari 2006) for a redundant aiming task using an air pistol with and without laser feedback. In this task, subjects were asked to aim an air pistol with and without laser at a target 10 m way by standing facing the target and 90 degree offset from the target (i.e. standing sideway with respect to the target). 30 markers were used to define the aiming position (body state variables) and the target was calculated from two markers at the end of the gun barrel. Therefore, the dimension of the body variables (28) was larger than the dimension of the goal (2). Thus there were 28 dimensional mapping where the changes in the body variables had no affect on the goal variables. By varying posture and perceptual cue (laser), they showed that while one could achieve similar performance for two distinct postures and perceptual conditions, the decomposition of goal level variability showed that standing sideway with laser on had best performance (lowest) variability and moderately good goal-relevant sensitivity. This result established the relationship between the body variables and the goal variables. The mapping of these variables arises naturally from the definition of the goal function. Therefore, for any task that could be represented by a goal function; you could characterize its performance by examining the goal equivalent manifold and sensitivity relationship between the goal and body variables. Therefore, the GEM approach provides a mean to estimate the sensitivity of goal level-error to body-level perturbation.

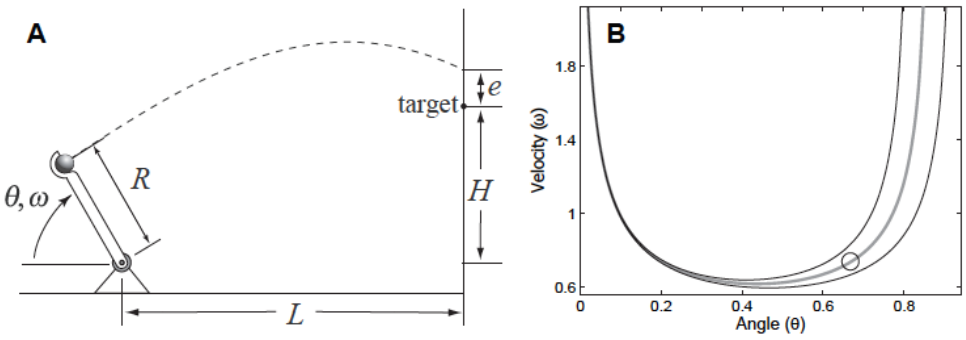

Figure 7: (A) An example of a throwing task where the target is mathematically defined by the release angle (θ) and the release velocity (ω). The goal manifold of the task with an ±10% error boundary (Cusumano and Dingwell 2013).

In the GEM approach, the task is defined using goal function, which defines the relationship between the goal of the task and the variables that are required to complete the task. Generally such goal function can be defined as

$$\mathbf{f}(\mathbf{x};\mathbf{p}) = 0 \tag{1}$$

Where $\mathbf{f}$ is the vector that define the goal of the task of dimension D_g and $\mathbf{x}$ define the body–level variable with dimension D_b and $\mathbf{p}$ defines other internal or external variables need to perfectly execute the task. Figure 7 show an example of a throwing task where the target is defined by

$$\mathbf{f}(\theta,\omega;H,R,L) = \frac{L+R\cos\theta}{\tan\theta} - \frac{g}{2}\left(\frac{L+R\cos\theta}{\omega R\sin\theta}\right) + R\sin\theta - H = 0 \tag{2}$$

Here $\mathbf{x} = (\theta,\omega)$ defines the body level variables and $\{H,R,L,g\}$ define other parameters within the task that are needed to accomplish the goal. Since, the dimension of the task (the target) is smaller than the dimension of the body-level variable ($\mathbf{x}$), there is a manifold in the θ-ω plane that defines a whole set of solution that will satisfy the goal of the task (Figure 7b) given that the vector $\mathbf{p}$ is constant. This defines the goal equivalent manifold for the task. Any point on this manifold will achieve task success. While a robotic system could be programmed to hit the target every time; humans are not

that precise; therefore variability exists from throw to throw. Thus this precipitates the exploitation of the redundancy in the task. How subjects exploit the variability and redundancy in the task provides important understanding of the underlying motor control mechanism.

AIMS OF DISSERTATION

Understanding how the nervous system accounts for motor noise and resolves redundancy can provide further insight on the underlying control mechanisms that govern movement. In this dissertation, we extend the current progress in motor theories to further investigate the effect of noise and redundancy in motor control.

In the first study, using a simple 2-dof of a planar arm model, the effect of noise on control was examined at the distal and proximal joint for a straight line reaching movement. Here we investigated how the nervous system partitioned control across proximal vs. distal joint in specific goal-directed task. It is not yet known precisely how the integration of distal and/or proximal control minimizes the effect of noise on task performance. Therefore, a rigorous analytical approach was implemented to investigate the distinct function of distal and proximal joints during movement. Such analysis would provide insights on how the nervous system mitigates the effect of noise within the motor control system. Current rehabilitation devices(Furuya and Kinoshita 2007) have been actively using proximal and distal control to develop more effective rehabilitation process; therefore understanding the effect of noise and control on motor can lead to development of more effective rehabilitation process.

One of the goals of this dissertation was to expand the framework developed by Cusumano to explain how the nervous system compensates for neuro-motor noise during a goal-redundant reaching task. In this study, we used an inter-trial controller to investigate the possible dynamical behavior display by subjects when performing a redundant reaching task. Furthermore, a better understanding of motor control can help develop diagnostic tools to identify neurological disorders and restore lost motor function. Rehabilitation technologies and exercises could be designed to incorporate only

the most *essential* control features to produce more physiologically compliant system that increases exercise efficiency. Ultimately, this process can increase therapy efficiency, reduce rehabilitation time and decrease overall healthcare cost. However, before the inter-trial controller could be used to hypothesize motor control and structure during a task and the validity of the control would need to be rigorously validated using experimental results. The goal was to be able to use the architecture of the inter-trial controller to provide further insights on the strategic differences between subjects during the task.

Chapter 3: Proximal vs. Distal Control of Neuromuscular Noise During Planar Reaching Task[1]

ABSTRACT

Determining how the human nervous system contends with neuro-motor noise is vital to understanding how humans achieve accurate goal-directed movements. Experimentally, people learning skilled tasks tend to reduce variability in distal joint movements more than in proximal joint movements. This suggests they might be imposing greater control over distal joints than proximal joints. However, the reasons for this remain unclear, largely because it is not possible experimentally to directly manipulate either the noise or the control at each joint independently. Therefore, this study used a 2 degree-of-freedom torque driven arm model to determine how different combinations of noise and/or control applied at each joint independently affected reaching accuracy and the total work required to make the movement. Signal-dependent noise was simultaneously and independently added to the shoulder and elbow torques to induce endpoint errors during planar reaching. Feedback control was then applied independently and jointly at each joint to reduce endpoint error due to the added neuromuscular noise. Movement direction and the inertia distribution along the arm were varied to quantify how these biomechanical variations affected system performance. Endpoint error and total net work were computed as dependent measures. When each joint was independently subjected to noise in the absence of control, endpoint errors were more sensitive to distal (elbow) noise than to proximal (shoulder) noise for nearly all combinations of reaching direction and inertia ratio. The effects of distal noise on endpoint errors were more pronounced when inertia was distributed more toward the forearm. In contrast, total net work decreased as mass was shifted to the upper arm for reaching movements in all directions.

[1] The work presented here in Chapter 2 has been published in the Journal of Biomechanical Engineering in 2012. Nguyen, H. P. and J. B. Dingwell (2012). "Proximal versus distal control of two-joint planar reaching movements in the presence of neuromuscular noise." J Biomech Eng **134**(6): 061007.

When noise was present at both joints and joint control was implemented, controlling the distal joint alone reduced endpoint errors more than controlling the proximal joint alone for nearly all combinations of reaching direction and inertia ratio. Applying control only at the distal joint was more effective at reducing endpoint errors when more of the mass was distributed more proximally. Likewise, controlling the distal joint alone required less total net work than controlling the proximal joint alone for nearly all combinations of reaching distance and inertia ratio. It is more efficient to reduce endpoint error and energetic cost by selectively applying control to reduce variability in the distal joint than the proximal joint. The reasons for this arise from the biomechanical configuration of the arm itself.

INTRODUCTION

Reaching is a very elementary task. However, it requires sophisticated control to overcome several fundamental challenges during movement. One of the most significant of these challenges is inherent neuromuscular noise. This noise emanates from both internal neuromuscular signals and external sources (Faisal, Selen et al. 2008; McDonnell and Ward 2011). Numerous control theories have attempted to explain how humans compensate for motor noise during movement (Harris and Wolpert 1998; Hamilton, Jones et al. 2004; Bays and Wolpert 2007; Guigon, Baraduc et al. 2008; Braun, Aertsen et al. 2009). Experimental studies at the muscle level have shown how increased co-contraction of shoulder (Laursen, Jensen et al. 1998) or elbow muscles (Osu, Kamimura et al. 2004) could be used to strategically minimize noise without compromising endpoint accuracy. Applying control to reduce the negative impacts of noise involves expending control effort (i.e., energy). The human nervous system must therefore decide how to most effectively apply control across the joints involved in any task in such a way as to maximize performance outcome, while also limiting the total energy expended. For the task of planar reaching, there are specific dynamic interactions between the torques applied at the shoulder and elbow (Gribble and Ostry 1999; Ketcham, Dounskaia et al. 2004) and these will also vary depending on the movement direction. It is not known how this biomechanical coupling influences how motor noise applied at each joint independently affects performance accuracy or the effectiveness of any control effort that is applied at either joint. Therefore, the purpose of this study was to determine how such biomechanical factors (arm configuration and differences in reaching direction) influence how different combinations of motor noise and/or control applied at each joint in turn affect reaching accuracy and energetic cost of reaching.

Noise and control at the proximal and distal joints may affect the dynamics and coordination of goal-directed movements differently (McDonald, Vanemmerik et al. 1989; Dounskaia 2005; Furuya and Kinoshita 2007; Konczak, vander Velden et al. 2009). For example, experiments suggest that people may first assert proximal joint control, followed by distal joint control, to help them learn new skilled tasks (McDonald,

Vanemmerik et al. 1989; Furuya and Kinoshita 2007). McDonald (McDonald, Vanemmerik et al. 1989) demonstrated in a dart throwing task that, with practice, the variability at the distal joints decreased and the cross-joint correlations between the distal and proximal joint also decreased. They suggested that people could adopt a control strategy of *freeing* and *freezing* different degrees of freedom in the system to learn this new task. Likewise, when using an experimentally controlled playing form, joint kinematics of novice violinists were more variable than those of experts (Konczak, vander Velden et al. 2009). However, as the novices practiced over time, variability at the distal joints decreased and approached the behavior exhibited by expert violinists. These experimental observations suggest that task performance may be more sensitive to controlling variability at distal joints than proximal joints. However, one cannot easily infer the nature of the underlying control process simply by observing the structure of the variability in the observed behavior (Valero-Cuevas, Venkadesan et al. 2009). A computational framework is required to independently manipulate the biomechanical and control factors and then measure their effects on task performance.

Understanding how the CNS regulates and structures movement variability is critical to understanding how humans perform skilled movements (Todorov and Jordan 2002; Körding and Wolpert 2004; Todorov 2004; Cusumano and Cesari 2006; Faisal, Selen et al. 2008). Trial-to-trial variability in most movement tasks is in fact *not* entirely random, but is structured in specific ways that have important implications for control (Todorov and Jordan 2002; Körding and Wolpert 2004; Todorov 2004; Cusumano and Cesari 2006). Geometry-based approaches to analyzing the structure of variability in experimental data (Scholz and Schöner 1999; Latash, Scholz et al. 2002; Cohen and Sternad 2009) have provided some insights into these issues. However, these approaches inherently ignore the question of how the biomechanical structure of the system performing the task (e.g., the arm, etc.) can themselves create structure in the measured task performance (Valero-Cuevas, Venkadesan et al. 2009). In fact, observed movement variability could be structured for any of *several* reasons *not* related to controlling the

task itself (Valero-Cuevas, Venkadesan et al. 2009). These might include the biomechanical structure of the system, the signal-dependent nature of neuromuscular noise, or a desire by the nervous system to satisfy other task goals like minimizing fatigue or exploring alternative control strategies. Theoretical approaches that tie these ideas to stochastic optimal control theory (Todorov and Jordan 2002; Todorov 2004; Cusumano and Cesari 2006) provide a more concrete computational framework for properly interpreting the specific control implications of such experimental observations (John and Cusumano 2007; Valero-Cuevas, Venkadesan et al. 2009; Dingwell, John et al. 2010). These concepts have not yet been applied to specifically address the question of how the nervous system might partition control across proximal vs. distal joints in specific goal-directed tasks. Thus, it is not yet known precisely how integrating distal and/or proximal control minimizes the effects of noise on task performance. Experimentally, one cannot manipulate these factors independently to separate the roles of distal vs. proximal noise and/or control on task performance. A rigorous computational analysis is needed to investigate the distinct functions of distal and proximal joints during movement.

Here, we used a 2 degree-of-freedom torque driven arm model to generate point-to-point reaching movements to fixed targets. We varied both movement direction and the inertia distribution along the arm to determine how these biomechanical factors impacted task performance. We then applied noise and feedback control in varying combinations at each joint torque. First, we examined how, in the absence of any additional control, adding *noise* to either the distal (elbow) *or* proximal (shoulder) joint torques independently affected endpoint errors and total net work. We hypothesized that, in the absence of any feedback control, performance in this reaching task would be more sensitive to distal (elbow) noise than to proximal (shoulder) noise. We also hypothesized that these effects would be strongly influenced by biomechanical factors (i.e. reaching direction and/or inertial properties).

Second, we quantified how, when noise was present at *both* the elbow and shoulder joint torques, applying feedback *control* to either the elbow joint torque, or

shoulder joint torque, or both, affected endpoint errors and total net work. Because we imposed reaching movements where the kinematics was fully specified, this yielded a one-to-one mapping from hand kinematics to joint torques. This then removed any *kinematic* redundancy in the system, and thus also any joint *torque* redundancy for the nominal (noise-free) movements themselves. However, there *was* redundancy in terms of where to apply *control* (i.e., at which joint torque), since the controller had the choice of applying limited control resources to reduce the effects of the applied noise either at the shoulder, *or* at the elbow, *or* both. Here again, geometry-based methods (Scholz and Schöner 1999; Latash, Scholz et al. 2002; Cohen and Sternad 2009) that consider only kinematic redundancy cannot address this important question. Here, we hypothesized that when noise was present at both joints, applying only distal (elbow) control would be more effective than applying only proximal (shoulder) control for maximizing task performance. We also hypothesized that these effects, like those above, would also be strongly influenced by biomechanical factors (i.e. reaching direction and/or inertial properties.

METHOD

Arm Model

A planar 2 degree-of-freedom (dof) torque-driven model of the right arm (Figure 8) was developed. This model was designed to specifically address how the biomechanics of the arm and the reaching task influences the options any controller might have to exploit *control redundancy* at the joint torque level. As with any model, this model represented a simplification from the true biological system. For example, our model did not include a wrist joint. Experimentally, humans exhibit minimal net torques and very little movement at the wrist (Galloway and Koshland 2002). Thus, many studies have used similar 2-joint models to simulate planar arm reaching movements (e.g., (Ohta, Svinin et al. 2004; Tee, Burdet et al. 2004; Secco, Valandro et al. 2005; Jagodnik and van den Bogert 2010)). Our model also did not include any muscle mechanics, spinal reflexes, or serial elastic elements (i.e., tendons), etc. However, increased biological noise at the *muscle* level has been shown to concurrently increase joint *torque* variability (Osu, Kamimura et al. 2004). Our goal here was to elucidate the general principles by which the biomechanics of the arm and the task influence the overall choice of where to apply control (proximal vs. distal). Our goal was *not* to explore any specific physiological implementation of that control. Thus, the model used here incorporated the necessary and sufficient level of complexity to address the specific control hypotheses posed.

Table 1 Model Parameters

Parameter Description	**Values for all IR**		
Length of upper arm (L_u) [m]	0.33		
Length of forearm (L_f) [m]	0.35		
COM of upper arm (d_u) [m]	0.14		
COM of forearm (d_f) [m]	0.018		
Segment Masses & Inertias	**IR = 0.25**	**IR = 1.05**	**IR = 4.00**
Mass of upper arm (m_u) [kg]	0.915	2.100	2.9905
Mass of forearm (m_f) [kg]	2.610	1.425	0.5345
Inertia of upper arm (I_u) [kg·m^2]	0.0291	0.0668	0.0951
Inertia of forearm (I_f) [kg·m^2]	0.1161	0.0634	0.0238

Standard anthropometric values were obtained assuming total body mass of M=75.0 kg and height of H=1.75 m (Table 1; (Winter 2005)). Inverse dynamics equations were derived from Ref. (Uno, Kawato et al. 1989). The *reference* joint torques ("τ_{ref}" in Figure 8b), $\left[\tau_s, \tau_e\right]^T$, for the noise-free / control-free reaches were given by

$$\begin{bmatrix}\tau_s \\ \tau_e\end{bmatrix} = \mathbf{H}(\theta)\begin{bmatrix}\ddot{\theta}_s \\ \ddot{\theta}_e\end{bmatrix} + \mathbf{B}\begin{bmatrix}\dot{\theta}_s \\ \dot{\theta}_e\end{bmatrix} + \mathbf{C}(\theta)\begin{bmatrix}\dot{\theta}_s\dot{\theta}_e \\ \dot{\theta}_s^2 \\ \dot{\theta}_e^2\end{bmatrix} \tag{1}$$

Where $\mathbf{H}(\theta)^{2x2}$ represents the inertial matrix, $\mathbf{B}^{2x2}$ denotes the torques due to damping, and $\mathbf{C}(\theta)^{2x3}$ denotes the torques due to Coriolis and centrifugal forces. In this model, we assumed that there were no external forces or perturbations acting on the system. The inertia matrix $\mathbf{H}(\theta)^{2x2}$ was given by

$$\mathbf{H}(\theta) = \begin{bmatrix} I_{uprox} + I_u + m_u\left(L_u^2 + d_f^2 + 2L_u d_f \cos(\theta_e)\right) & I_{fprox} + m_f\left(L_u d_f \cos(\theta_e)\right) \\ I_{fprox} + m_f\left(L_u d_f \cos(\theta_e)\right) & I_{fprox} \end{bmatrix} \tag{2}$$

Where L_u is the length of the upper arm and d_f denotes the distance from elbow joint to the center of mass of the forearm. m_f and m_u are the mass of the forearm and

upper arm respectively. I_u and I_f represent the inertias of the upper arm and forearm with respect to the center of mass of the segment. $I_{uprox}=[I_u+m_u d^2{}_u]$ and $I_{fprox}=[I_f+m_f d^2{}_f]$ are the inertias of the upper arm and forearm with respect to the proximal end of the segment. Values of these parameters are given in Table 1. $\left[\theta_s,\theta_e\right]^T$ defines the angles of the shoulder (s) and elbow (e) joints. The torques generated by the Coriolis and centrifugal forces were given by

$$\mathbf{C}(\theta)=\begin{bmatrix} -m_f L_u \sin(\theta_e) & 0 & -2m_f L_u d_f \theta_e \\ 0 & m_f L_u d_f \sin(\theta_e) & 0 \end{bmatrix} \tag{3}$$

The damping constants (Stroeve 1999) were included to provide an estimate of the damping effect due to the viscoelastic structures around the joints. The damping matrix was defined as

$$\mathbf{B}=\begin{bmatrix} 0.3 & 0.2 \\ 0.2 & 0.3 \end{bmatrix} \quad (Nms) \tag{4}$$

Eq. (1) was used to formulate the differential equations to calculate the forward kinematics.

$$\begin{bmatrix} \ddot{\theta}_s \\ \ddot{\theta}_e \end{bmatrix}=\mathbf{H}^{-1}(\bar{\theta})\left(\begin{bmatrix} \tau_s \\ \tau_e \end{bmatrix}-\mathbf{B}\begin{bmatrix} \dot{\theta}_s \\ \dot{\theta}_e \end{bmatrix}-\mathbf{C}(\bar{\theta})\begin{bmatrix} \dot{\theta}_s\dot{\theta}_e \\ \dot{\theta}_s^2 \\ \dot{\theta}_e^2 \end{bmatrix}\right) \tag{5}$$

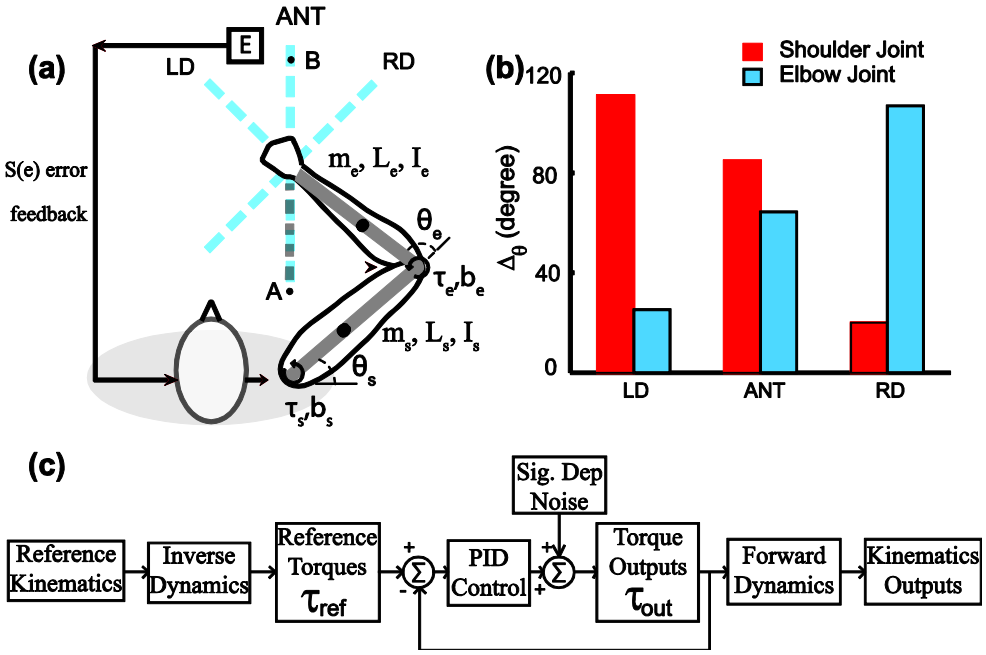

Figure 8: (a) A 2-dof torque driven arm model used to simulate three different reaching movements: Anterior (ANT), Left Diagonal (LD), and Right Diagonal RD) (b) Total ranges of motion for each joint for each reaching movement (c) Schematic of the PID controller.

The differential equations were solved by using numerical integration with trapezoidal rule (step size=0.002). A simple numerical integration code was implemented in Matlab® (The Math Works Inc., Natick, MA) to solve the differential equation. Although Matlab® offers numerous alternatives to solving the differential equations, our code yielded similar results at a smaller computational cost.

This model was used to simulate reaching movements in three distinct directions: Anterior (ANT), Left Diagonal (LD), and Right Diagonal (RD) (Figure 8a). These directions were chosen to test a wide range of motion of the shoulder and elbow joints (Figure 8b). For the right arm, a LD reach required a larger range of movement at shoulder, but less at the elbow. While a RD reach required a larger range of movement at the elbow, but less at the shoulder. Simulating these three directions allowed us to further highlight differences of proximal versus distal control in the presence of noise and biomechanical variation. Furthermore, these directional tasks provided a broader scope

within which to capture the diversity of underlying control mechanisms across different reaching tasks (Goble, Zhang et al. 2007; Levin, Forner-Cordero et al. 2008; Dounskaia, Goble et al. 2011). This allowed us to explicitly explore how the nervous system could exploit redundancy in the choice of where to apply *feedback control* (i.e., at the proximal vs. distal joint vs. both joints) to maximize task performance, even in a task that exhibited no kinematic redundancy.

Nominal Reaching Movement

The distance from each starting point to each target was set at 50 cm to yield slightly less than fully extended reaching movements in all reaching directions for a model with a total arm length of 68 cm (Table 1). For anterior movements, the starting pose of arm was set at 10 cm anterior to the shoulder joint (Figure 8a). For diagonally directed movements, the starting positions were offset at 45° in the corresponding direction (Figure 8a). The movement time was set at 1 sec. Within each trial, the nominal movement was defined by a feed-forward Minimum Jerk trajectory (Hogan 1984; Flash and Hogan 1985). Minimum Jerk is just one of many computational models that accurately predict average trajectories of the hand during reaching (Collins 1995; Alexander 1997; Engelbrecht 2001; Scott 2004). For straight-line reaching movements, this model accurately predicts the basic kinematic features exhibited by humans during reaching. The Minimum Jerk theory states that humans tend to minimize the net jerk (i.e., the derivative of acceleration) of the hand during the reaching movement. The cost function to be minimized is thus:

$$C = \frac{1}{2}\int_0^{t_f}\left(\left(\frac{d^3x}{dt^3}\right)^2 + \left(\frac{d^3y}{dt^3}\right)^2\right)dt \qquad (6)$$

Where (x, y) denotes the Cartesian coordinates of the hand and $t_f = 1$ sec is the total duration of the reaching movement. Assuming that motion starts and ends with zero velocity and zero acceleration and that (x_0, y_0), and (x_f, y_f) denote the initial and final positions of the hand, respectively, the solution of Eq. 5 yields a trajectory of the hand that is described in the Cartesian plane as a 5th order polynomial:

$$x(t) = x_0(x_0 - x_f)(-6\zeta^5 + 15\zeta^4 - 10\zeta^3)$$
$$y(t) = y_0(y_0 - y_f)(-6\zeta^5 + 15\zeta^4 - 10\zeta^3) \quad (7)$$

Where $\zeta = 1/t_f$. Once this nominal hand trajectory was specified, joint kinematics was calculated using inverse kinematics. Nominal joint torques required to achieve this trajectory were then calculated using inverse dynamics (Eq. 1). Because the task was restricted to the 2D plane, there was a one-to-one mapping of the endpoint (i.e., hand) motion to these joint torque profiles. Here we considered only reaching movements directed away from the body. Movements directed towards the body would have yielded the same kinematics and inverse dynamics (Figure 9), except in reverse time.

Signal-Dependent Noise

Motor noise was added to the feed-forward profiles of the elbow and shoulder joint torques (Figure 9) to determine the relative sensitivity of the system to distal and/or proximal noise. This noise was specified to be signal-dependent (Harris and Wolpert 1998; Hamilton, Jones et al. 2004), such that the noise amplitude increased proportionally with an increase in muscular activity (Figure 9). Osu (Osu, Kamimura et al. 2004) demonstrated that increases in *muscle* (i.e., EMG) variability resulted in increased joint *torque* variability. Therefore, while *neuromuscular noise* initially arises from muscle forces and/or activations, the inherent signal-dependent noise (Harris and Wolpert 1998; Hamilton, Jones et al. 2004) generated during muscle activation is also reflected in the resulting joint torques (Osu, Morishige et al. 2009). We therefore assumed the noise added to these net joint torques reasonably reflected the net effect of the neuromuscular noise in the system. In the model, this noise was added either to the elbow torque only, to the shoulder torque only or simultaneously to both the elbow and shoulder torques (Figure 9).

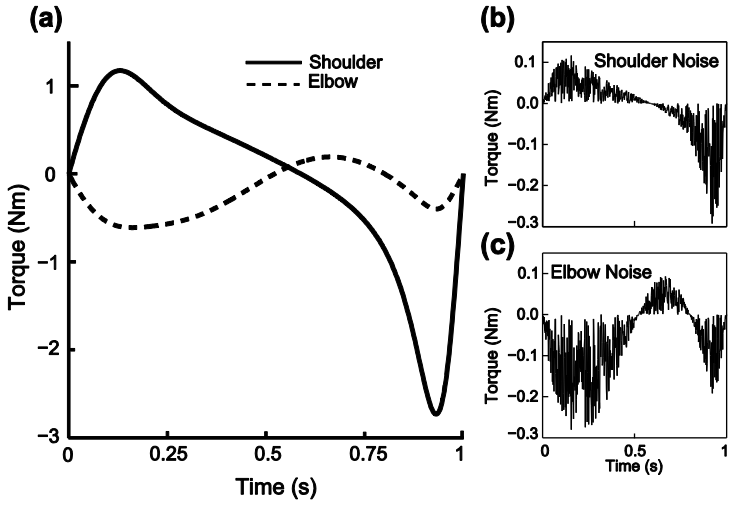

Figure 9: (a) Nominal torque profiles for the shoulder and elbow joint during anterior reaching without the influence of noise (b) Shoulder joint signal-depending noise profile (c) Elbow joint signal-dependent noise profile.

The applied signal-dependent-noise, $\bar{\mathbf{N}}_i$, was randomly distributed and scaled to be proportional to the torque output (τ) at each joint (Figure 9b):

$$\bar{\mathbf{N}}_i = \begin{bmatrix} N_{s,i} \\ N_{e,i} \end{bmatrix} = 0.3 \cdot \begin{bmatrix} \tau_{s,i} \cdot \eta_{s,i} \\ \tau_{e,i} \cdot \eta_{e,i} \end{bmatrix} \tag{8}$$

Where *i* denotes the individual time step within the reaching movement and the $\eta_{\bullet,i}$ terms were random values chosen from a uniform distribution on the interval [–1, +1] generated using the Matlab® "rand" function. Typical profiles of the noise at the shoulder and elbow joint are shown in Figure 9b. This noise was then added to the nominal torque required to make each reaching movement.

Control Model

While motor noise is ubiquitous in movement (Faisal, Selen et al. 2008), humans do use sensory feedback to help mitigate its effects on task performance. Therefore, within each trial, standard Proportional-Integrative-Derivative (PID) controllers (Figure 8c) were implemented to simulate within-trial torque adjustment. The same PID controller was used to control the elbow and shoulder joint torques either independently

or jointly. Similar types of controllers (Gribble, Ostry et al. 1998; Peterka 2003) have been shown to adequately capture the dynamics of relatively typical reaching movements. These controllers adjusted the performance of the system proportionally to the torque error output and its derivative. This control law was given by

$$\mathbf{V}(t) = \mathbf{k_p} \cdot \mathbf{e}(t) + \mathbf{k_i} \cdot \int \mathbf{e}(t)dt + \mathbf{k_d} \cdot \frac{d}{dt}\mathbf{e}(t) \tag{9}$$

Where $\mathbf{e}(t)$ was the relevant torque error (i.e., elbow or shoulder) and $\mathbf{V}(t)$ was the feedback control effort required to correct for deviations in the torque due to motor noise at the relevant joint(s). Given the one-to-one mapping between hand kinematics and joint torques, correcting these torque errors was equivalent to correcting endpoint errors. Control was only applied when noise was present at both the elbow and shoulder joint. To apply control at the elbow only, we took $\mathbf{e}(t) = \begin{bmatrix} 0 & e_e(t) \end{bmatrix}^T$ and $\mathbf{V}(t) = \begin{bmatrix} 0 & V_e(t) \end{bmatrix}^T$. To apply control at the shoulder only, we took $\mathbf{e}(t) = \begin{bmatrix} e_s(t) & 0 \end{bmatrix}^T$ and $\mathbf{V}(t) = \begin{bmatrix} V_s(t) & 0 \end{bmatrix}^T$. To apply control simultaneously at both the elbow and shoulder, we took $\mathbf{e}(t) = \begin{bmatrix} e_s(t) & e_e(t) \end{bmatrix}^T$ and $\mathbf{V}(t) = \begin{bmatrix} V_s(t) & V_e(t) \end{bmatrix}^T$. For all 3 controllers, the control constants were diagonal matrices:

$$\mathbf{k_p} = \begin{bmatrix} k_p & 0 \\ 0 & k_p \end{bmatrix}, \quad \mathbf{k_i} = \begin{bmatrix} k_i & 0 \\ 0 & k_i \end{bmatrix}, \text{ and } \quad \mathbf{k_d} = \begin{bmatrix} k_d & 0 \\ 0 & k_d \end{bmatrix} \tag{10}$$

where k_p=0.3, k_i=0.2, and k_d=0.1 were the controller gains. These proportionality constants were determined using Ziegler-Nichol rule (Franklin, Powell et al. 2002), which heuristically tuned the controller to find constants that satisfied specified performance requirements. The same control values were used for all simulations for all conditions to ensure the results did not depend on the optimization of these parameters. The controller iteratively minimized the noise at every time step during each movement until the noise was eliminated within a specified tolerance. Although more sophisticated control schemes certainly do exist that are more physiologically "realistic" (indeed, real biological controllers are far less effective than the controllers used here), the critical

aspect to *this* study is that we applied the *same* type of control to both joints in the same way.

Simulations and Analyses

Simulations:

Two different sets of conditions were simulated to determine how noise and control affected endpoint error and net work during planar reaching. The first set of simulations compared the effect of noise at the elbow versus noise at the shoulder on endpoint error and net work in the absence of any control at the joints. The second set of simulations compared how, when noise was present at both joints, applying distal and/or proximal control affected endpoint error and net work.

To investigate the effects of inertial distribution in the upper extremity, we manipulated the masses of the upper arm and forearm to generate different inertia ratios (Figure 10) while keeping the total mass and total length of the arm constant. The total mass of the arm was kept constant to prevent introducing additional loads into the system. The inertia ratio (IR) was defined as

$$IR = \frac{I_u}{I_f} \equiv \frac{Inertia\ of\ upper\ arm}{Inertia\ of\ \ forearm} \tag{11}$$

Where I_u and I_f define the inertia of the upper arm (u) and forearm (f) with respect to the center of mass of each segment. Three inertia ratios were tested (Figure 10). The anthropometric arm, based on standard human data, had an IR $\approx$ 1.05 (Table 1). The other two ratios (IR = 0.25 and IR = 4.0) were chosen to represent dramatic shifts of the inertia in both directions. While these two alternative IR's do not represent biologically realistic systems, the results from these simulations allowed us to explicitly determine how the biomechanical properties of the human arm might influence the choice of any control strategy the nervous system might choose to use to minimize noise.

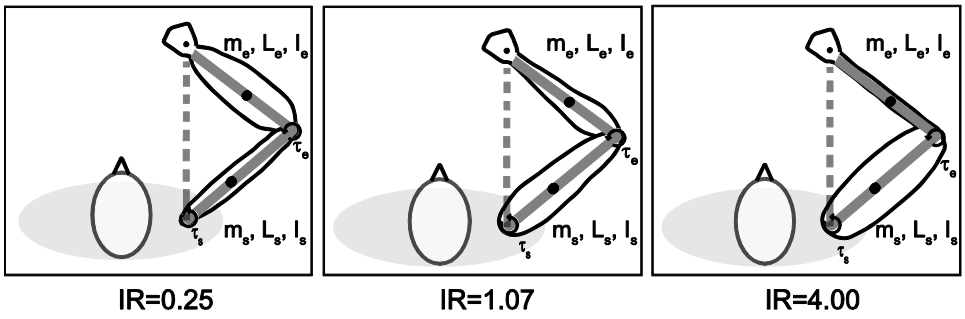

Figure 10: The biomechanical properties of the arm were manipulated by varying the inertia distribution along the arm.

Simulations were implemented in Matlab® (The Math Works Inc., Natick, MA). Each condition was simulated for 30 trials and the average values were recorded.

Dependent Measures:

Endpoint error is a direct measure of the success in the task. Endpoint errors in position were calculated as the absolute deviation from the desired endpoint location (x_d, y_d), as specified by the nominal feed-forward Minimum Jerk trajectory (Eq. 7). This error was defined as

$$Err_j = \sqrt{\left(x_j - x_d\right)^2 + \left(y_j - y_d\right)^2} \tag{12}$$

where (x_j, y_j) denoted the endpoint location at the completion of each trial, j. The Minimum Jerk reaching trajectories used here imposed zero velocity and zero acceleration at the beginning and end of each reaching movement, which also yielded zero torque (Figure 9a). Since the noise applied was proportional to these torques (Figure 9b), we assumed that any errors in torque, velocity, or acceleration would be quite small compared to the position errors.

Total net work (TNW) is a direct measure of the work required to complete the task. This assumes that people try to complete the task as accurately as possible with as little effort as necessary. Alexander (Alexander 1997) demonstrated that *one* possible strategy that drives human arm trajectories is to minimize energy cost (Sparrow and Newell 1998; Nishii and Taniai 2009). Therefore, it is possible that the distal-proximal

control strategy could yield more energetically efficient movements. Here energetic cost was only used as performance metric and not as an optimization parameter for the system. *TNW* was calculated as the total net work (in Joules) required to drive the system to the reference state under the presence of noise. The reference state was fully specified by the Minimum Jerk motion. *TNW* included the feedback (PID controller), feed-forward (Minimum Jerk), and noise components of the effort required to execute each movement. The TNW for each trial was thus calculated by numerically integrating the absolute value of the power curve:

$$TNW_j = \sum_{i=1}^{k} \left| \tau_{t(i)} \cdot \dot{\theta}_{t(i)} \right| \Delta t \tag{13}$$

Where k denotes the number of discrete time steps within each trial (k=500) and $\tau_{t(i)}$ denotes the total *output* torque ("τ_{Out}" in Figure 8b) at each joint, including the torque due to noise and feedback controller.

Statistical Analyses:

Endpoint error (*Err*) and total net work (*TNW*) were analyzed for both sets of simulations. To analyze the effects of adding *noise* (in the absence of control) on endpoint error and net work, 3-factor ANOVAs were used to determine both main effects and interaction effects across noise locations (distal or proximal), directions (ANT, LD, RD), and the 3 inertia ratios. Estimated marginal means tests were used to make individual post-hoc comparisons across the different levels of each factor. Within each direction, 2-factor ANOVAs were used to identify significant effects of noise and inertia ratio on endpoint error and net work.

To analyze the effects of applying *control* (in the presence of noise) on endpoint error and net work, 3-factor ANOVAs were used to determine both main effects and interaction effects across the joint control schemes (no control, shoulder control only, elbow control only, elbow+shoulder control), directions (ANT, LD, RD), and the 3 inertia ratios. Estimated marginal means tests were used to make individual post-hoc comparisons across the different levels of each factor. Within each direction, 2-factor

ANOVAs were used to identify significant effects of control and inertia ratio on endpoint error and net work.

RESULT

Distal vs. Proximal Noise

Endpoint Error:

In the absence of any control at the joints, there were significant differences in endpoint error (Err) across all reaching directions ($p<0.05$), inertia ratios ($p<0.05$), and noise locations ($p<0.05$) (Figure 11) when noise was applied either at the proximal (shoulder) joint or distal (elbow) joint independently. For movements in the anterior (ANT) direction, noise applied at the elbow resulted in significantly larger endpoint errors (Err=5.77 cm) than noise applied at the shoulder (Err=1.48 cm, $p<0.05$). The same trend was observed across all inertia ratios for movements in the ANT direction. As more mass was shifted toward the upper arm, creating a larger inertia ratio, there were significant increases in endpoint error due to noise at distal joint (from 2.89 cm to 9.53 cm, $p<0.05$), but not due to noise at the proximal joint.

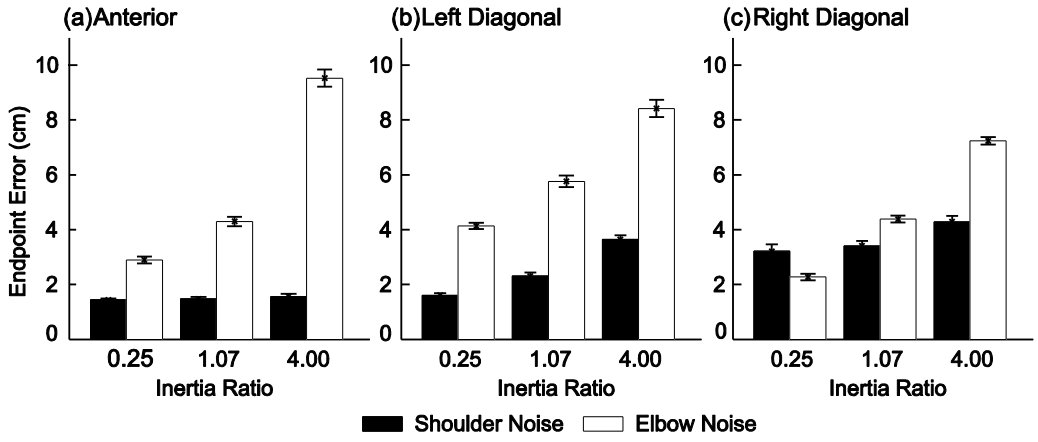

Figure 11: Endpoint errors for reaching movements in the (a) anterior direction, (b) left diagonal direction and (c) right diagonal direction when noise was applied at the elbow and shoulder joint independently. Error bars indicate ± standard deviations.

Similar trends were also observed for movements in the left diagonal (LD) direction (Figure 11b). Noise applied at the distal joint had a significantly larger effect on endpoint error (Err=6.107 cm) than noise applied at the proximal joint (Err=2.52 cm,

$p<0.05$). This was true across all inertia ratios. Similarly, as the inertia ratio increased, endpoint error due to distal noise also increased (from Err=4.13 cm to Err=8.4 cm, $p<0.05$). In contrast to the ANT, proximal noise also generated more endpoint error (from Err=1.6 cm to Err=3.64 cm, $p<0.05$) with increases in inertia ratio.

For movements in the right diagonal (RD) direction (Figure 11c), noise at the distal joint also generated greater endpoint error (Err=4.63 cm) than noise applied at the proximal joint (Err=3.63 cm, $p<0.05$). Similar to the LD direction, higher inertia ratios also yielded greater endpoint error when noise was applied at the distal joint (from Err=2.7 cm to Err=7.2 cm, $p<0.05$) and proximal joint distal (from Err=3.2 cm to Err=4.2 cm, $p<0.05$). The lowest inertia ratio in the RD direction generated the only instance where the proximal noise (Err=3.2 cm) generated more endpoint error than the distal noise (Err=2.27 cm, $p<0.05$).

Net Work:

Similar to endpoint error, there were significant differences in the net work across different reaching directions ($p<0.05$), inertia ratios ($p<0.05$), and noise locations ($p<0.05$) (Figure 12). In general, the average net work in the LD direction (Figure 12b) (TNW=3.94 J) was significantly larger than average net work in the ANT direction (Figure 12a) (TNW=1.83 J, $p<0.05$) and RD direction (Figure 12c) (TNW=1.89 J, $p<0.05$). In addition, the between-trial variances on the energetic cost were significantly smaller than the between-trial variances for endpoint error due to distal and proximal noise. Thus, TNW was less *sensitive* to changes in noise than endpoint errors (Err).

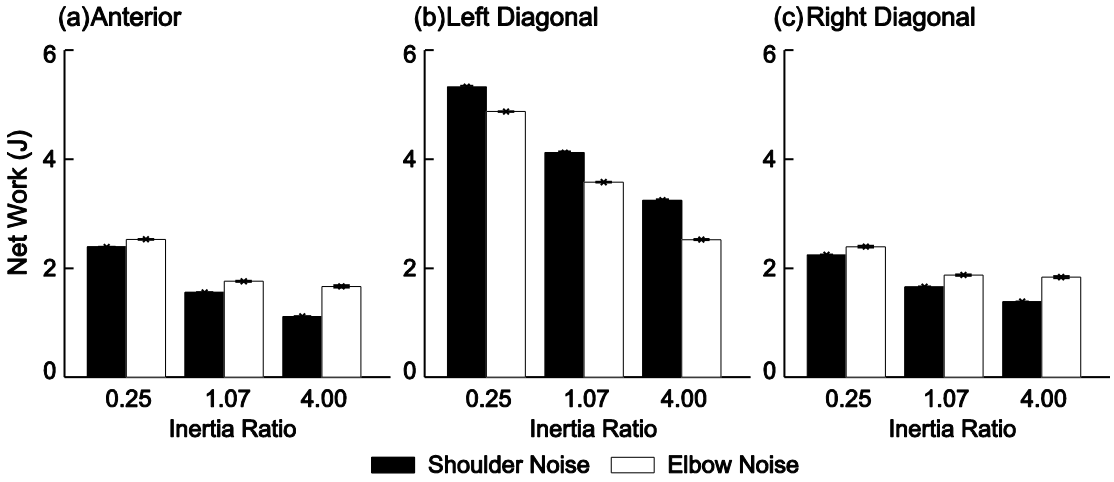

Figure 12: Total net work for reaching movements in the (a) anterior direction, (b) left diagonal, and (c) right diagonal when noise was applied at the elbow and shoulder joint independently. Error bars indicate ± standard deviations.

In the ANT direction (Figure 12a), net work was more affected by distal noise (TNW=1.98 J) than by proximal noise (TNW=1.68 J, $p<0.05$). However, their mean difference was small (Δ=0.293 J). As inertia ratio increased, the effect of distal noise (TNW=2.53 J to TNW=1.67 J, $p<0.05$) and proximal noise (TNW=2.39 J to TNW=1.11 J, $p<0.05$) on net work decreased. This is true across all three directions. However, in the LD direction, the opposite trends were observed (Figure 12b) when applying distal and proximal noise. Noise applied at the *proximal* joint (TNW=4.23 J) generated more energetic cost than noise applied at the *distal* joint (TNW=3.65J, $p<0.05$). The RD direction (Figure 12c) exhibited similar trends to the ANT (Figure 12a). Net work on average was significantly larger when noise was applied at the distal joint (TNW=2.0 J) than when noise was applied at proximal (TNW=1.76 J, $p<0.05$).

Distal Control vs. Proximal Control

Endpoint Error:

When noise was present at both the shoulder and elbow joint simultaneously, there were significant differences in endpoint error across all directions ($p<0.05$), inertia ratios ($p<0.05$), and control locations ($p<0.05$) (Figure 13).

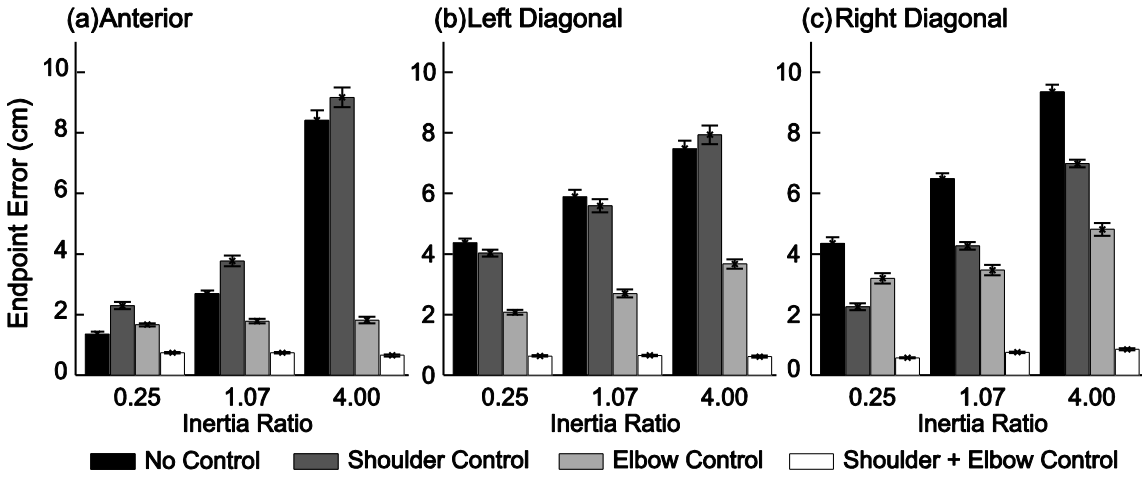

Figure 13: Endpoint errors due to change in control scheme for reaching movements in the (a) anterior direction, (b) left diagonal, and (c) right diagonal when noise was present at both joints. Error bars indicate ± standard deviations.

In the ANT (Figure 13a), applying control at the proximal joint (Err=5.08 cm) generally *increased* endpoint error compared to the no control condition (Err=4.12 cm, $p<0.05$). However applying control at either the distal joint (Err=1.75 cm) or both joints (Err=0.714 cm) significantly *reduced* endpoint error when compared to the no control condition ($p<0.05$). Generally, applying control at both joints simultaneously improved task performance over conditions where only the distal joint was controlled. There were also significantly larger increases in endpoint error for the no control condition (from 1.36 to 8.4 cm, $p<0.05$) and proximal joint control condition (2.29 to 9.17 cm, $p<0.05$) when more mass was shifted to upper arm. Yet, the increases in inertia ratio did not affect the endpoint error generated by elbow control or shoulder+elbow control condition.

This trend was also observed in the LD and RD direction. In the LD direction (Figure 13b), there were significant differences between the no control condition (Err=5.92 cm) and shoulder control condition (Err=5.85 cm) ($p<0.05$) across all inertia ratios. However, the mean difference was small (Δ=0.07 cm). Applying elbow control (Err=2.81 cm) and shoulder+elbow control (Err=0.63 cm) greatly reduced endpoint error when compared to the no control ($p<0.05$) and shoulder control conditions ($p<0.05$). For

movements in the RD direction (Figure 13c), all combinations of joint control significantly reduced endpoint errors from the no control condition (p<0.05). Applying shoulder control reduced endpoint error from Err=6.7 cm to Err=4.5 cm (p<0.05) while applying elbow control reduced endpoint error to Err=3.82 cm (p<0.05). Furthermore, when both joints were controlled simultaneously, endpoint error was reduced to Err=0.73 cm (p<0.05).

Total Net Work:

When noise was present at both the shoulder and elbow joint simultaneously, there were significant differences in net work across all different directions (p<0.05), inertia ratios (p<0.05), and control locations (p<0.05) (Figure 14).

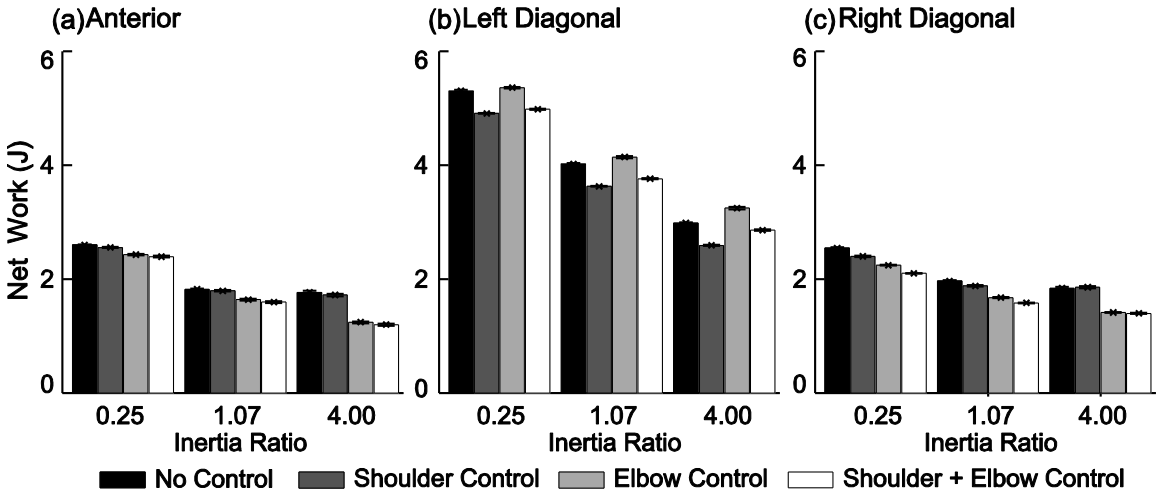

Figure 14: Total net work due to change in control scheme for reaching movements in the (a) anterior direction, (b) left diagonal, and (c) right diagonal when noise was present at both joints. Error bars indicate ± standard deviations.

For movements in the ANT (Figure 14a), applying control at either the shoulder, elbow, or both joints reduced net work compared to the no control condition. While shoulder control was statistically significant when compared to the no control condition, their mean differences were very small (Δ=0.03 J). Applying control at elbow significantly reduced net work (TNW=1.77 J) compared to no control condition

(TNW=2.07 J) (p<0.05). Similarly, applying control at both joints reduced net work to TNW=1.73 J (p<0.05). As inertia ratio increased, there were significant decreases in net work across all control schemes. Net work decreased from TNW=2.60 J to TNW=1.77 J (p<0.05) for the no control condition and from TNW=2.55 J to TNW=1.72 J (p<0.05) for shoulder control condition as inertia ratio increased. Similarly, as inertia ratio increased, net work decreased from TNW=2.43 J to TNW=1.24 J (p<0.05) during elbow control condition and from TNW=2.39 J to TNW=1.2 J (p<0.05) when control was applied at both joints.

For movements in the LD direction (Figure 14b), applying shoulder control (TNW=3.71 J) required significantly less energetic cost than all other conditions (p<0.05). Using only elbow control (TNW=4.25 J) generated the most energetic cost even when compared to the no control condition (TNW=4.1 J) (p<0.05). This trend was different than the anterior or RD directions. When control was applied at both joints, the energetic cost (TNW=3.8 J) was significantly less than applying elbow control (p<0.05), but greater than shoulder control (p<0.05). However, the mean difference was very small (Δ=0.69 J). As inertia ratio increased, there were significant decreases in energetic cost across all control conditions. The no control and shoulder control conditions reduced energetic cost by 2.32 J (p<0.05) as inertia ratio increased. Similarly, as the inertia ratio was increased, net work decreased by 3.2 J (p<0.05) during elbow only control and by 1.11 J (p<0.05) when control was applied at both joints.

Movements in the RD direction (Figure 14c) exhibited similar trends to ANT (Figure 14a). The no control condition generated the greatest energetic cost (TNW=2.11 J) while controlling both joints required the least energetic cost (TNW=1.69 J). While there were statistically significant differences between the shoulder control and no control conditions (p<0.05), the mean value difference was small (Δ=0.07 J). Controlling either the elbow only (TNW=1.78 J) or both joints significantly decreased energetic cost from no control condition (p<0.05). Furthermore, while there were statistically significant differences between these two conditions, the mean difference was again

small (Δ=0.09 J). Similar to ANT movements, as inertia ratio increased net work decreased across all control conditions. During no control condition, energetic cost reduced by 0.7 J (p<0.05) while during shoulder control energetic cost decreased by 0.55 J (p<0.05) as inertia ratio increased. Similarly, as inertia ratio increased, net work decreased by 0.84 J (p<0.05) during elbow control condition and by 0.55 J (p<0.05) when control was applied at both joints.

DISCUSSION

Determining how the nervous system deals with inherent redundancy is one of *the* central questions of motor control research (Todorov and Jordan 2002; Scott 2004; Todorov 2004). Likewise, one of the most fundamental issues the nervous system has to deal with in solving this problem is the ubiquitous noise that is inherent in biological systems (Harris and Wolpert 1998; Faisal, Selen et al. 2008; McDonnell and Ward 2011). Here, we studied a planar reaching task that did not exhibit kinematic redundancy, but *was* redundant in the sense that any controller trying to regulate the movements of that arm has to decide whether to apply more or less effort to reduce the influence of noise emanating from either the proximal (shoulder) joint, or the distal (elbow) joint, or both joints equally. We specifically determined how the biomechanical factors of the arm (inertia ratio) and the task (reaching direction) influenced how different combinations of motor noise and/or control applied at each joint torque in turn affected reaching accuracy and total net work.

In general, for all 3 reaching directions and all 3 inertia ratios (IR) tested, adding noise to the elbow (distal) joint always incurred significantly greater endpoint errors than imposing noise at the shoulder (proximal) joint (Figure 11a-c) with only one exception at the lower inertia for movements in the RD direction (Figure 11c). Conversely, the total net work required to eliminate the effects of this noise was either not different, or slightly greater, when the noise was applied to the shoulder (proximal) joint than to the elbow (distal) joint (Figure 12a-c). These results largely confirmed previous experimental observations (Scholz, Schöner et al. 2000; Konczak, vander Velden et al. 2009). While the movements in the ANT and RD directions showed that shoulder control had slightly lower energetic cost than elbow control, the differences where very small. The small increases in energetic cost were greatly outweighed by the significant decreases in endpoint error. Since the *only* difference between these conditions in our simulations was where this noise was applied, these results confirm that the noise applied at the shoulder was dampened by the larger inertial load of the upper arm plus forearm, whereas the noise applied at the elbow was transmitted mostly unimpeded to the endpoint.

Likewise, when noise was simultaneously imposed at both joints, applying distal control was always more effective than applying proximal control for improving endpoint accuracy (Figure 13a-c) with only one exception at the lower inertia ratio for movements in the RD direction (Figure 13c). However, the magnitudes of these reductions varied for the 3 different movement directions. Additionally, using distal control generally required less total net work than proximal control (Figure 13a, c). However, during LD movements, more net work was required during distal control than proximal control. For LD movements, the task required greater shoulder motion (Figure 8b); therefore it is possible that controlling the elbow would require larger net work. However, the small increase in energetic cost was compensated by the larger reduction in endpoint error (Figure 13b). These results suggest that applying distal control is the most energetically efficient strategy to maximize task performance. Together, these results strongly confirm both of our first two hypotheses, namely that (1) reaching performance in all cases was far more sensitive to distal (elbow) noise than to proximal (shoulder) noise, and that (2) applying only distal (elbow) control was far more effective than applying only proximal (shoulder) control.

The results also showed significant effects of biomechanics on task performance. As the inertia distribution was shifted to the upper arm (IR=4.0), endpoint errors increased. When noise was applied at the distal joint, at smaller IR, the inertia was concentrated at the distal joint, so the forearm provided a natural biological damper to the noise in the system. As the inertia distribution was shifted to the upper arm, the inertia load at the upper arm essentially had no effect on the noise at the distal joint independent of the direction of the task. The inertia effects were also evident in the net work. When the forearm was large (IR=0.25), more *net* work was required to both move and control the mass of the distal segment. As the mass was shifted to the upper arm, less total net work was required. These results were consistent across all reaching directions, noise conditions, and control conditions (Figure 14). These results also explained why less net work was expended for movements in the RD direction than in the LD direction. For RD

movements, which required more elbow extension, the noise and net work depended mainly on the distal joint. For LD movements, where the noise was mainly driven by the shoulder torque, more net work was expended to move and control the arm.

Somewhat counter-intuitively, for most reaching directions and inertia ratios, the total net work required to both move *and* control the system tended to decrease as control was applied at more joints (Figure 14). In general, applying additional control to reduce noise will increase energy expenditure. However, Figure 14 shows that controlling both joints simultaneously can be more efficient overall because it allows the system to exploit the natural mechanical coupling between the two joints. This natural passive mechanical coupling helps cancel the effects of the noise across both joints more rapidly, thus reducing the total net work required to both move and control the system.

Endpoint accuracy was significantly different depending on the direction of the reaching task (Figure 11). When movements relied heavily on elbow extension (RD; Figure 11c); noise at the shoulder joint had far greater effects on endpoint performance when compared to the shoulder intensive (LD; Figure 11b) or balanced (ANT: Figure 11a) directions. Again, when the source of the noise depended on the torque of the distal joint, this had the most significant effect on endpoint error. Therefore, controlling that noise naturally reduced endpoint error with less net work. Similar trends were also exhibited for the net work across all three reaching directions (Figure 12). The net work required in the RD direction was significantly less than in the LD direction. These results emphasize the critical function of distal noise and control during reaching movements. Within each inertia ratio for all noise conditions, there were significant decreases in net work as more inertia was shifted to the upper arm (i.e., IR = 4.0). Generally, a relatively larger forearm required more net work for all conditions, except for movements in the LD direction where the task is more shoulder intensive. Together, these results also confirm our third hypothesis, namely that (3) the effects of noise and control are strongly influenced by biomechanical factors (i.e. reaching direction and/or inertial properties).

Noise is always present in the human neuro-musculo-skeletal system (Harris and Wolpert 1998; Faisal, Selen et al. 2008; McDonnell and Ward 2011). During movement, this noise is selectively suppressed or ignored by the nervous system. Determining how the nervous system compensates for this noise is vital to understanding movement coordination (Scott 2004; Todorov 2004; Dingwell, John et al. 2010). Experimental paradigms lack the ability to unequivocally determine how or if the nervous system uses distal-proximal control strategies to compensate for motor noise and generate desired movements. The present study provides a rigorous computational analysis which clearly demonstrates that biomechanical factors related to both the system configuration (e.g., arm inertial properties) and the task being performed (e.g., reaching directions) play a defining role in determining how the nervous system should most effectively apply control effort across the shoulder and elbow joints so as to maximize system performance, while also limiting expended energy cost. These insights help reveal a more comprehensive picture of why the nervous system chooses to control certain parameters more than others during these types of tasks.

The simplified model used here does not fully represent all of the intrinsic complexities of the biological system at the muscle or neural level, nor does it capture the abundance of redundancy in the motor system. Individual muscles can transmit or absorb power from limb segments not directly connected to those muscles (Zajac 2002). Likewise, agonist and antagonist muscle groups likely play different roles during dynamic and isometric tasks (Stroeve 1998; Schouten, de Vlugt et al. 2001; Gribble, Mullin et al. 2003; Kutch, Kuo et al. 2008; Gerus, Rao et al. 2010). These interactions could significantly affect how the nervous system controls movements. However, implementing a more complicated muscle-driven model would have introduced additional layers of redundancy (i.e., now at the muscle level as well as at the joint level). This would have in turn made it far more difficult to determine precisely which differences we observed might be due to redundancy at the joint level versus the muscle level. Thus, the torque-driven model implemented here did provide an appropriate tool to

examine at the macroscopic level how even the simplest redundancy can significantly affect task performance.

Biomechanically, there are advantages in applying distal control over proximal control. The location of the noise and the inertia distribution of the arm affect the performance of the task as well as the total control effort required to minimize the noise in the system. These results could potentially explain how humans learn or adapt to different tasks based on the sequential control of proximal-to-distal joints (McDonald, Vanemmerik et al. 1989; Furuya and Kinoshita 2007). Humans could potentially initially acclimate to the task using proximal control and then later refine their movements using more effective distal control, similar to the hypothesis posed in Ref. (Dounskaia 2005). Furthermore, humans could exploit the greater sensitivity of the distal joint to noise to generate more accurate movements using minimal energy. Our results demonstrate that the human nervous system potentially takes advantage of these control strategies to minimize the effects of noise within the neuromuscular system during movement.

Our simulations provide a well-grounded theoretical framework from which to interpret previous experimental results (McDonald, Vanemmerik et al. 1989; Dounskaia 2005; Furuya and Kinoshita 2007; Konczak, vander Velden et al. 2009), which suggest that humans appear to prefer to impose greater control over distal joints than over proximal joints, but do not explain *why*. Our results provide the first analytical evidence to concretely determine why this is: because it is both more effective and less costly. Although it has often been hypothesized that human generate arm trajectories that minimize muscle energy, a number of studies have questioned this assumption (e.g., (Goble, Zhang et al. 2007; Kistemaker, Wong et al. 2010)) and there remains much debate about exactly what is being *optimized* during arm movement (Engelbrecht 2001). Here, our model made no explicit attempts to optimize energy expenditure. Instead, we used energy cost merely as an output metric to quantify performance. Our result demonstrated that by applying the appropriate control (i.e., distal vs. proximal) in the

presence of noise could led to lower energy consumption. Thus, our findings support the idea that people adopt control strategies based at least partly on the "Minimum Intervention Principle" (Todorov and Jordan 2002; Todorov 2004; Cusumano and Cesari 2006; John and Cusumano 2007; Dingwell, John et al. 2010). That is, they expend far less effort to minimize fluctuations at the proximal joints because those fluctuations have only minimal effects on final task performance.

Chapter 4: Experimental Setup and Results

One of the goals of this dissertation was to evaluate and validate whether a model of an inter-trial controller could provide insights on the movement to movement dynamics during a reaching task. This model of the controller was developed by Cusumano (John and Cusumano 2008) to study performance during a redundant throwing task. It had also been used to model stride to stride fluctuation during treadmill walking (Dingwell, John et al. 2010) and a virtual shuffle board task (Cusumano and Dingwell 2013). These studies utilized the model of the control in conjunction with experiment data to investigate the movement to movement dynamics that were limited in experimental analysis. In this study, the model of the inter-trial controller was extended to analyze redundant reaching task. Therefore, experimental data were taken from a prior experiment to understand whether subject could learn and perform redundant reaching task.

While experimental results demonstrated that subjects could learn and perform the specified reaching task and exploit the inherent redundancy in the task to improve their performance, the experimental analysis alone could not provide any insights on the different strategies used by different subjects during the performance of the tasks. Here, a brief summary of the experimental protocol and main results from the experiment are presented to understand how the inter-controller could be used to estimate the movement to movement variability during performance of the Task. In the next chapter, the experimental data were compared with the results from an inter-trial controller to analyze the differences in strategy adopted by each subject during the execution of the task. This will provide insights on how each subject resolve the inherent redundancy and noise associated with this reaching task.

This work was entirely done by **Rachel Smallwood** as part of her master thesis. The summary of the work is included to provide context to the modeling results in the

next chapter. The results from the experimental work had been published in the *Journal of Neurophysiology* (Dingwell, Smallwood et al. 2013).

One of the basic questions in motor control is how the nervous system regulates and generates repeatable goal-directed movements in the present of multiple redundancies. The redundancy could come from biological noise and abundant numbers of degrees of freedom that are present in the human motor control system. The abundant numbers of degree of freedoms give rise to equifinality; thus, there are an infinite number of ways to perform the same action (goal equivalent). Not only is there redundancy at the motor control level; there is also redundancy at the task level. The Goal Equivalent Manifold (GEM) approach provides a rigorous mathematical model that hypothesizes how people resolve the task redundancy.

The objective of the experiment was to determine if subjects could learn and exploit the redundancy at the task level for two distinct tasks. These tasks were defined by two task level variables: reaching distance (D) and reaching time (T). At the task-level, any reaching movement can be described by the reaching distance and time. If the objective of the task is to reach at constant speed, there are infinite combinations of reaching distance and time that satisfy the goal of the task. These solutions define the goal manifold of the task. More generally, one can define an entire class of reaching movements defined by the family of goal functions: the goal of the task during reaching can be defined by:

$$G\left(D_k, T_k\right) = D_k^m \cdot T_k^m - c = 0 \;\Rightarrow D_k^m \cdot T_k^m = c \qquad (1)$$

Where n and m are positive integers and c is a positive constant. The goal of the task is to drive the goal function to zero. Given the equation, a concrete mathematical relation is then formulated to investigate the underline strategies people might use to achieve any given specific task.

Experimentally, two specific goal functions $n=-m$ and $n=+m$ (Figure 15) were studied. In both cases, each goal function was defined entirely by the corresponding task

variables, completely independent of how subjects chose to move with respect to the GEM. Task 1 has an intuitive "speed" control profile while Task 2 lacks any direct physical analogue.

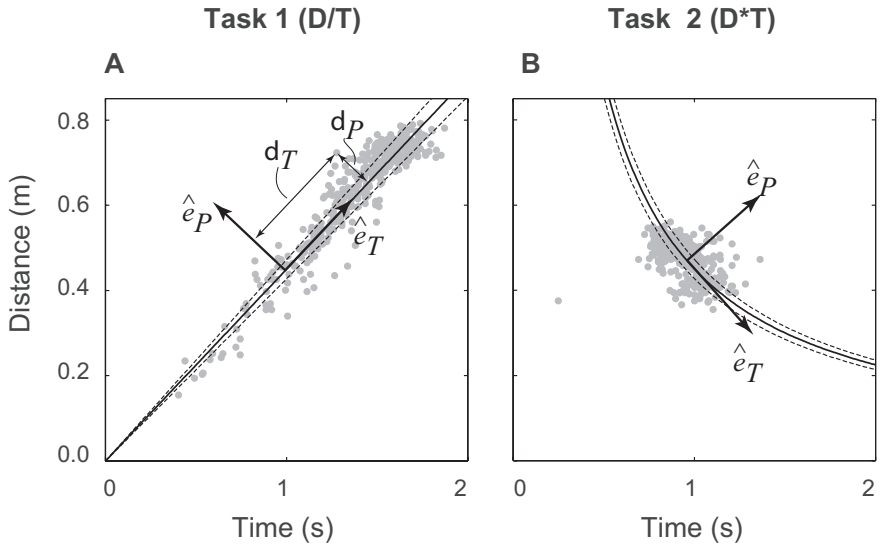

Figure 15: Different goal functions could be constructed by changing the value of m, n, and c. Two goal functions were tested in the experiment: (A) Task 1 (D/T=v) and (B) Task 2 (D·T = v).

EXPERIMENTAL PROTOCOL

Ten young healthy right-handed adults participated in the experiment. Subjects were tested on two pairs of consecutive days. Day 1-2 and days 3-4 were on consecutive, with day 1 and 2 being at least five days apart. On each pair of days, one of 2 different goal functions was used (Figure 15):

$$\begin{aligned} D_k^{+m} \cdot T_k^{-m} &= \left(D_k / T_k\right)^m = \left(0.45\ m/s\right)^m \\ D_k^{+m} \cdot T_k^{+m} &= \left(D_k \cdot T_k\right)^m = \left(0.45\ m \cdot s\right)^m \end{aligned} \tag{2}$$

Subjects sat in a chair attached to the testing device. Subjects rested their arm in the arm support and grasped a handle attached to a slider mounted on a low-friction rail (Figure 16a). Subjects were only instructed to start close to the body and make a smooth, continuous out and back reaching movement. They were instructed to reach as far as

they wanted, at whatever speed they desire. For each reaching movement, the reaching distance and reaching time were recorded.

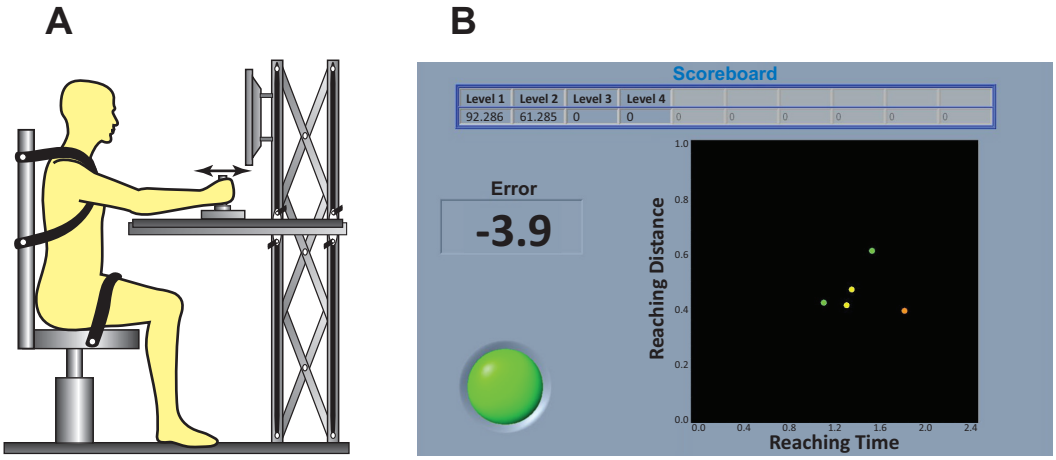

Figure 16: Experimental setup of device. There were four stages of data collection however only the last 400 trials of the testing phase were used to validate the model. (B) Subjects were presented with visual feedback of the last 5 movements. Error feedback and total score were presented to motivate subject to improve performance.

After each reaching movement, subjects received feedbacks in terms of his or her last five reaching movements and a score that indicated how well the subject performed the reaching movement. On the display screen in front of them, the error was displayed and a marker was plotted in the [T, D] plane located at their reaching time and distance and score (Figure 16b). The size and color of the marker indicated the magnitude of their error. The GEM was never directly shown to the subject and subjects were only told that different combinations of reaching distance and time could achieve the goal. Subjects were told that a low error would yield a high score; therefore their goal was to achieve the highest score possible.

Net reaching distances (D) and times (T) were recorded. Subjects made a total of 900 movements for each task; however only the last 400 movements from the second day were used to investigate the movement-to-movement dynamics. This assumed that learning and exploration were achieved during the first 500 reaching movements.

Subjects performed 2 trials of these 400 reaching movements for both tasks on two consecutive days.

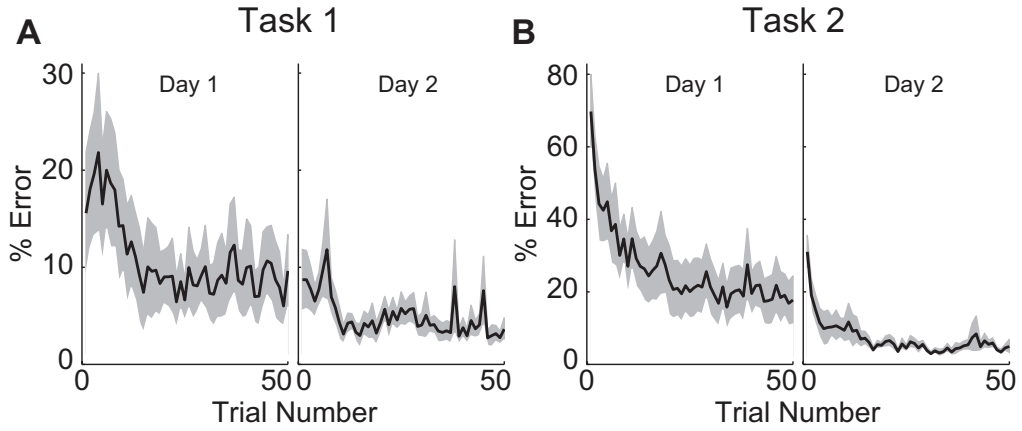

Figure 17: For both tasks, the error significantly decreased after the first 50 reaching movements. This indicated that subjects were able to learn and perform the task well even without explicit instruction on the exact nature of the task.

One of the concerns during the experimental design was whether subjects could learn such a novel task without any specific information about the nature of the task. Subjects were only provided minimal feedback to perform the task; and were only instructed to try and minimize their error and achieve best possible score by manipulating their reaching distance and reaching time. The reduction in the error indicated that after sufficient practice trials subjects were able to learn and performed the task well under minimal feedback. Furthermore, it also showed that subject quickly minimized their error within the first 50 reaching movements (Figure 17). It was critical to the modeling of the inter-trial controller that subjects could learn and perform the task; otherwise the correlations to the experimental data and model would be meaningless and irrelevant.

Several analyses were performed to quantify the final task performance and determine if and to what extent subjects exploited the redundancy inherent in each task. Analyses were performed in two coordinate systems: The [T, D] plane and the [δ_T, δ_P] plane. The analyses in the [T, D] plane investigated how the distance and time changes from movement to satisfy the goal. Reaching distance and reaching time worked

harmoniously to find the solution near or on the goal manifold. However, the fluctuation in the $[\delta_T, \delta_P]$ direction was deemed more pertinent to control and exploitation of redundancy during the execution of the task. Fluctuations along the goal manifold (δ_T) would not directly affect the goal of the task, but fluctuations in the perpendicular direction (δ_P) to the goal manifold would affect the goal of the task.

The $[\delta_T, \delta_P]$ coordinate system lied along and perpendicular to the goal manifold (Figure 15). For both tasks, the coordinate system was moved to the preferred operating point (POP) of each subject. The POP $[T^*, D^*]$ was defined as the average reaching distance and reaching time of each subject over the entire trial. Thus the new coordinate system centered at this operating point, $T_k^{'} = T_k - T^*$ and $D_k^{'} = D_k - D^*$, where k is the index for the reaching movement. The fluctuations tangential and perpendicular to the goal manifold were calculated by the equations described below for Task 1 and Task 2. The magnitude of c $(\|0.45\|)$ was the same for both tasks. The value of c was chosen from the experimentally piloted data.

For Task 1

$$\begin{bmatrix} \delta_T \\ \delta_P \end{bmatrix} = \frac{1}{\sqrt{1+c^2}} \begin{bmatrix} 1 & c \\ -c & 1 \end{bmatrix} \begin{bmatrix} T_k^{'} \\ D_k^{'} \end{bmatrix} \tag{3}$$

Similarly for Task 2

$$\begin{bmatrix} \delta_T \\ \delta_P \end{bmatrix} = \frac{1}{\sqrt{1+\left(D^*/T^*\right)^2}} \begin{bmatrix} 1 & -D^*/T^* \\ D^*/T^* & 1 \end{bmatrix} \begin{bmatrix} T_k^{'} \\ D_k^{'} \end{bmatrix} \tag{4}$$

The details of the derivation of these equations can be found in the published article in the journal of Neurophysiology (Dingwell, Smallwood et al. 2013); however, the details are omitted here.

The mean and standard deviation of the variables in these two coordinate systems were calculated. The times series of each variable $(T, D, \delta_T, \delta_P)$ was used to analyze the

movement to movement fluctuation (Figure 18) for both tasks. The movement to movement variability was measured using a linear model estimation of the correlation from one movement to the next.

$$X_{k+1} = \lambda X_k + \xi \tag{5}$$

Where X indicated any of the relevant time series and ξ is the noise term. For the experimental and modeling analysis $X = \{T, D, \delta_T, \delta_P\}$. This linear estimation is based on the inherent noise from movement to movement in biological system (van Beers, Haggard et al. 2004; Faisal, Selen et al. 2008). The movement variability could be attributed the noise in the neuro-control system (van Beers, Haggard et al. 2004). While the human can perform the task repeatedly with high accuracy, there is also persistence of variability from one movement to the next.

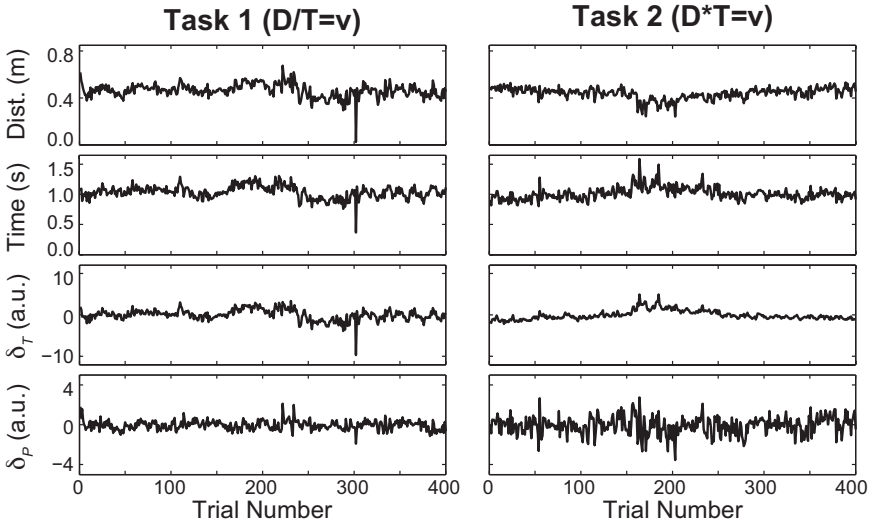

Figure 18: Typical time series of the reaching distance, reaching time, δ_T, and δ_P for Task 1 and Task 2. The time series was used to calculate the λ's that correlates the movement to movement variation.

λ quantifies the strength of the relative correlation between consecutive movements. If λ = 0, the movement to movement variability is white noise. In such case, the next movement is not driven or affected by the previous movement. When λ > 0, it indicates statistical persistence: increases (or decreases) in the value of X are more

likely to be followed by further increases (or decreases) in X (i.e. subjects are less responsive to correct for deviation and tend to drift before correction). In contrast, when $\lambda < 0$, it indicates anti-persistence: increases (or decreases) in X are more likely to be followed by subsequently decrease (or increases) in X. In this case subjects immediately correct for the deviation away from X.

The dependent measures of interest in this experiment were the mean and variance of: D, T, δ_T and δ_P. In addition, the one step auto correlation of both the original time series and λ_D and λ_T and GEM variable λ_{δ_P} and λ_{δ_P} were calculated to analyze the movement to movement dynamics.

SUMMARY OF THE RESULTS

For both tasks, subjects exhibited greater variability along each GEM than perpendicular to it Figure 19a). Relative to the Task 1, the standard deviation in the δ_P direction was significantly smaller than the standard deviation in the δ_T direction ($p<0.0005$). Relative to the goal manifold for Task 2, the standard deviation of δ_P was still significantly smaller than δ_T. λ for the distance and time variables were all above zero, indicating statistical persistence (Figure 19b).

Additionally, subjects actively corrected for deviations perpendiculars to the GEM faster than deviation along the GEM (Figure 19c). On average, subjects exploited the redundancy in Task 2 to the same degree as the redundancy in Task 1, despite exhibiting greater variance ratios for Task 2.

As a group, subjects were more variable in the direction along the GEM and less variable in the direction perpendicular to the GEM. While the data for both days are presented here, only the data from the Day 2 were used to evaluate the model. From the results, there were not significantly differences between Day 1 and Day 2.

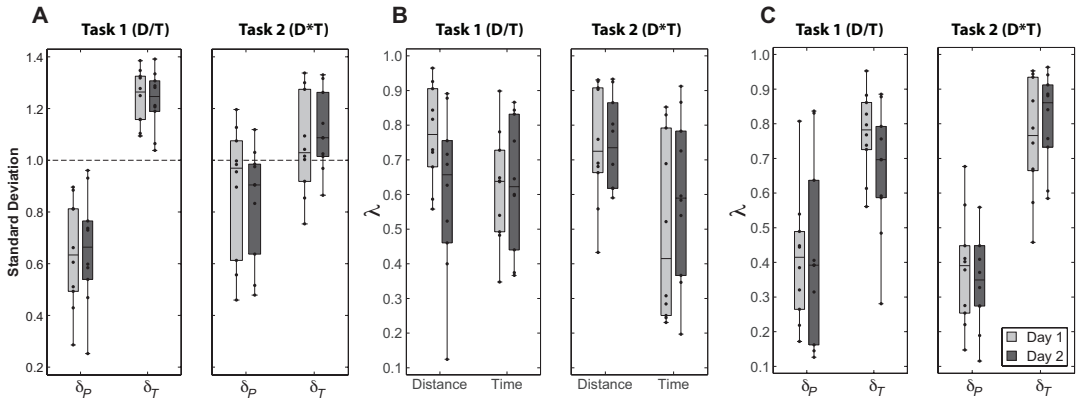

Figure 19: Summary of the results from the experiment. (A) shows the standard deviation along the tangential perpendicular direction with respect to the GEM (B) shows the one-step linear correlation in the reaching distance and reaching time, while (C) shows the movement to movement correlation in the tangential and perpendicular direction on the GEM.

IMPACT OF EXPERIMENTAL DATA ON MODELING

While the general trends were significant across all subjects, there were also clearly many differences between subjects. This suggested that maybe not all subjects adopted the same control strategy, or were not successful in performing the task. The experimental analysis lacks the tool to analyze the different strategies between each subject as they performed the task. Furthermore, relying on a singular metric such as variance to indicate control sometime could lead to false positive. Studies have shown that sometimes the structure variances were irrelevant to the control mechanism during the execution of the task (Valero-Cuevas, Venkadesan et al. 2009; Dingwell, John et al. 2010) Therefore, an inter-trial controller was used to estimate the movement to movement dynamics exhibited by *each* subject during the performance of the task.

From the structure of the controller, it is possible to hypothesize the how each individual performed the task; therefore, it is possible to identify the strategy differences between subjects. The model could potential reveal whether subjects were performing the task well or not at all. Based on the experimental analysis, subject could be satisfying the objective of the task while completely ignoring the GEM. Analyzing the variance and the λ's from the experimental analysis in conjunction with the structure of the inter-

trial controller provided more details on what the subjects were actually controlling during the performance of the task. However, before the inter-trial model could be use to extrapolate control; it must be evaluated and validated using the experimental data. Once the inter-trial controller is validated, it could be used to analyze the movement-to-movement dynamics in these reaching tasks.

Chapter 5: Modeling Trial-to-Trial Control Strategies Used by Subjects During Redundant Reaching

INTRODUCTION

Humans can perform highly redundant tasks with high accuracy and repeatability; yet the control mechanisms that drive these behaviors are still unknown. Experimental (Scholz, Schoner et al. 2000; Scholz, Kang et al. 2003; Sternad, Abe et al. 2011; Chu, Sternad et al. 2013) and mathematical approaches (Todorov 2004; Guigon, Baraduc et al. 2008) have strived toward capturing the processes by which the nervous system retrieves sensory information, compensates for biological uncertainty, and drives motor neurons to execute the desired movements. Using optimality, motor coordination is viewed as finding the best possible path for a given task (Bizzi, Accornero et al. 1984; Flash and Hogan 1985; Uno, Kawato et al. 1989; Harris and Wolpert 1998). These principles change how the nervous system solves redundant tasks and compensates for uncertainties (internal and external) that arise during the execution of the task.

Studies have shown that during redundant tasks (Todorov and Jordan 2002), there is less variability in the direction that is relevant to the task goal from trial-to-trial. This phenomenon translates to strongly controlling in the direction that is relevant to the task. More specifically, the nervous system imposes the greatest control when the internal or external perturbation affects the goal and less control when the perturbations do not affect the task goals. These observations lead to the emergence of stochastic optimal control as principle for explaining variability during motor coordination for redundant task. This principle provides an analytical framework to resolve the redundancy and stochastic noise. *Minimum Intervention Principle (MIP)*, an intrinsic property of stochastic optimal control, states that the controller only corrects for perturbations when they directly affect

the performance of the goal. The controller does not correct for perturbations that are irrelevant to task performance. This selective control mechanism significantly reduces control effort, thus minimizing over-correction during the task. However, stochastic optimal control does not completely account for the movement to movement dynamics. Therefore, within the framework of stochastic optimal control, the *Goal Equivalent Manifold (GEM)* approach provides a mechanism to understand and analyze the trial to trial fluctuations.

While many theories have been proposed (Uno, Kawato et al. 1989; Scholz and Schoner 1999; Muller, Frank et al. 2007) to explain how coordination is organized during these redundant tasks; it is still unclear what underlying mechanisms drive the selection of a particular distance and time during a reaching task. Is the nervous system designed to minimize motor noise (Harris and Wolpert 1998), energy expenditure(Alexander 1997), or the variance in the system to select the optimal solution while resolving the redundancy in the task? To address these questions, the GEM approach utilizes both the model of the task (goal functions) and a model of the controller to explore different control variables that are responsible for the organization and execution of the task. It provides a tool to understand how humans coordinate movement during redundant tasks and elucidate different strategies adopted by people to resolve the redundancy. This approach provides a rigorous analytical and mathematical framework for reconciling issues of optimality, redundancy, and stochasticity (noise) in human control.

The Goal Equivalent Manifold (GEM) approach was first introduced by Cusumano et. al (Cusumano and Cesari 2006) for a redundant aiming task using an air pistol with and without laser feedback. In this task, subjects were asked to aim an air pistol with and without laser at a target 10 m way by standing facing the target and 90 degree off set from the target (i.e. standing sideway with respect to the target). 30 markers were used to define the aiming position (body state variables), however, the target was calculated from two markers at the end of the gun barrel. Therefore, the dimension of the body variables (28) was larger than the dimension of the goal (2). Thus

there were 28 dimensional mapping where the changes in the body variables had no affect on the goal variables. By varying posture and perceptual cue (laser), they showed that while one could achieve similar performance for two distinct postures and perceptual conditions, the decomposition of goal level variability showed that standing sideway with laser on had best performance (lowest) variability and moderately good goal-relevant sensitivity. This result established the relationship between the body variables and the goal variables. The mapping of these variables arises naturally from the definition of the goal function. Therefore, for any task that could be represented by a goal function; you can characterize its performance by examining the goal equivalent manifold and sensitivity relationship between the goal and body variables. This approach captures the dynamics of how the variability of the body variables changes with the goal of the task and provides insight into how people control their movements along the manifold to satisfy the task goal.

The goal function for any given task can be generalized as

$$\mathbf{f}(\mathbf{x};\mathbf{p}) = 0 \tag{1}$$

Where is **f** a vector-valued goal function of dimension D_g and x is the body-level state vector of dimension D_b which defines the task execution; therefore, the goal function can be satisfied by any combinations of the body-level variables (**x**). For a redundant system the dimension of D_b is greater than the dimension of D_g $(D_b > D_g)$. In this study, the GEM approach was used to explain how movements were coordinated during reaching, more specifically, what variables in the system were actively controlled during the execution of the task. These goal-directed reaching movements were derived from the mathematical functions that define the goal of the task.

A trial-to-trial planar reaching task is fully defined by the reaching distance (D) and reaching time (T). A family of goal functions can be generated by varying the relationship between D and T (Cusumano and Cesari 2006; Dingwell, Smallwood et al. 2013). The goal function for a planar reaching task can be defined as

$$G\left(D_k, T_k\right) = D_k^m \cdot T_k^m - c = 0 \;\Rightarrow D_k^m \cdot T_k^m = c \tag{2}$$

Where m and n are positive integers, and c is a positive constant. Any combination of $\left(D_k, T_k\right)$ will satisfy the task and drives the goal function to zero. The perfect execution of the task is when the combination of $\left(D_k, T_k\right)$ lies on the goal manifold. Different reaching tasks can be generated by changing the parameter values of m, n, and c. Changing the value of m and n changes the location and shape of the GEM while c specified the goal of the task.

METHOD

While the experimental results (Chapter 4) provided insight on how subjects in general performed in redundant reaching task; it lacked the tool to analyze how each individual subject adopted different strategies to resolve the same redundancy in the task. In this study, a stochastic model of the control was used to hypothesize one way subject could strategize their movement to achieve the task. From the totality of the structure of the controller, it is possible to hypothesize the type of strategy subjects could adopted to resolve this redundancy. The inter-trial controller was evaluated and validated by comparing the output from the model with the experimental data where subjects where asked to perform two redundant reaching tasks (see Chapter 4 for details).

In general the goal of the planar reaching task can be defined as

$$f\left(D_k, T_k\right) = D_k^m \cdot T_k^n = c \tag{3}$$

By varying the different values of m, n and c we can generate infinitely unique goal manifolds. For the tasks investigated in the study, $m = n = \pm 1$ and $c = c^m = 0.45$. Therefore, the equations of the two specific reaching tasks examined were given by

$$\begin{aligned} D_k^{+m} \cdot T_k^{-m} &= \left(D_k / T_k\right)^m = \left(0.45\ m/s\right)^m \\ D_k^{+m} \cdot T_k^{+m} &= \left(D_k \cdot T_k\right)^m = \left(0.45\ m \cdot s\right)^m \end{aligned} \tag{4}$$

The aim of the inter-trial controller was to model and capture the possible strategic differences between individual subjects when performing the task. The goal was to see if the inter-trial controller could generate and estimate the kinematics and dynamics characteristics of the experimental data. The experimental data showed that there was a clear difference between Task 1 and Task 2 (see Chapter 4). However, simply replicating the experimental results would not provide sufficient insight on the strategic differences between subjects during the performance of the task. In this study, a systematic analytical approach was adopted to estimate the dynamics of the experiment

and a stochastic optimal controller was deployed to find to the best structure of the inter-trial controller that could explain the strategies adopted by each subject during the task.

The inter-trial controller is not intended to characterize how reaching movement are generated, theories on how the within-trial reaching movements are regulated are rich and vary (Flash 1987; Uno, Kawato et al. 1989; Dornay, Kawato et al. 1996; Alexander 1997; Karniel and Inbar 1997; Harris and Wolpert 1998; Nishii and Taniai 2009). While the within-trial model is important and would help explain how movements are generated, it is not important to this study. In this study, only the outcome [T_k, D_k] of the reaching movement were considered and modeled. Thus this controller allows us to investigate and analyze the how movement outcomes vary across movements regardless of which within-trial model generates the reaching movements. Therefore, the inter-trial controller has the potential to impact experimental studies and complex computation models of reaching.

Stochastic Optimal Controller

The discrete inter-trial controller employed to model the movement to movement for a reaching task is fundamentally expressed as (John and Cusumano 2008)

$$\mathbf{x}_{k+1} = \mathbf{x}_k + \mathbf{G}\left[\mathbf{I} + \mathbf{N}\right]\mathbf{u}\left(\mathbf{x}_k\right) + \eta \tag{5}$$

Where $\mathbf{x}_{k+1} = \left[T_{k+1}, D_{k+1}\right]^T$ is a 2x1 matrix denoting the next state and $\mathbf{x}_k$ denotes the current state of the body variable. $\mathbf{I}$ is identity matrix. $\mathbf{G}$ is the gain matrix, $\mathbf{N}$ is the multiplicative noise, $\mathbf{u}$ is the controller inputs (efforts), and η is the additive noise. The structure of Eq. 5 provides a reasonable representation of the behavior exhibited in repeated reaching task. For example, in the absence of noise $\left(N = 0;\ \eta = 0\right)$, the performance of the subject will be constant, i.e. $\mathbf{x}_{k+1} \approx \mathbf{x}_k$. Furthermore, in the absence of any control, $\mathbf{u} = 0$, the system would yield Brownian motion due to the fluctuation in the Gaussian white noise $\left(\eta\right)$, thus the next state is defined by $\mathbf{x}_{k+1}\mathbf{x}_k + \eta$. The controller provides a reasonable balance between performing perfect repetition of the

task and random oscillation behavior about the state space. This inter-trial controller was used to predict the dynamic variability from movement-to-movement for the specified goal-directed reaching task.

The multiplicative noise and additive noise were defined as

$$\mathbf{N} = \begin{bmatrix} \sigma_1 v_1 & 0 \\ 0 & \sigma_2 v_2 \end{bmatrix}, \quad \eta = \begin{bmatrix} \sigma_3 v_3 \\ \sigma_4 v_4 \end{bmatrix} \tag{6}$$

Where $v_k \left(k \in \{1,2,3,4\} \right)$ are independent random variables with zero mean and unit variance and σ_k are the standard deviations of each noise term. Combining Equ 6 and Eq. 3, the inter-trail controller can be expanded to represent the movement to movement fluctuations of the reaching task $\mathbf{x}_k = \left[T_k, D_k \right]$ as the state variable.

$$\begin{bmatrix} T_{k+1} \\ D_{k+1} \end{bmatrix} = \begin{bmatrix} T_k \\ D_k \end{bmatrix} + \begin{bmatrix} g_1 & 0 \\ 0 & g_2 \end{bmatrix} \begin{bmatrix} 1+\sigma_1 v_1 & 0 \\ 0 & 1+\sigma_2 v_2 \end{bmatrix} \begin{bmatrix} u_1(\mathbf{x}_k) \\ u_2(\mathbf{x}_k) \end{bmatrix} + \begin{bmatrix} \sigma_3 v_3 \\ \sigma_4 v_4 \end{bmatrix} \tag{7}$$

The above state update equation with the control inputs was designed to model the inter-trial dynamics during reaching, and not the dynamic *within* each reaching movement. The control effort, $\mathbf{u}(x_k)$, was determined by solving a classic quadratic optimal control problem in which $\mathbf{u}(x_k)$ was chosen to be optimal with respected to the expected value of the cost function with the form:

$$C = \alpha e^2 + \beta p^2 + \gamma u_1^2 + \delta u_2^2 \tag{8}$$

This controller is not designed to account for all neural processes employed by the nervous system during a repetitive reaching task; however, it highlights some important characteristics to the performance of repetitive task.

The trial-to-trial controller emphasizes the cost of performance on four key components. The first term, αe^2, penalizes the deviation about the specified goal manifold. *e* defines the error of each reaching distance and time from the GEM. A large α indicates that subjects are doing more correction to get back or stay on the goal manifold; conversely a small α indicates that subjects are weakly correcting for deviation

perpendicular to the GEM. The second term, βp^2, penalizes the deviation about a preferred operating point (POP). The POP is defined as

$$p^2 = \left(T_k - T^*\right)^2 + \left(D_k - D^*\right)^2 \tag{9}$$

Where $[T^*, D^*]$ denotes the POP. T^* was calculated by taking the average of reaching time of the whole trial (400 movements) and D^* was correlated by the goal function for each task. Based on previous modeling work, in the absence of β, the controller failed at containing the distribution of the experimental data because the solution could be infinitely spread along the manifold (Dingwell, John et al. 2010). Preliminary results also showed that without β, the controller only needed to satisfy the GEM error (e); therefore, it did not have any knowledge or limitation of the work space. Furthermore, in these repetitive reaching tasks, it is feasible for subject to find a preferred region and stay near that combination of reaching distance (D) and reaching time (T) without further incentive to explore other feasible locations along the GEM. Therefore, the β term is necessary to constraint the controller to a physical workspace of the subject, but also provides contrasting strategy adopted by subjects during the task. A large β coupled with a small α might indicate that subjects preferred to operate at a specific operating point without exploiting the redundancy in the task. Therefore the combination α and β can provide some indication of the movement to movement strategy adopted by subjects.

γ and δ represent the effort exerted by the controller. The cost function thus balances control effort versus the need to correct for deviation about the goal of the task.

Task 1

The goal manifold for Task 1 was mathematically defined as

$$e = \frac{D_k}{T_k} = c = v \Rightarrow e = D_k - vT_k = 0 \tag{10}$$

c was redefined as v to indicate that the goal of the task was to reach at a constant speed v. The derivation of the controller for Task 1 is given below as an example of how the optimal control efforts were solved. (for more detail see (Dingwell, John et al. 2010).

By substituting the expression for e and p as defined by Eq. 9 and 10 respectively. Furthermore, incorporating the equation for the next reaching distance and reaching time as defined by Eq. 5, where

$$C = \alpha\left(D_{k+1} - vT_{k+1}\right)^2 + \beta\left[\left(T_{k+1} - T^*\right)^2 + \left(D_{k+1} - D^*\right)^2\right] + \gamma u_1^2 + \delta u_2^2 \tag{11}$$

Giving that the state-update equation was

$$\begin{aligned} T_{k+1} &= T_k + g_1\left(1 + \sigma_1 v_1\right)u_1\left(x_k\right) + \sigma_3 v_3 \\ D_{k+1} &= D_k + g_2\left(1 + \sigma_2 v_2\right)u_2\left(x_k\right) + \sigma_4 v_4 \end{aligned} \tag{12}$$

The cost function was expanded as

$$\begin{aligned} &C = \alpha\left(D_k + g_2\left(1 + \sigma_2 v_2\right)u_2 + \sigma_4 v_4 - v\left(T_k + g_1\left(1 + \sigma_1 v_1\right)u_1\left(x_k\right) + \sigma_3 v_3\right)\right)^2 + \\ &\beta\left[\left(T_k + g_1\left(1 + \sigma_1 v_1\right)u_1\left(x_k\right) + \sigma_3 v_3 - T^*\right)^2 + \left(D_k + g_2\left(1 + \sigma_2 v_2\right)u_2 + \sigma_4 v_4 - D^*\right)^2\right] + \gamma u_1^2 + \delta u_2^2 \end{aligned} \tag{13}$$

Next, Eq. 13 was expanded and simplified by taking its expected value $\bar{C} = E[C]$ using the fact that the noise processes have zero mean, unit variance and are uncorrelated. Therefore, the expected values of the variance were derived by setting $E\left[v_k^2\right] = 1$ and $E\left[v_k\right] = 0$ for $k \in \{1, 2, 3, 4\}$ and $E\left[v_k v_m\right] = 0$ for $k \neq m$. Thus the expected value of C was

$$\begin{aligned} &\bar{C} = 2u_1\left(\alpha T_k v^2 - \alpha D_k v - \beta T^* + \beta T_k\right) + u_1^2\left[\left(\sigma_1^2 + 1\right)\alpha v^2 + \left(\sigma_1^2 + 1\right)\beta + \gamma\right] + \left(\alpha T_k^2 + \sigma_3^2\alpha\right)v^2 - \\ &2u_2\left[\alpha T_k v + \beta D^* + \left(-\alpha - \beta\right)D_k\right] - 2\alpha D_k T_k v - 2u_1 u_2 \alpha v + \beta T^{*2} - 2\beta T_k T^* + \beta D^{*2} - 2\beta D_k D^* + \\ &\beta T_k^2 + \left(\alpha + \beta\right)D_k^2 + u_2^2\left[\delta + \left(\sigma_2^2 + 1\right)\alpha + \left(\sigma_2^2 + 1\right)\beta\right] + \sigma_4^2\alpha + \left(\sigma_4^2 + \sigma_3^2\right)\beta \end{aligned} \tag{14}$$

Similar to the inter-trial controller developed for throwing task (John and Cusumano 2008) and treadmill walking (Dingwell, John et al. 2010) the controller was

required to be unbiased means that on average the expected value of the goal function (F) was zero (Eq. 15)

$$\bar{F} \equiv E\left[D_{k+1} - vT_{k+1}\right] = 0 \tag{15}$$

Substituting for $\left[T_{k+1}, D_{k+1}\right]$ in F and taking the expected value of F

$$-\left(u_1 - T_k\right)v + u_2 + D_k \tag{16}$$

To solve for the optimal controller effort, $\boldsymbol{u}$, the control gains were initially set to unity (i.e. $g_1 = g_2 = 1$) and solved for the augmented Lagrangian, Λ, where

$$\Lambda = \bar{C} - \mu\bar{F} \tag{17}$$

Where μ is the Lagrangian multiplier and $\bar{F}$ is the requirement that the unbiased single-step controller, on average, is *expected* to be perfect on the next movement. Thus the minimum of $\bar{C}$ occurs when the reaching movement is on the GEM (e = 0). However, in the presence of the noise terms, the state variable will not converge onto the GEM.

The optimal control efforts were solve by differentiate the augmented Lagrangian equation with respect to the expected value of C' and F'.

$$\frac{\partial\bar{C}}{\partial u_i} - \mu\frac{\bar{F}}{\partial u_i} = 0, \quad i = 1,2 \tag{18}$$

From the differentiation, we obtained a system of equations (Eq. 19 & 20) as a function of the control effort **u**. These equations correlate the control inputs to the parameters of the cost function ($\alpha, \beta, \gamma, \delta$) and the multiplicative noise (σ_1 and σ_2) as well as the state space variable, $\left(T_k, D_k\right)$. Notice that the additive noise terms (σ_3, σ_4) were zeroed out due to the assumption about the nature of the noise (i.e. unit variance, zero mean).

$$2\left[\left(\sigma_1^2+1\right)\alpha v^2+\left(\sigma_1^2+1\right)\beta+\gamma\right]u_1+2\alpha T_k v^2+\left(\mu-2\alpha D_k\right)v-2u_2\alpha v-2\beta T^*+2\beta T_k=0 \tag{19}$$

$$-2\alpha T_k v-2u_1\alpha v-2\beta D^*+\left(2\alpha+2\beta\right)D_k-\mu+2\left[\left(\sigma_2^2+1\right)\alpha+\left(\sigma_2^2+1\right)\beta+\delta\right]u_2=0 \tag{20}$$

Solving for the optimal control inputs, we derived the equation for the control input u_1 and u_2.

$$u_1=\frac{-T_k\left[\delta+\sigma_2^2\alpha+\left(\sigma_2^2+1\right)\beta v^2+\beta\right]+\left[\beta D^*+\left(\delta+\sigma_2^2\alpha+\sigma_2^2\beta\right)D_k\right]v+\beta T_p}{\left[\delta+\left(\sigma_2^2+\sigma_1^2\right)\alpha+\left(\sigma_2^2+1\right)\beta\right]v^2+\left(\sigma_1^2+1\right)\beta+\gamma} \tag{21}$$

$$u_2=\frac{T_k v\left(\sigma_1^2\alpha v^2+\sigma_1^2\beta+\gamma\right)+\left[\beta D^*-\left(\sigma_1^2\alpha+\beta\right)D_k\right]v^2+\beta T^* v+\left[-\left(\sigma_1^2+1\right)\beta-\gamma\right]D_k}{\left[\delta+\left(\sigma_2^2+\sigma_1^2\right)\alpha+\left(\sigma_2^2+1\right)\beta\right]v^2+\left(\sigma_1^2+1\right)\beta+\gamma} \tag{22}$$

Based on the derivation, there could be up to active eight parameters (including g_1 and g_2) in the controller. Preliminary attempts to understand the trial-to-trial dynamics by using all either parameters results in confounded results due to the under constraint nature of the system and the flatness in the solution space. There were redundant solutions manifolds that made it possible to understand the meaning of the control parameters. Therefore a more systematic approach was adopted and a few assumptions were made to derive a functional version of the control inputs.

From the derivation of the control inputs, it could be written as a linear combination of the current reaching distance and reaching time $\mathbf{u}=\mathbf{A}\mathbf{x}+\mathrm{B}$, where $\mathbf{u}=\left[u_1,u_2\right]^T$, $\mathbf{x}=\left[D_k,T_k\right]^T$ and $\mathbf{B}^{2\mathrm{x}1}$ is the noise vector. Therefore, it might be possible to use linear regression analysis to estimate the dynamic of the controller by fitting the experimental data to the **A** matrix and **B** vector.

Setting the multiplicative noise to zero reduced the number of parameters, $N=0$. The multiplicative noise represents the motor noise. To estimate the nature of the multiplicative noise would require the modeling the motor dynamics that drive the arm within the reaching movement. In this repetitive reach task, the movement to movement noise was assume to be minimal since subjects were expected to perform this task at a steady state. The additive noise represents the effect of the perceptual, motor, and

environmental (i.e. feedback) sources were estimated from the experiment. Rather than modeling the additive noise, it was more important to understand how the reaching strategies were organized under the presence of additive noise. The main focus was to understand how or if people exploited the redundancy inherent in the task. The estimations of these noise terms from the experimental data do not affect the fundamental structure of the controller to answer this question.

However, it was problematic to assume that multiplicative noise was zero since it nullified important parameters of the controller, α (Eq. 23 and 24). Therefore a modification from the previous approach was made to retain the α parameters.

$$u_1 = \frac{-T_k\left[\delta + \beta v^2 + \beta\right] + \left[\beta D^* + \delta D_k\right]v + \beta T_p}{\left[\delta + + \beta\right]v^2 + \left(\sigma_1^2 + 1\right)\beta + \gamma} \tag{23}$$

$$u_2 = \frac{T_k v\gamma + \left[\beta D^* - \beta D_k\right]v^2 + \beta T^* v + \left[-\beta - \gamma\right]D_k}{\left[\delta + \beta\right]v^2 + \beta + \gamma} \tag{24}$$

This was accomplished by removing the unbiased requirement in the single step controller from the previous method. This means that on average the movement is not expected to be perfect and that the preferred operating is not required to be on the GEM but is expected to be close to the GEM.

Furthermore, to track the subject fluctuation from movement-to-movement about their preferred operating point, the fluctuations were transformed to the preferred operating point by defining

$$\begin{aligned} T_k^{'} &= T_k - T^* \\ D_k' &= D_k - D^* \end{aligned} \tag{25}$$

Where $\left(T^{'}, D^{'}\right)$ was the new coordinate system and $\left(T^*, D^*\right)$ was the preferred operating point of each subject. Therefore the new control inputs were found by assuming the multiplicative is zero, removing the unbiased control requirement and supposing the POP is close to the GEM. Following the same procedure as outlined above and transformation

to the new coordinate system, the control inputs were expressed a linear combination of the current teaching distance and reaching time (Eq. 26 & 27).

$$u_1 = -\frac{\left[(\alpha\delta+\beta\alpha)v^2+\beta\delta+\beta\alpha+\beta^2\right]}{(\alpha\delta+\beta\alpha)v^2+(\beta+\gamma)\delta+(\beta+\gamma)\alpha+\beta^2+\gamma\beta}T_k^{'}+\frac{\alpha\delta v}{(\alpha\delta+\beta\alpha)v^2+(\beta+\gamma)\delta+(\beta+\gamma)\alpha+\beta^2+\gamma\beta}D_k^{'} \tag{26}$$

$$u_2 = \frac{\gamma\alpha v}{(\alpha\delta+\beta\alpha)v^2+(\beta+\gamma)\delta+(\beta+\gamma)\alpha+\beta^2+\gamma\beta}T_k^{'}-\frac{\left[\beta\alpha v^2+(\beta+\gamma)\alpha+\beta^2+\gamma\beta\right]}{(\alpha\delta+\beta\alpha)v^2+(\beta+\gamma)\delta+(\beta+\gamma)\alpha+\beta^2+\gamma\beta}D_k^{'} \tag{27}$$

Given the linearity of the controller input in the state space $\left(T_k^{'}, D_k^{'}\right)$, we can rewrite mapping of the fluctuation from trial-to-trial as

$$\mathbf{x_{k+1}^{'} = x_k^{'} + GIAx_k^{'}} + \eta \tag{28}$$

Where the control input vector $\mathbf{u}^{2x1}$ is defined by the state variables and the 2x2 $\mathbf{A}^{2x2}$ matrix, $\mathbf{u = Ax_k^{'}}$. The optimal **A** matrix was derived by setting the gain matrix, $G = I$; thus when $G \neq I$, the effective controller matrix A was sub-optimal with respect to the cost function. This is an important feature of the controller since subjects do not have to be *optimal* all the time. It is possible that being optimal might not be the best way to perform the task and exploit the redundancy and over variability during the task.

To explicitly derive the A matrix, we let Ω defines the denominator of the control inputs as show in Eq. 24 and Eq. 25.

$$\Omega = (\alpha\delta+\beta\alpha)v^2+(\beta+\gamma)\delta+(\beta+\gamma)\alpha+\beta^2+\gamma\beta \tag{29}$$

The state-update equation was redefine set setting let $\varepsilon^{'}$ denotes the movement to movement fluctuation in the new coordinate system, Eq. 5 could be rewritten as a linear combination of the reaching distance and reaching time (Eq. 30)

$$\varepsilon^{'} = \begin{bmatrix} -g_1\dfrac{(\alpha\delta+\beta\alpha)v^2+\beta\delta+\beta\alpha+\beta^2}{\Omega} & g_1\dfrac{\alpha\delta v}{\Omega} \\ g_2\dfrac{\gamma\alpha v}{\Omega} & -g_2\dfrac{\beta\alpha v^2+(\beta+\gamma)\alpha+\beta^2+\gamma\beta}{\Omega} \end{bmatrix}\begin{bmatrix} T_k^{'} \\ D_k^{'} \end{bmatrix}+\begin{bmatrix} \eta_T \\ \eta_D \end{bmatrix} \tag{30}$$

Where the general **A** matrix of the optimal and suboptimal control inputs controller inputs was defined by

$$A = \begin{bmatrix} -g_1 \dfrac{(\alpha\delta + \beta\alpha)v^2 + \beta\delta + \beta\alpha + \beta^2}{\Omega} & g_1 \dfrac{\alpha\delta v}{\Omega} \\ g_2 \dfrac{\gamma\alpha v}{\Omega} & -g_2 \dfrac{\beta\alpha v^2 + (\beta + \gamma)\alpha + \beta^2 + \gamma\beta}{\Omega} \end{bmatrix} \tag{31}$$

The A matrix represents the controller inputs that correlates the movement-to-movement fluctuation to the current state variables. Therefore, the parameters of the A matrix provide a mechanism to estimate the possible strategy adopted by each subject during the experiment. α and β provide estimation of the control strategies employed by subject during the task. Therefore possible control strategy could be hypothesized by comparing the parameters of the A matrix between subjects. Some subjects might favor exploiting the redundancy along the GEM resulting a larger α value, while some subjects might refrain from exploiting such redundancy and settle at a fix operating region thus resulting in larger β. However, based on the structure of our inter-trial controller and cost function associated with finding the control efforts, there were still numerous parameters within the system to construct viable control architecture to simulate the results demonstrated by the experimental subject. Given the larger number of *degree of freedom* in the controller, it is still possible to generate different combinations of these parameters to replicate the experimental data. However, care must be taken in interpreting these values in the controller because of the interaction across all six parameters of the controller $\{\alpha, \beta, \gamma, \delta, g_1, g_2\}$.

Task 2

Similar approach could be used to solve for Task 2. The goal manifold for Task 2 was mathematically defined as

$$e = D_k \cdot T_k = z \Rightarrow e = D_k - \frac{z}{T_k} = 0 \tag{32}$$

Where z now defines the goal of the task. The cost function and the definition of the preferred operating point of Task 2 were similar to Task 1. Therefore, by substituting the expression for e and p as defined by Eq. 9 and 10 respectively. Thus the cost function for Task 2 was expressed by

$$C = \alpha\left(\frac{D_{k+1}T_{k+1} - z}{T_{k+1}}\right)^2 + \beta\left[\left(T_{k+1} - T^*\right)^2 + \left(D_{k+1} - D^*\right)^2\right] + \gamma u_1^2 + \delta u_2^2 \tag{33}$$

Similarly, the state-update equation was given by

$$\begin{aligned} T_{k+1} &= T_k + g_1\left(1 + \sigma_1 v_1\right)u_1\left(x_k\right) + \sigma_3 v_3 \\ D_{k+1} &= D_k + g_2\left(1 + \sigma_2 v_2\right)u_2\left(x_k\right) + \sigma_4 v_4 \end{aligned} \tag{34}$$

The cost function was then expanded as

$$\begin{aligned} C = \alpha&\left(\frac{\left(D_k + g_2\left(1 + \sigma_2 v_2\right)u_2\left(x_k\right) + \sigma_4 v_4\right)T_k + g_1\left(1 + \sigma_1 v_1\right)u_1\left(x_k\right) + \sigma_3 v_3 - z}{T_k + g_1\left(1 + \sigma_1 v_1\right)u_1\left(x_k\right) + \sigma_3 v_3}\right)^2 + \\ \beta&\left[\left(T_k + g_1\left(1 + \sigma_1 v_1\right)u_1\left(x_k\right) + \sigma_3 v_3 - T^*\right)^2 + \left(D_k + g_2\left(1 + \sigma_2 v_2\right)u_2\left(x_k\right) + \sigma_4 v_4 - D^*\right)^2\right] + \\ &\gamma u_1^2 + \delta u_2^2 \end{aligned} \tag{35}$$

Similar to Task 1, the control inputs were solved by deriving the augmented Lagrangian for Task 2 with the multiplicative noise assumed to be zero and required that controller on average be perfect on the next movement (Eq. 36).

$$\bar{F} = D_k + u_2 - \frac{z}{T_k + u_1} \tag{36}$$

Differentiating the augmented Lagrangian equation, we derived a system of equations that related the control input with the Lagrangian multipliers.

$$2u_1\left(\beta + \gamma\right) + 2\beta\left(T_k - 2T_p\right) - \frac{\alpha z^2\left(2T_k + 2u_1\right)}{\left(T_k + u_1\right)^4} + \frac{-\mu z + 2\alpha z u_2 + 2\alpha z D_k}{\left(T_k + u_1\right)^2} = 0 \tag{37}$$

$$2u_2\left(\beta + \alpha + \delta\right) - \mu + 2\left(\alpha + \beta\right)D_k - 2\beta D_p - \frac{2\alpha V}{T_k + u_1} = 0 \tag{38}$$

Notice that these equations are nonlinear with respect to u_1 and it is not possible to find an explicit expression for the control input u_1 and u_2 as in Task 1. While numerical techniques could be invoked to find possible solutions for the controller, the computation complexity could further diminished the meaning of the parameters found for the controller; therefore, a simpler approach was adopted to investigate the trial to trial dynamics for Task 2.

For Task 2, rather than defining the goal function as $D_k \cdot T_k = z$, the reaching time could be transformed to reaching frequency where ($F = 1/T\ s^{-1}$). The goal function was then rewritten as

$$D_k \cdot T_k = z \Rightarrow D_k \cdot \frac{1}{1/T_k} = z \Rightarrow \frac{D_k}{F_k} = z \tag{39}$$

Therefore, the equations that were derived for Task 1 could be applied to Task 2. This coordinate transformation had been shown to retain the exactly same trial to trial dynamics (Dingwell, Smallwood et al. 2013) as the original time.

Multivariate Linear Regression

Given that the A matrix is central to our understanding how subject solve the task redundancy in the problem; it is utmost important for us to capture the dynamics of the A matrix from the experimental data. Multivariate Linear Regression was used to estimate the movement to movement fluctuation for each subject. Multivariate linear regression is a statistical method of estimate the interaction of different variables within the system. The generalized form of the regression model is express as

$$\mathbf{Y} = A\mathbf{X} + \mathbf{U} \tag{40}$$

Where **Y** is the output matrix, **A** is the design matrix, **X** is the state variable and **U** is the noise or error matrix. Linear regression provides a methodological process of estimating the parameters in the controller using the experiment data. This approach also provides greater integrity to the model because the process is not to simply replicate the measurable outputs, but estimate the overall dynamics of the system. Using numerous

optimization algorithms available (Simplex, Iterative Search, Genetic Algorithm, etc.), one could easily replicate the experimental outputs by generating an optimal set of parameters that statistically replicate the output model. However, such approach would not provide sensible meaning to the control parameters and it would not provide meaningful interpretations of the strategy adopted by each subject. Linear regression only estimate the dynamics of each subject by modeling how the controller would behave, whether the system could replicate the measure output is a secondary objective. Under ideal experimental condition, we expected the controller to generate qualitatively similar output to the experimental data. However, it is possible that the model is simply not sufficient to capture "other" strategies adopted by the experiment or that subject did not follow any structure laws in performance the task.

Using linear regression we could estimate the A matrix for each subject from the experimental data. The experimental structure of the movement to movement fluctuation, $\varepsilon'_{\exp}$, was then formulated as follows

$$\varepsilon'_{\exp} = \begin{bmatrix} A_{11} & A_{12} \\ A_{21} & A_{22} \end{bmatrix}_{\exp} \begin{bmatrix} T'_k \\ D'_k \end{bmatrix} + \begin{bmatrix} \eta_T \\ \eta_D \end{bmatrix} \tag{41}$$

This process allowed the extraction of the A matrix and the residual noise associated with each subject from the experimental data and compared with the explicit form that defines the controller input to find the parameters, $\{\alpha, \beta, \gamma, \delta, g_1, g_2\}$. A simple Iterative Search optimization algorithm was implemented to find the parameters values that would give the best estimation to the experimental A matrix.

$$\begin{bmatrix} A_{11} & A_{12} \\ A_{21} & A_{22} \end{bmatrix}_{\exp} = \begin{bmatrix} -g_1 \dfrac{(\alpha\delta+\beta\alpha)v^2+\beta\delta+\beta\alpha+\beta^2}{\Omega} & g_1 \dfrac{\alpha\delta v}{\Omega} \\ g_2 \dfrac{\gamma\alpha v}{\Omega} & -g_2 \dfrac{\beta\alpha v^2+(\beta+\gamma)\alpha+\beta^2+\gamma\beta}{\Omega} \end{bmatrix} \tag{42}$$

The residual noises of the reaching distance and reaching time were calculated by using Matlab® (MathWorks, built-in function *mvregress)*. The residual noise provides

an estimate of the residual noise in the system. This is critical in simulating the trial-to-trial movement strategy adopted by the controller.

Optimization

The parameters of the controller were found by optimizing the error difference between the element of the experimental A matrix, $\left(A^E\right)$, matrix and the element of the model A matrix $\left(A^M\right)$. Different cost functions were tested; however, Eq. 33 generated the most consistent and robust solutions

$$\min\left\{S = \sum_{i=1}^{2}\sum_{j=1}^{2}\left(A_{ij}^{M} - A_{ij}^{E}\right)^2\right. \tag{43}$$

Preliminary analysis showed that the solution space of these six parameters was relatively flat (i.e. different optimal solutions were found for different starting conditions); therefore a global search algorithm was implement in an attempt to find the best possible solution. Rather just find *a solution*, it continues to compare another 100 starting condition and keep the best results. Thus the algorithm can overcome local minimums within the solution manifold. While using such semi-brute force algorithm might not find the best optimal solutions it does provide a computationally more efficient method to overcome the flatness in the solution space where a more complex optimal algorithm might not provide sufficient improvement at greater computational cost.

The parameters for two different controllers were calculated by finding the parameters that minimize the sum of the error between the elements of the experimental A matrix and the model A matrix.

<u>*Optimal Control*</u>: The gain matrix g_1 and g_2 were set to unity $g_1 = g_2 = 1$. The optimization algorithm minimized the sum of the error of the A matrix to estimate the optimal parameters $(\alpha, \beta, \gamma, \delta)$ for the controller. This controller is defined as the optimal controller. Due to the flatness of the solution manifold, the initial conditions were set to correspond to the variance along the direction tangential and perpendicular to the goal

manifold. The variances tangential and perpendicular to GEM were calculated from the experimental data. The initial conditions for the control effort parameters, γ and δ, were randomly set so that $\gamma = \delta$. These initial conditions were especially important when computing the parameters for the optimal controller. This scheme is know as the *optimal controller*.

Suboptimal Control: In this scheme the parameters $(\alpha, \beta, \gamma, \delta, g_1, g_2)$ of the controller were allowed to change simultaneously. In contrast to the optimal controller, here we assume that subject might not perform the task optimally. There is no restriction on how subject performed the task; therefore, it is unreasonable to assume that every subject will perform the task optimally with respect to the cost function C. Again, as previously stated, subject could perform the task in ignorant of the GEM requirement since the task was not structured to limit or constrain the subject to a specific strategy. However, the parameters $(\alpha, \beta, \gamma, \delta)$ found in the optimal controller were used as the starting guesses for this condition. This assumes that people will operate near optimal but explore other solutions that might provide better fit while localizing the search region. This controller is referred as the *suboptimal controller*.

The Matlab ® built-in *fmincon* was used as the optimization algorithm to minimize the error in the A matrix

ANALYSIS

Applying the optimization process, we can estimate the parameters of the A matrix of the model to hypothesize the type of control adopted by each subject; however, the A matrix itself only reveals the possible strategy with respect to the GEM adopted by the subject to perform the task. It does not provide any direct insight on the actual trial-to-trial dynamics. Furthermore, it does not indicate whether the model is accurate in estimating the behavior exhibited by each subject. We used the parameters that define the A matrix to yield the model output that allow us to evaluate and compare the output from the model with the experimental output to determine the robustness of our model in capturing the dynamics of the task for each individual subject. More specifically, we used it to predict a set of reaching distance and reaching time as defined by

$$\mathbf{x}'_{\mathbf{k+1}} = \mathbf{x}'_{\mathbf{k}} + \mathbf{GIA}\mathbf{x}'_{\mathbf{k}} + \eta \tag{44}$$

Where $\mathbf{x}_{\mathbf{k}} = \left[T_k, D_k\right]$ defines the state variable reaching distance and reaching time and η denotes the estimation of the residual or noise of the fluctuation in the reaching distance and reaching time derived from the linear regression of the experimental data. The optimization algorithm was used to find the parameters of the controller that minimized the optimization objective function. From this parameters, an A matrix was constructed and used to calculate a time series of 400 reaching distance (D) and reaching time (T). From the time series of the reaching distance and reaching time, the time series along (δ_T) and perpendicular (δ_P) to the GEM were also calculated. From these time series several dependent measures were calculated to determine the fitness of these two controllers and to compare the model output with the experimental data. These are: mean and standard deviation of these time series, stability multipliers (κ), and linear correlation (λ). Results from 30 different trials (A matrices) were calculated and compared with the experimental data.

Dependent Measures

Once the optimal and suboptimal control parameters were identified for each subject and the output time series were obtained, several dependent measures were identify to evaluate the "goodness of fit" of each model to the experimental data. These relevant dependent measures were extracted separately and independently from the model and the experimental data time series data.

Lambdas (λ)

Lambdas show the linear correlation between the current movement $(\mathbf{x}_k)$ and the next movement $(\mathbf{x}_{k+1})$. In this experiment, correlations were investigated: fluctuations in reaching time (T), reaching distance (D), fluctuation in the direction tangential to the GEM (δ_T) and perpendicular to the GEM (δ_P). The reaching distance and reaching time series comprised the 400 trials performed by the experimental data and generated by the models. The correlations in the T and D are map by defining by

$$\mathbf{x_{k+1}} = \lambda \mathbf{x_k} + \xi \tag{45}$$

Where λ denotes the correlations from movement to movement and ξ represents the residual noise in the linear regression.

Or more explicitly as

$$\begin{bmatrix} T_{k+1} \\ D_{k+1} \end{bmatrix} = \begin{bmatrix} \lambda_T & \lambda_D \end{bmatrix} \begin{bmatrix} T_k \\ D_k \end{bmatrix} + \begin{bmatrix} \xi_T \\ \xi_D \end{bmatrix} \tag{46}$$

The $[\lambda_T, \lambda_P]$ values indicate how rapidly subjects correct for the reaching distance and reaching time based on the previous movement.

Deviations in the tangential and perpendicular direction were calculated by calculating the error away from the preferred operating point. For Task 1, the deviation in the tangential and perpendicular direction is given by

$$\begin{bmatrix} \delta_T \\ \delta_P \end{bmatrix} = \frac{1}{\sqrt{1+c^2}} \begin{bmatrix} 1 & c \\ -c & 1 \end{bmatrix} \begin{bmatrix} \tilde{T}_k \\ \tilde{D}_k \end{bmatrix} \tag{47}$$

Where c define the goal function constant and $\tilde{T}_k = T_k - T^*$ and $\tilde{D}_k = D_k - D^*$. Similarly, the deviation in the tangential and perpendicular for Task 2 is given by

$$\begin{bmatrix} \delta_T \\ \delta_P \end{bmatrix} = \frac{1}{\sqrt{1+\left(D^*/T^*\right)^2}} \begin{bmatrix} 1 & D^*/T^* \\ -D^*/T^* & 1 \end{bmatrix} \begin{bmatrix} \tilde{T}_k \\ \tilde{D}_k \end{bmatrix} \tag{48}$$

In terms of control, the λ in the tangential and perpendicular direction provide indication how rapidly do subject correct for perturbation about the goal manifold. $\lambda > 0$ indicates statistical persistence: increases (or decreases) in the value of $\mathbf{x}_k$ are more likely to be followed by increase (or decreases in $\mathbf{x}_k$). $\lambda = 0$ corresponds to uncorrelated or "white noise" and $\lambda < 0$ indicates anti-persistence: increases (or decreases) in $\mathbf{x}_k$ are more likely to be followed by subsequent decreases (or increases) in $\mathbf{x}_k$.

Stability Multipliers (κ)

Given that the noise in the trial-to-trial controller is small, we linearized the controller about the prefer operating point as define above in Eq. 32. Where the A matrix map the fluctuation from movement to movement; therefore the eigenvalues and eigenvectors of the A matrix indicate the dynamics stability properties of the system.

If the eigenvalues of A is real and distinct, when $|\kappa_i| < 1$ for $(i = 1,2)$, it indicates that the operating point is asymptotically stable about the operating point. This means that over time, in the absence of noise, the fluctuations would decay to zero. In contrast, when $|\kappa_i| > 1$, the system is unstable about the operating point and the fluctuation will grow over time. Given the restriction in the workspace of the experimental data, we expect the real eigenvalue value to be stable. Lastly, when $|\kappa_i| = 1$, this indicates a *neutrally stable* fluctuation about the operating point. In such case, the nature of the

noise term determines the local stability about the operating point. However, given that the experimental data might not be structured in the most optimal way with respect to the goal manifold, it is possible to obtain complex eigenvalue. Complex eigenvalues indicate and oscillatory stability about the operating point. The real part of the eigenvalue still indicates the growth and decay nature of the movement to movement dynamics while the imaginary part indicates the fluctuation or exploitation about the operating point. It is possible that subject *tries* other strategies before adopting a *best* strategy.

Bootstrap

Bootstrapping is a statistical method of resampling a population to give an estimate of the accuracy of a measurement of the model, (Efron 1979). The results from the bootstrap allow us to make inference about the integrity of the data and the estimate of the uncertainty in a measurement of interest. Furthermore, results from the probability distribution function allow us additional tool to evaluate the dynamic of the task as in terms of how well each subject actually exploited the prescribed redundancy in the task.

Since there was only one trial collected during the experiment for each subject and for each task, it was important to estimate the uncertainty of the measured parameters. Bootstrapping provided a simple statistical tool to estimate the uncertainty in these parameters by subsampling the population. We can compare if the uncertainty exhibited in the model is within tolerance of the bootstrapping of the data. The uncertainty in the system was estimated by calculating the variance of the subsampling. The variance obtained from the bootstrapping was then used to evaluate how well the model predicted the experimental results. For the bootstrapping method, 300 samples were subsampled from each trial (400 total samples). This was repeated for 2000 trials. For trial-to-trial correlation (λs) calculation, we sampled the *k* and *k+1* trial as a pair. These trials were then evaluated to look at the mean and standard deviation of each metric.

The bootstrap were performed on the element of the A matrix to estimate the error in the dynamics of the system as well as the optimal and suboptimal parameters. This was done by estimating the corresponding control parameters for each subsample A matrix. The results were used to compare to the parameters estimated by the model. Bootstrapping was also performed on the dependent measures to compare if the outputs calculated from the model are a good estimation of the single-trial experimental data. These dependent measures are (κ, λ).

RESULTS

The experimental study had been done to analyze differences in subjects during the performance of Task 1 and Task 2 (Dingwell, Smallwood et al. 2013). However, the experimental analysis did not provide a mechanism to analyze the strategic differences between subjects in performing the task. Therefore, a trial-to-trial controller was proposed to estimate the movement-to-movement dynamics. From the structure of the controller, we can compare the differences in control strategy among subjects. From these results, we can generalize how (or if) a subject exploited the redundancy that was inherent at the task level. However, before the optimal and suboptimal models can be used to generalize the dynamics exhibited by each subject, bootstrapped data were analyzed to determine if the results from the model were a good estimation of the experimental data.

A Matrix

The control parameters $(\alpha, \beta, \gamma, \delta, g_1, g_2)$ were derived from the estimation of the A matrix. The A matrix represents the fluctuation from movement to movement about the preferred operating point. As previously stated (see Method), the A matrix was calculated from the experimental data by using a linearized model about the preferred operating point.

Figure 20 shows the experimental (*Exp.*) and bootstrap results (*Exp. Bootstrap*) of the A matrix. The results showed that fluctuation in time was negatively related to current reaching time and positively related to current reaching distance. However, the fluctuation in distance was more negatively related to current reaching distance ($\overline{A}_{21} = 0.0627,\ \sigma_{A_{21}} = 0.0757$). This might indicate that subjects relied on both distance and time feedback to adjust their reaching time. The most sensitive element was element A_{12}. Across subjects, there were significant differences between the experimental data and the bootstrap ($p<0.005$). This trend was also consistent in Task 2.

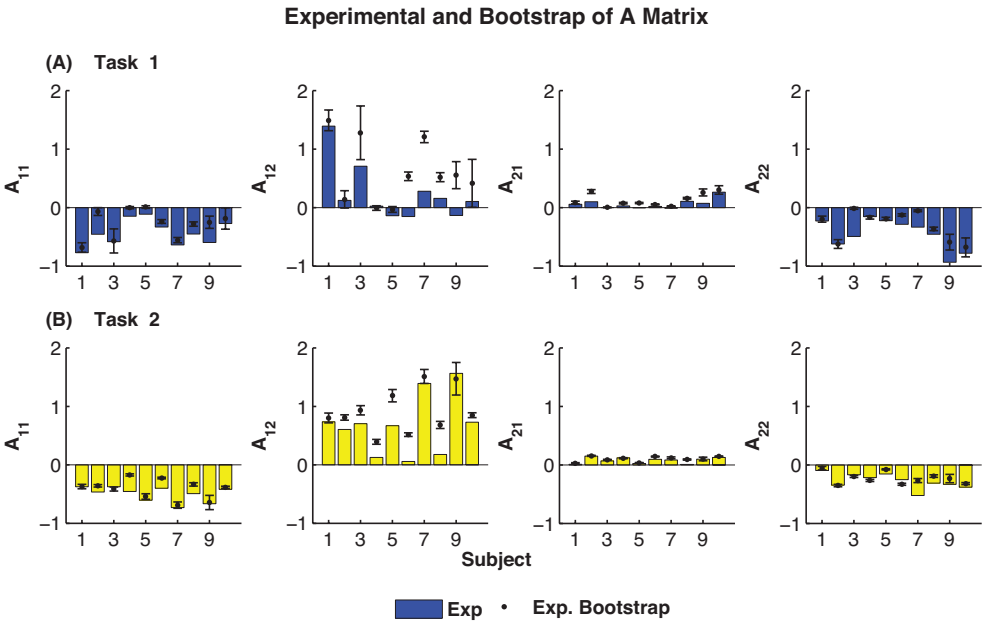

Figure 20: Experimental and bootstrap estimate of A matrix for both GEMs (A) Task 1 (B) Task 2. The *Exp*. represents the single trial from the experimental data while *Exp*. *Bootstrap* denotes the estimates from bootstrapping the experimental data.

Since the experiment was designed so that subjects were intentionally giving the minimal instruction and feedback required to perform the task. Since, very little instruction concerning the nature of the task, we did not expect the bootstrap of A to perfectly map the A matrix. Furthermore, the linear regression of A matrix only *estimates* the dynamics from movement-to-movement; therefore there could be more noise in capturing the dynamics from trial to trial. However, given the nature of the experiment and the statistical estimation implemented; the bootstrap data generally followed the same trend as the experimental data. In addition, the magnitudes of the correlation in the magnitude were relative small. The A matrix was subsequently used find the parameters of the controller that were used to generate the time series for reaching distance and reaching time. From these time series, we calculated the dependent measures to determine the fitness of model based on the experimental A matrix. It is possible that the A matrix does not need to be perfectly matched as long as the general dynamics of the task are captured.

Optimization Parameters

These parameters were found by optimizing the mean square differences between the A matrix of the experimental data through linearization about the preferred operating point and the explicit form derived for the inter-trial controller. The A matrices are summarize below:

$$\begin{bmatrix} A_{11} & A_{12} \\ A_{21} & A_{22} \end{bmatrix}_{\exp} = \begin{bmatrix} -g_1 \dfrac{(\alpha\delta+\beta\alpha)v^2+\beta\delta+\beta\alpha+\beta^2}{\Omega} & g_1 \dfrac{\alpha\delta v}{\Omega} \\ g_2 \dfrac{\gamma\alpha v}{\Omega} & -g_2 \dfrac{\beta\alpha v^2+(\beta+\gamma)\alpha+\beta^2+\gamma\beta}{\Omega} \end{bmatrix} \tag{49}$$

Since only one experimental trial was collected for each subject, bootstrapping was used to estimate the uncertainty in the parameters of the optimal and suboptimal controller. This is important in determining if there is consistency in these parameters because they provide the comparative differences between each individual subject.

Parameters of the Optimal Controller

The optimal parameters of the controller were obtained by setting $g_1 = g_2 = 1$ for both Task 1 (Figure 21) and Task 2 (Figure 22). In the figures the *Model* denotes the data from the simulated data while *Exp*. *Bootstrap* represents the experimental data with the standard deviation estimated from the bootstrap of the experimental data. For Task 1, the general trends in parameters value were consistent with the estimation of using the experimental data. Since the A matrix was not well behaved during bootstrapping, we did not expect the parameters to be perfectly match; however, model estimation of these parameters were within the uncertainty based on the bootstrapping of the experimental data. For Task 1, it was notable that subject 5 and 6 have an α value of about zero $\left(a_{5,6} = 0.00 \pm 0.00\right)$. Overall, the model generally did a good job of replicating the experimental results across subjects for Task 1.

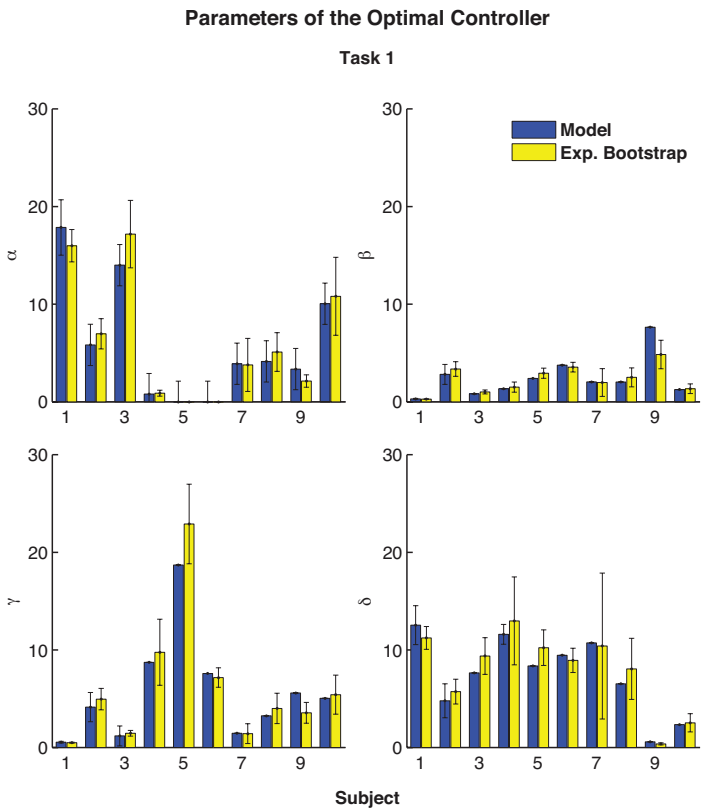

Figure 21: The parameters of the optimal model as derived from the optimization of the A matrix and the explicit form of the model A matrix. The optimal controller (*Model*) was defined when the gain was unity, $g_1 = g_2 = 1$. *Exp. Bootstrap* represents the mean from the single experimental data with the standard deviation esimated from bootstrapping the experimental data.

Figure 22 shows the parameter of the optimal controller for Task 2 as compared to data from the bootstrapping of the experimental data. Since Task 2 lacked the physical intuitiveness of Task 1, we expected the controller to have a more difficult time in capturing the dynamics of this task. However, overall the parameters found by controller were consistent with the experimental data across all subjects. While most subjects exhibited controller parameters within the same magnitude of each other, Subject 7 and 9 exhibited significantly different behavior than other subjects.

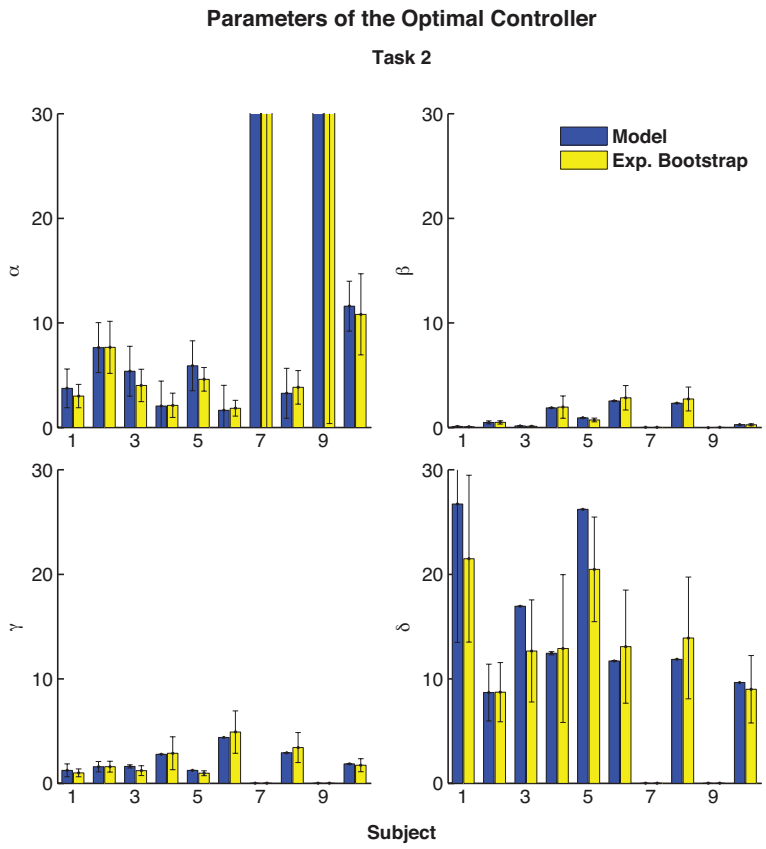

Figure 22: Optimal parameter of the controller of Task 2. The optimal controller was defined when the optimal gains =1.

While the α values for most subjects ranged from $\alpha_6 = 1.648 \pm .0728$ to $\alpha_{10} = 11.605 \pm 2.6955$ the α for subject 7 and 9 were $\alpha_7 = 48.024 \pm 79.488$ and $\alpha_9 = 50.193 \pm 43.360$. Furthermore, the β parameters for these subjects were close to zero $\left(\beta_7 = 3.211E-05 \pm 3.335E-05,\ B_9 = 0.0 \pm 0.0\right)$. These trends also extended to the control parameters γ for subject 7 $\left(\gamma_7 = 6.91E-05 \pm 7.10E-05\right)$ and for subject 9 $\left(\gamma_9 = 3.023E-04 \pm 3.028E-04\right)$. This was similar for the δ parameters for subject 7. $\left(\delta_7 = 8.0247E-04 \pm 7.1053E-05\right)$ and subject 9 $\left(\delta_9 = 0.0034 \pm 8.2664E-04\right)$ of Task 2. This data confirmed that subjects tend to exert strong correction for deviation perpendicular to the GEM (Domkin, Laczko et al. 2002; Todorov 2004; Valero-Cuevas, Venkadesan et al.

2009; Dingwell, John et al. 2010) and weakly control for deviation about the preferred operating point ($\alpha > \beta$).

While the individual parameter of the controller has a unique function within the inter-trial control, it is possible that there are interactions between these parameters. Here we are interested in how the ratio of these parameters changes (α/β and γ/δ). The α/β represents the tendency to correct for deviation along the goal manifold and the gravitation toward a preferred operating point. The γ/δ represents the interaction between the control efforts.

Figure 23 (A-D) shows the ratio of the α/β and γ/δ for Task 1 and Task 2. The results showed that there were several unique trends across different subjects. For both tasks, the ratio of γ/δ was significantly smaller than the ratio α/β ($p<0.005$) across all subjects. This was more evident in the Task 2. The variances of these ratios were essential zero, indicating the consistency of these paired parameters across all trials. For Task 2, two subjects exhibited significantly different behavior than the other subjects. Given that $\delta_9 = 0$, the ratio for subject 9 was undefined and the ratio for subject 7 was significantly large given that $\delta_7 \approx 0$. Overall, the model estimation generally captured the experimental data across all subjects.

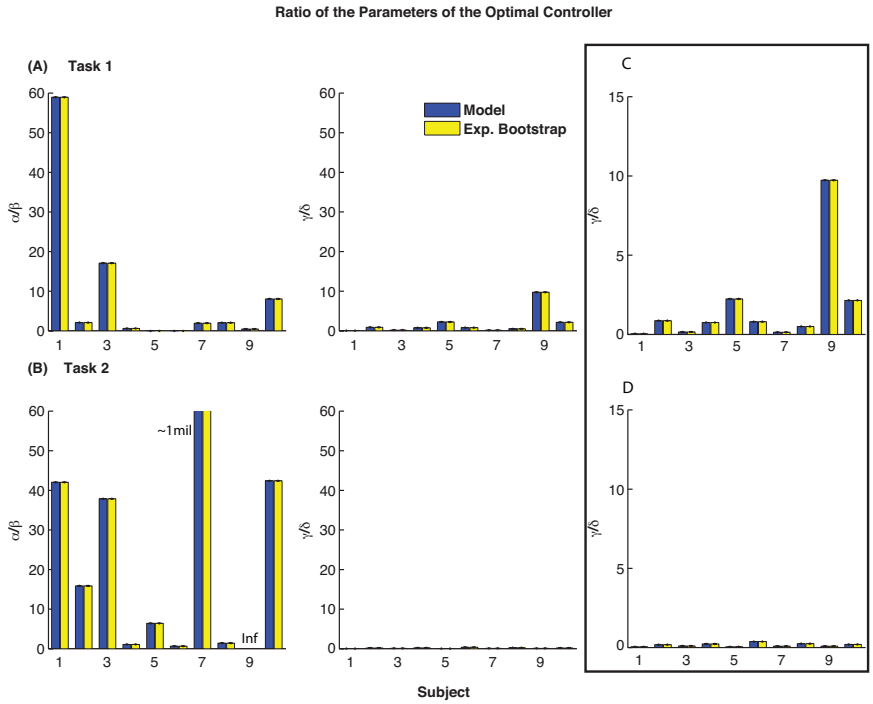

Figure 23: The ratio of the parameters of the optimal for (A) Task 1 and (B) Task 2. (C and (D) show the rescale of the γ/δ ratios for Task 1 and Task 2. Exp. Bootstrap indicates the mean from the single trial and the standard deviation from bootstrapping the experimental data.

Parameters of the Suboptimal Controller

In the suboptimal condition, rather than fixing controller parameter (g_1, g_2), we allowed all six parameters to change simultaneously. However, the parameters found for the optimal controller for both tasks were used as the starting point for the suboptimal search (Figure 21). Here we assumed that best solution would be *near* optimal where $g_1 = g_2 = 1$.

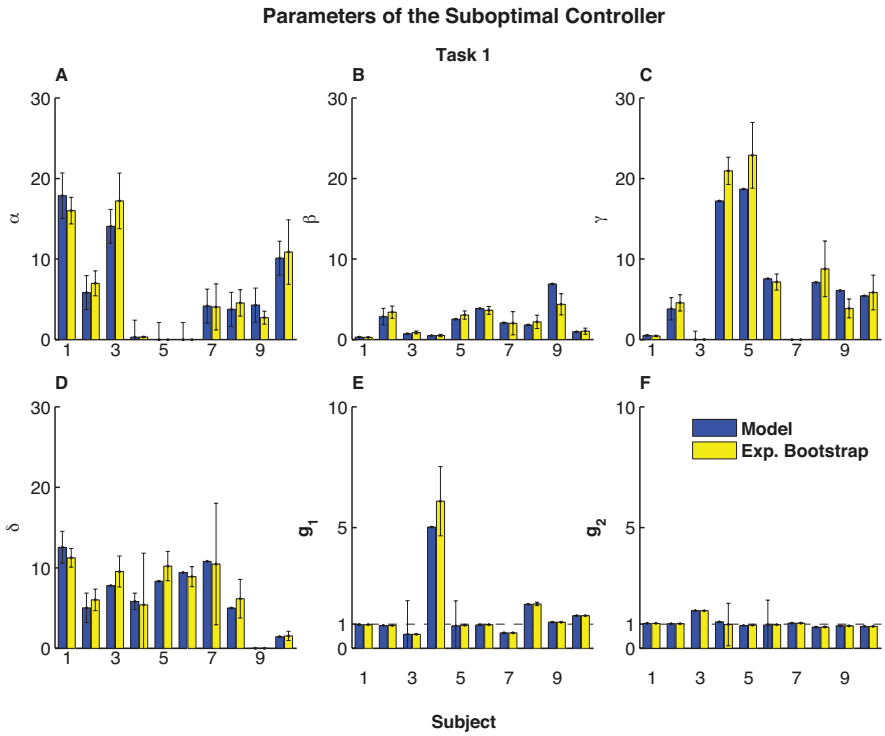

Figure 24: Parameters of the suboptimal controller for Task 1. For Task 1, on average $\alpha > \beta$ and the gains were approximately unity for most subjects. The *Model* indicates the simulated results from the suboptimal control and the *Exp. Bootstrap* denotes the mean from the experimental data (single trial) and the standard deviation from the bootstrapping of the experimental data.

Overall, the model generally captured the general trend in the experimental data. While the model did not perfectly match the experimental data, it generally provided good estimations of the dynamics. For Task 1, in general, the parameters for the suboptimal controller were within the region of the optimal controller ($p<0.005$) (Figure 21). Most subjects had an estimated gain that was approximately unity except for subject 4 $\left(g_{1,4} = 5.020 \pm 1.570\right)$.

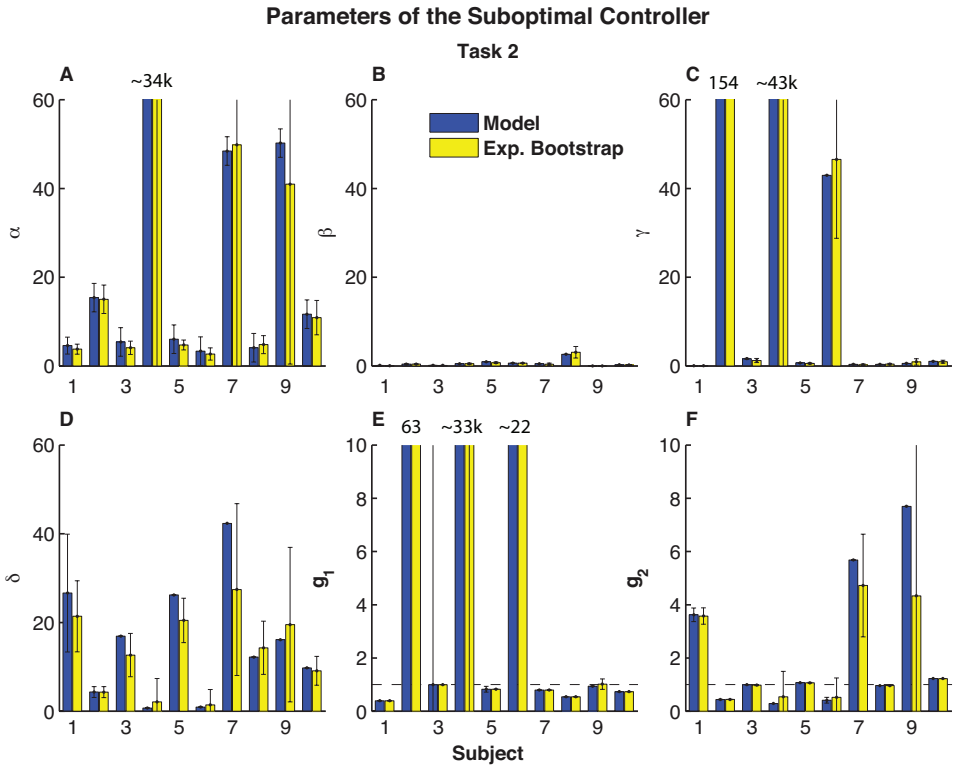

Figure 25: Parameters of the suboptimal controller for Task 2. Similar to Task 1, the α's were significantly larger then β. While the gains for most subjects were with the expected range (~1), some subjects exhibited significantly large gain value.

Figure 25 shows the parameters of the suboptimal controller for Task 2. From the experimental data, it showed that the estimation of these parameters were more variable for Task 2 than Task 1. However, in general, the model parameters were within the uncertainty of the experimental data. The model was able to capture the general dynamics across all subjects. In general, the estimation of the β and γ (Figure 25 B, C) were significantly smaller as compared to α and δ (Figure 25 A, D). A few subjects exhibited larger estimate of γ. While most subjects remained close to the optimal solution, some subjects deviated significantly from their predicted optimal solutions. Subject 4 $\left(\alpha_{4,opt} = 2.046 \ \pm 1.108\right)$ moved away significantly from the starting point once

the gain parameters were relaxed $\left(\alpha_{4,subopt} = 34,284 \ \pm 90015\right)$ (p<0.005); this was evident by a significant increase in the gain parameter g_1 $\left(g_{1,4,subopt} = 33,239 \ \pm 86115\right)$.

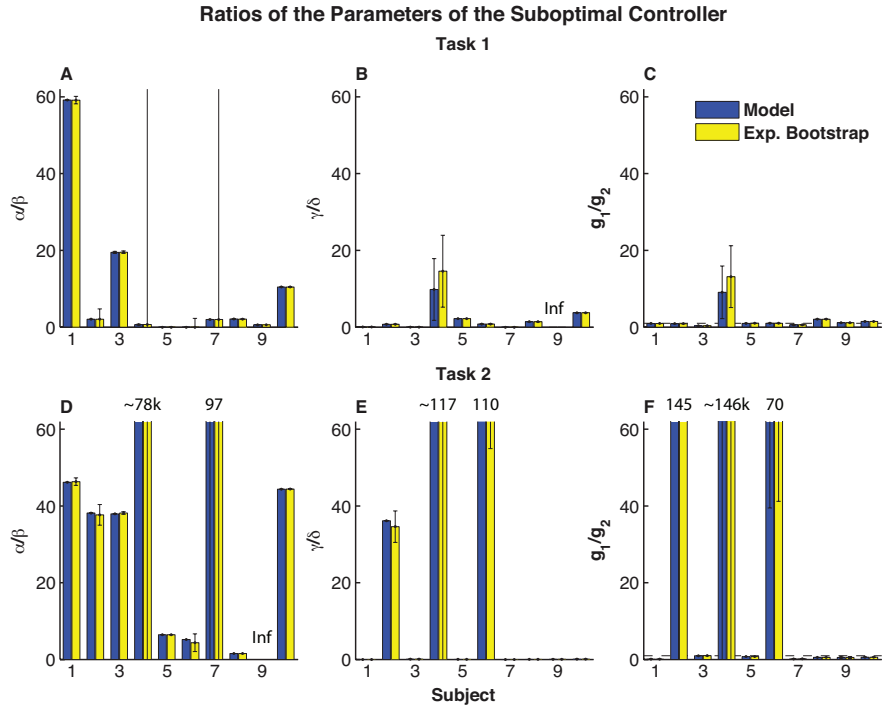

Figure 26: Ratios of the parameters of the suboptimal controller for (A) Task 1 and (B) Task 2.

Figure 26 shows the ratio for both Task1 (A-C) and Task 2 (D-F). In general, the model estimations of the experimental data were very consistent and had very small variance. This was similar to the results from the optimal controller.

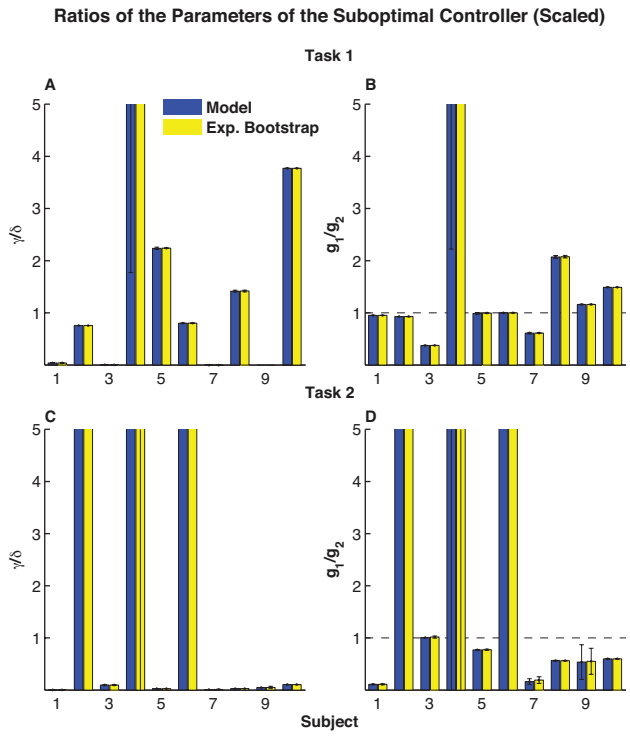

Figure 27: The results from Figure 26 is rescaled and presented here. Ratios of the parameters of the suboptimal control scaled to show the lower value for the γ/δ and g_1 / g_2 ratios.

For Task 1, while most subjects exhibited relatively small ratios of these parameters (Figure 26(A-C)), subject 1 exhibited a larger α/β ratio $\left(\alpha / \beta_{1,subopt} = 59.154 \pm 0.065\right)$. Furthermore, the ratio of the of the gain parameters, g_1 / g_2, remained approximately 1 for the suboptimal controller. This is more evident when the ratio is rescaled (Figure 27 B).

For Task 2, the ratios of the α/β (Figure 26 D) were significantly larger than the ratio for Task 1. Furthermore, for most subjects the ratios of γ/δ were relatively small (~ 0). From the results, there were distinct overall differences between the strategy adopted for Task 1 and Task 2. The ratios of the gain parameters were slightly less then unity for most subjects (Figure 27 D). Three subjects (2,4 and 6) exhibited a significantly large gain ratio.

Comparison of Dependent Measures

Overall, the model provided very good estimations of the experimental data. The inter-trial controller, in general, captured the dynamics and unique behavior of these subjects during the performance of Task 1 and Task 2. Furthermore, there were clear and distinct differences in the strategies adopted for Task 1 and Task 2 based on the structure of the controllers estimated by the optimization algorithm. Here, the inter-trial controllers (both optimal and suboptimal) derived during the optimization process were used to generate 30 simulated trials of 400 reaching movements to investigate whether these controllers could capture more concrete measured outputs from the experimental data. Since, only one set of time series was available from the experimental data, similar bootstrapping was implement on these parameters to evaluate fitness of the results from both the optimal and suboptimal inter-trial controller.

A matrix

The A matrix correlated the movement to movement fluctuation during the reaching task. The A matrix was also used in the construction of the optimization cost function to find the parameters of the controller. Here we recalculated the A matrix from the reaching distance and reaching time generated by the model. The bootstrapping data of the A matrix for Task 1 and Task 2 are shown in Figure 20.

Figure 28 shows the comparison of the A matrix of the optimal and suboptimal controller for Task 1. The results from the controller were compared with the *single* trial calculated from the experimental data. The variances from the bootstrapping (*Exp. Bootstrap*) of the experimental data are also plotted to provide an estimate of the level of uncertainty in the experimental data. The results show that both controllers demonstrated consistent prediction for all element of the A matrix. From the bootstrapping results, we expected that the A_{12} matrix was more variable than the other component. However, the controller did a better job of estimating these parameters than the variance shown in the bootstrapping results. Again, there was no significant different between the optimal and suboptimal controller ($p<0.005$).

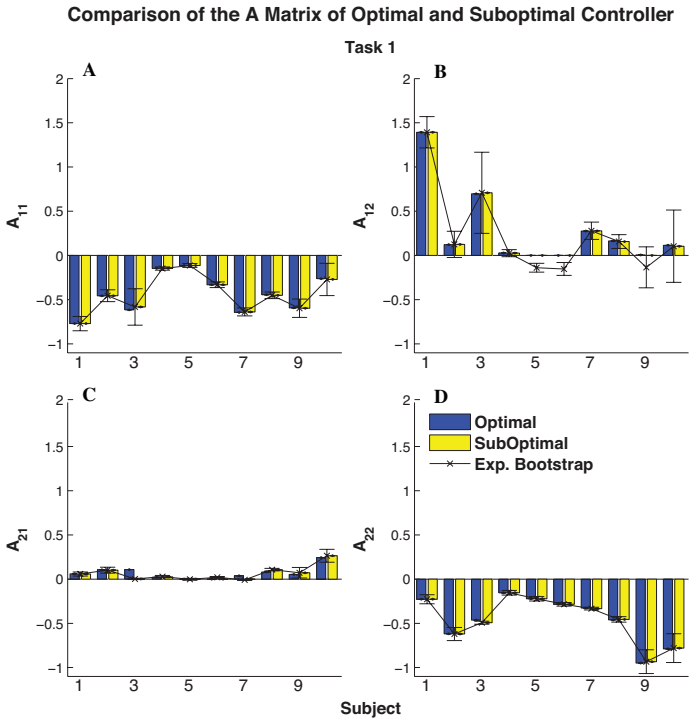

Figure 28: A matrix of the optimal and suboptimal controller for Task 1 compared to the experimental estimation of the A matrix with bootstrapping.

Figure 29 shows the A matrix generated from the optimal and suboptimal controller for task 2. Similar to Task 1, both controllers accurately captured the experimental results. Furthermore, all the estimations were within the uncertainty of the experimental data. Surprisingly, the estimations of the elements of the A matrix for Task 2 were more consistent than for Task 1, even for the A_{12} component (Figure 29 B). Again, there were no significant differences between the optimal and suboptimal controllers ($p<0.005$).

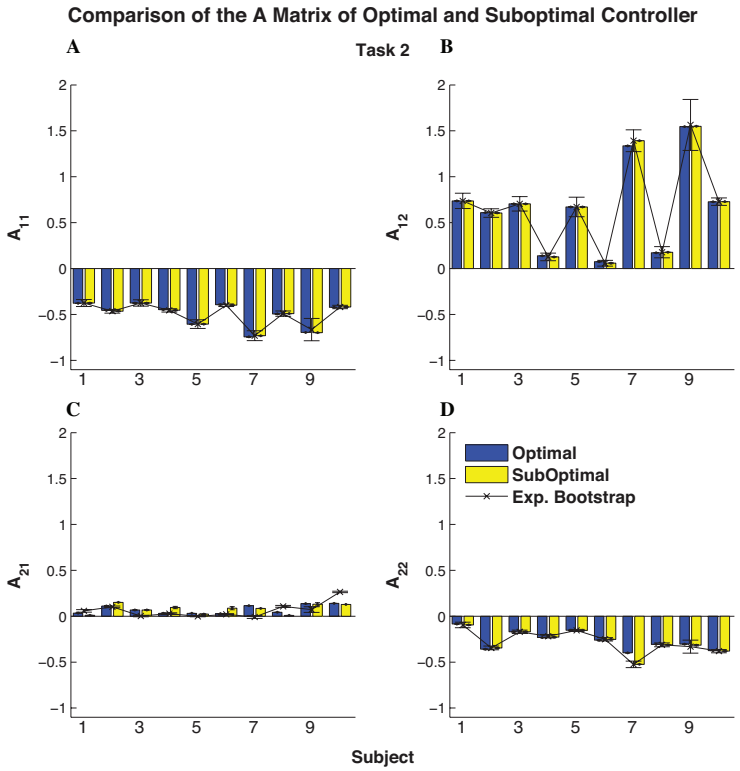

Figure 29: Comparison of the A matrix of the optimal and suboptimal controller compared with the bootstrapping of the experimental trial for Task 2.

Stability Multiplier ($\varkappa$)

The stability multiplier ($\varkappa$) represents the dynamics stability of the A matrix that correlates the movement to movement fluctuation. These stability multipliers are the eigenvalue of the A matrix.

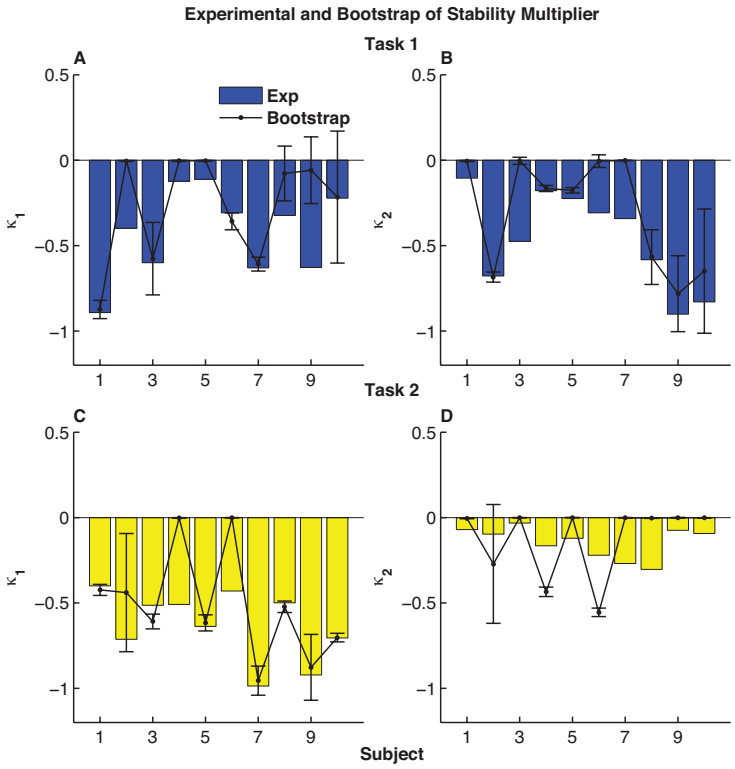

Figure 30: Stability multipliers of the experimental and bootstrap data for Task 1 (A-B) and Task 2 (C-D).

The estimation of the stability multiplier is shown in Figure 30. Overall, the bootstrapping data showed that there were some inconsistencies in the stability multiplier across all subjects for Task 1 and Task 2. While the data showed that subjects were asymptotically stable across all subject for Task 1 and Task 2, the bootstrapping results sometime indicated a marginally stable system $(\kappa = 0)$ (Figure 30 D).

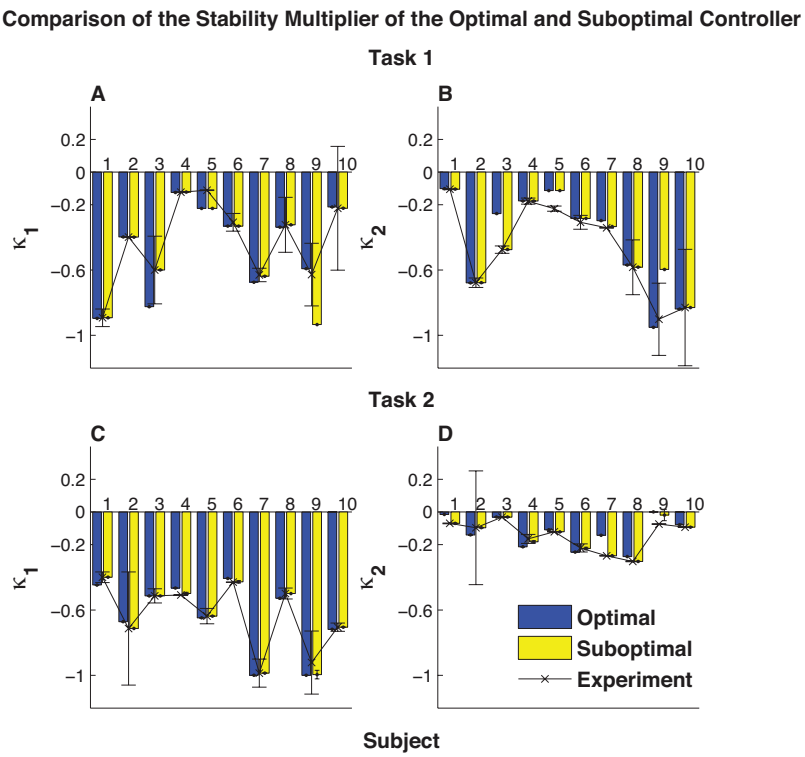

Figure 31: Stability multipliers of the optimal and suboptimal controller across two different goal-direct tasks (A) Task 1 and (B) Task 2 as compared to the experimental data with the standard deviation derived from the bootstrapping of the experimental data.

The results of both controllers accurately captured the dynamic stability in the correlation matrix of the fluctuation from movement to movement for both Task 1 and Task 2. While there were instances when the suboptimal did a better job of fitting the experimental data than the optimal controller, both controllers captured the general trends of the subjects in the task and the results were within the uncertainty of the experimental data. It was not in our interest to replicate the experimental data exactly. Here we used these calculated outputs to determine if the controller could in general behave similar to the subject.

Reaching Distance and Reaching Time

While the A matrix and the stability multipliers provided insight on the structure of the inter-trial controller and the dynamic stability of subject performing the task, the

reaching distance and reaching time provided metric to evaluate the integrity of the optimal and suboptimal controller. The raw reaching distance vs. reaching time is shown Figure 33 and Figure 34.

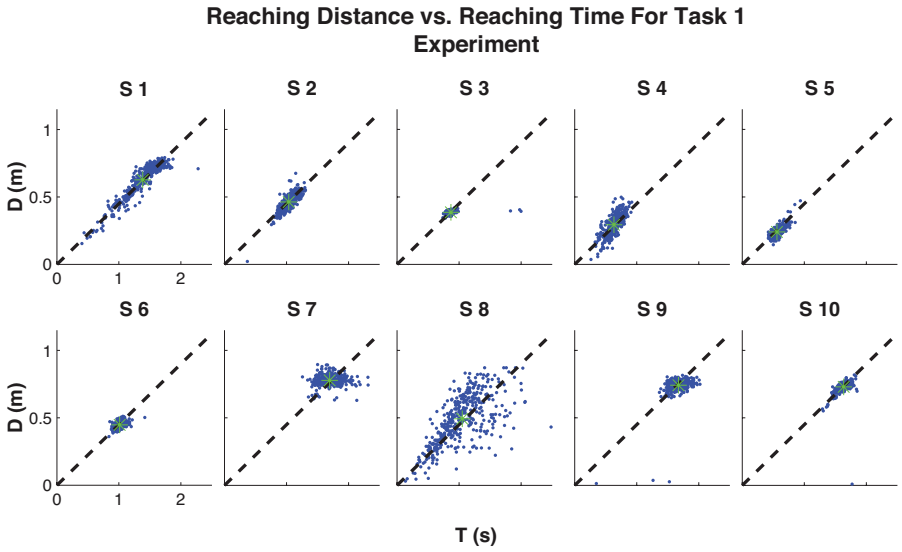

Figure 32: The reaching distance vs. reaching time for all 10 subjects during the experiment Task 1. The dash line (--) indicates the goal specified for the task.

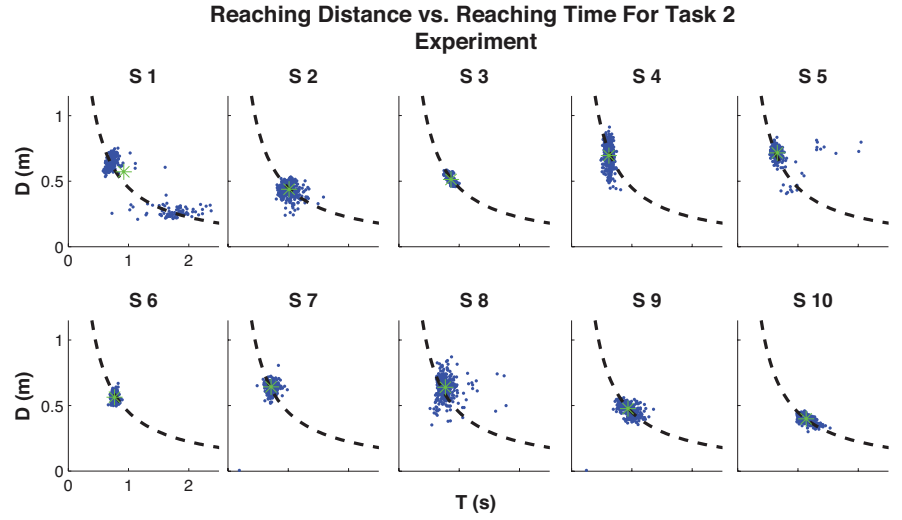

Figure 33: The reaching distance vs. reaching time for all 10 subjects during the experiment for Task 2. The dash line (--) indicates the goal specified for the task.

Figure 34 shows the bootstrapping data and the experimental results for Task 1 and Task 2. Overall, the data suggested that subjects consistently achieved the same mean reaching distance and time (Figure 34). This was consistent for both Task 1 and Task 2.

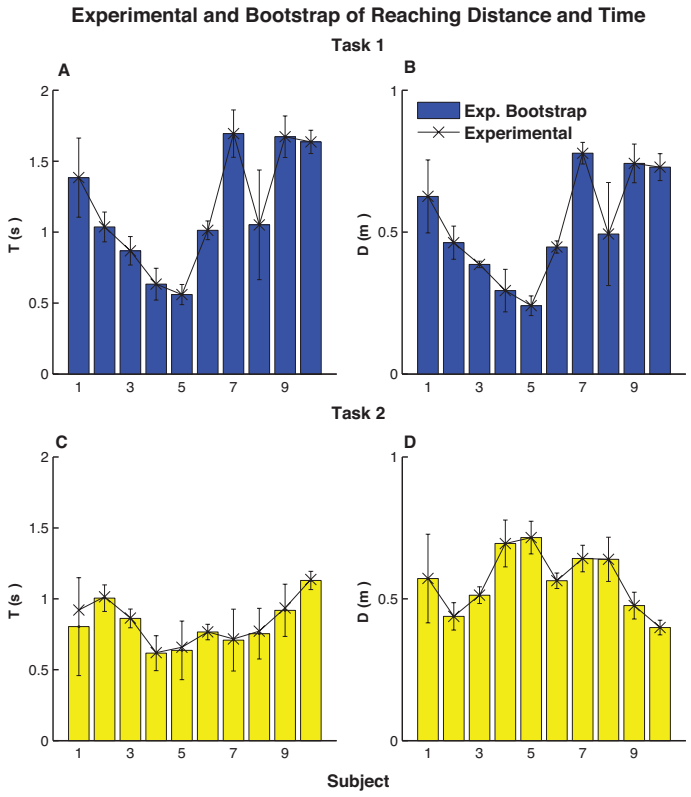

Figure 34: Plot of the each subject's experimental reaching distance (D) and reaching time (T) for (A-B) Task 1 and (C-D) Task 2. The mean and standard deviation of the bootstrap data are also shown.

The most basic comparison of the validity of the model was whether the model could capture the mean of the reaching time and distance. Here we looked at the mean reaching distance and time of the optimal and suboptimal model and evaluate how effective they were at reproducing the mean of the reaching time and distance. Here the average of 30 trials was calculated and each trial contains 400 reaching movements. The results shown in Figure 35 indicated that the model consistently generated the mean

reaching distance and time for each subject. For most subjects, the optimal and suboptimal results were very similar.

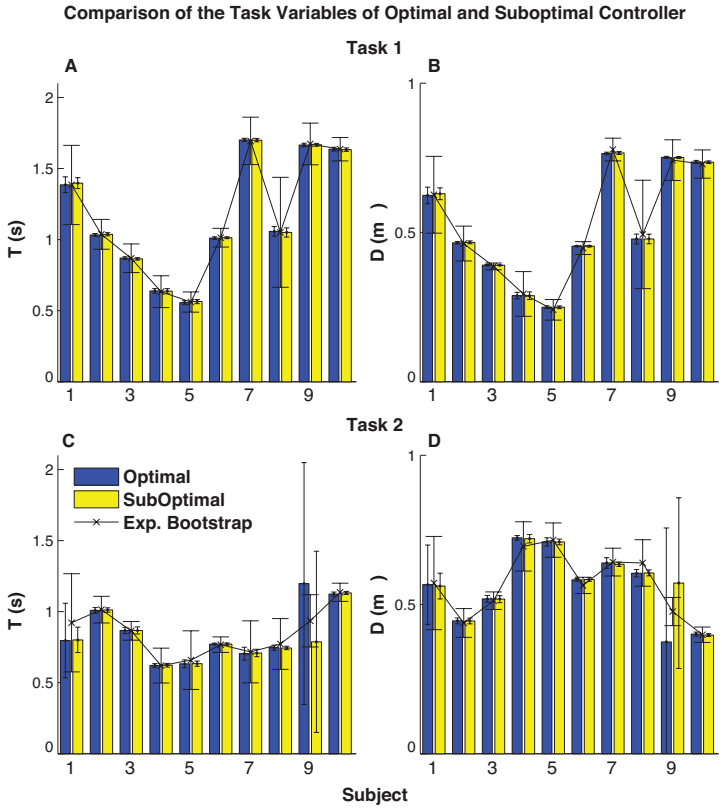

Figure 35: Comparison of the reaching distance and time of the optimal and suboptimal controller for Task 1 (A-B) and Task 2 (C-D).

Lastly we examined the linear correlation from the generated movement from the inter-trial controller for the reaching distance and reaching time and evaluate whether the controllers were capable of exhibiting similar behavior displayed by each subject in the experiment.

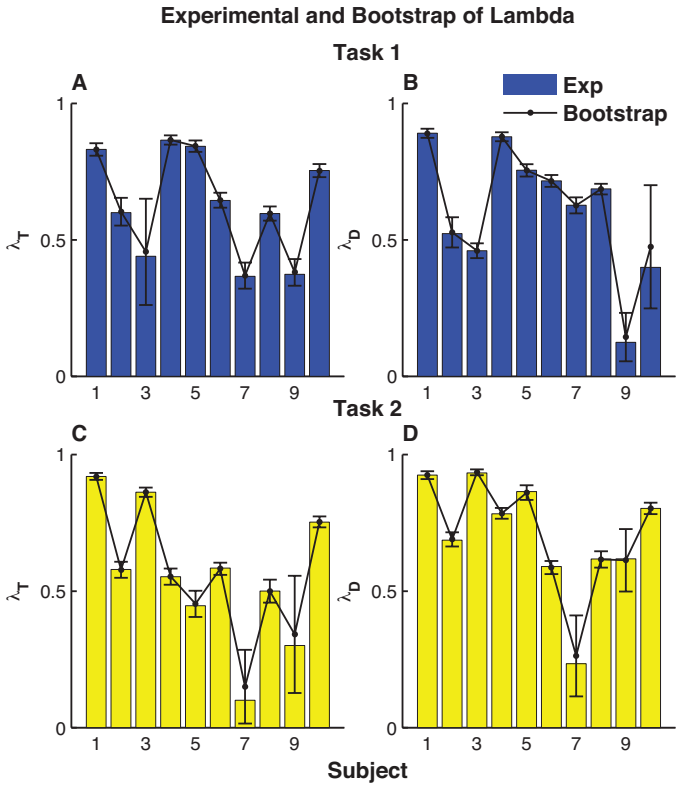

Figure 36: Experimental and bootstrap results Task 1 (A-B) and Task 2 (C-D).

Overall, the bootstrapping of the movement to movement was very consistent throughout the trial (Figure 36). The λ accounts for the correlation in reaching distance and reaching time separately. The results for the optimal and suboptimal as compared to the experimental data are shown in Figure 37 below.

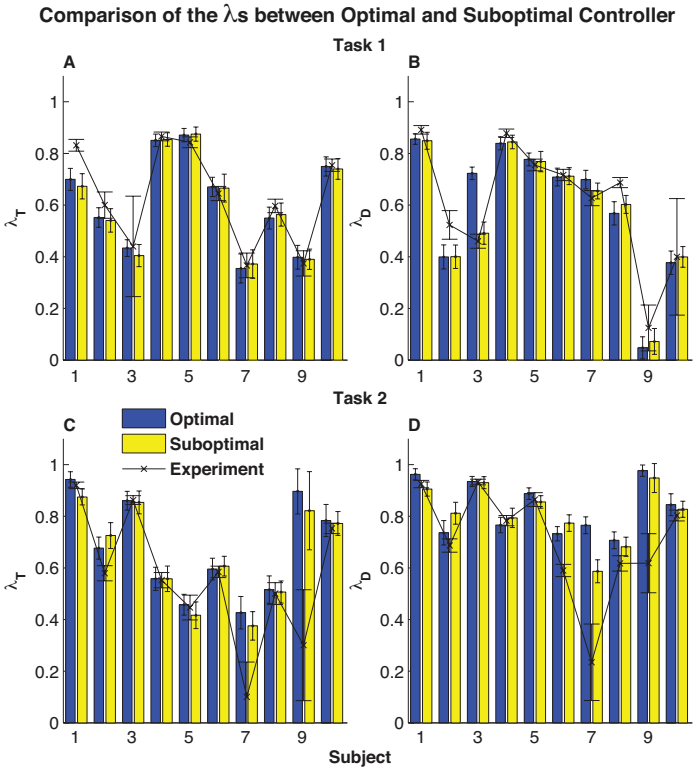

Figure 37: Comparison of the lambdas estimated by the suboptimal and optimal controller versus the experimental data for Task 1 (a-b) and Task 2 (c, d).

Overall for Task 1, the optimal and suboptimal did a pretty good job of capturing the linear correlation for the reaching and reaching time. Furthermore, the controllers were able to estimate lambdas within the uncertainty of the experimental model. Our intent here was not to *replicate* the experimental data exactly; however these results showed that the models, in general, were able to parse the unique differences in reaching strategy between subjects. For Task 1, there was one instance (subject 3) where the suboptimal controller $\left(\lambda_{D,3,subopt} = 0.4912 \ \pm 0.0430\right)$ did a significantly better job then optimal controller $\left(\lambda_{D,3,opt} = 0.7230 \ \pm 0.0241\right)$ in estimating the experimental data linear correlation (Figure 37b).

Even though Task 2 was less intuitive, both controllers seemed to capture the movement-to-movement correlation of the reaching distance and reach time across

subject. Furthermore, the optimal and suboptimal models generated similar λ's for both the correlation in the reaching time and reaching distance. However, there were subjects where neither controller performed as well against the experimental data: Subject 7 and 9. For example, the average λ for the optimal and suboptimal controller of the reaching time for subject 7 $\left(\bar{\lambda}_{T,7,con} = 0.401 \pm 0.0591\right)$ was significantly larger than the experimental data $\left(\bar{\lambda}_{T,7,\exp} = 0.100 \pm 0.135\right)$. Similarly, The average λ for the optimal and suboptimal controller of the reaching distance for subject 7 $\left(\bar{\lambda}_{D,7,con} = 0.676 \pm 0.0385\right)$ was significantly larger than the experimental data $\left(\bar{\lambda}_{D,7,\exp} = 0.2344 \pm 0.1482\right)$. These were similar to subject 9.

Goal Manifold Variation (δ_T & δ_P)

The reaching distance and reaching time analysis examined the correlation in the task variables; however, it did not address the fluctuations along or perpendicular to the goal manifold. δ_T and δ_P denoted the coordinates tangential and perpendicular to the GEM, respectively. The dynamics of these coordinates provided further insights on whether subjects exploit the redundancy inherent in these tasks. The time series for the tangential and perpendicular direction were calculated using Eq. 47 and 48.

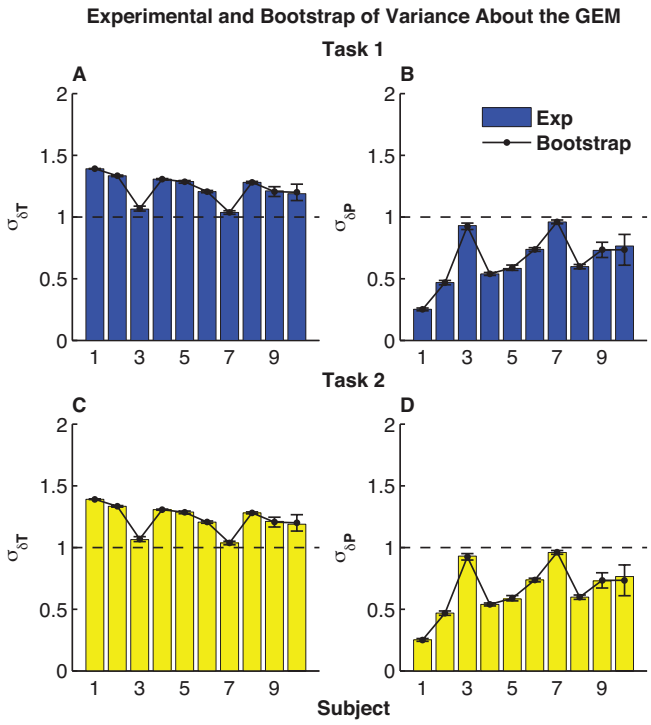

Figure 38: Comparison between the bootstrap and experimental data for the standard deviation of the fluctuation in the direction perpendicular (δ_P) and along (δ_T) the goal manifold for (A) Task 1 and (B) Task 2.

Figure 38 shows the results from the bootstrapping of the experimental data set. Here the standard deviation was normalized to unit variance (Dingwell, John et al. 2010; Dingwell, Smallwood et al. 2013); therefore, the results were compared relative to a standard deviation of 1. Overall, results from the bootstrapping indicated that the fluctuations exhibited by subject were consistent with the experimental data across the 400 reaching movements.

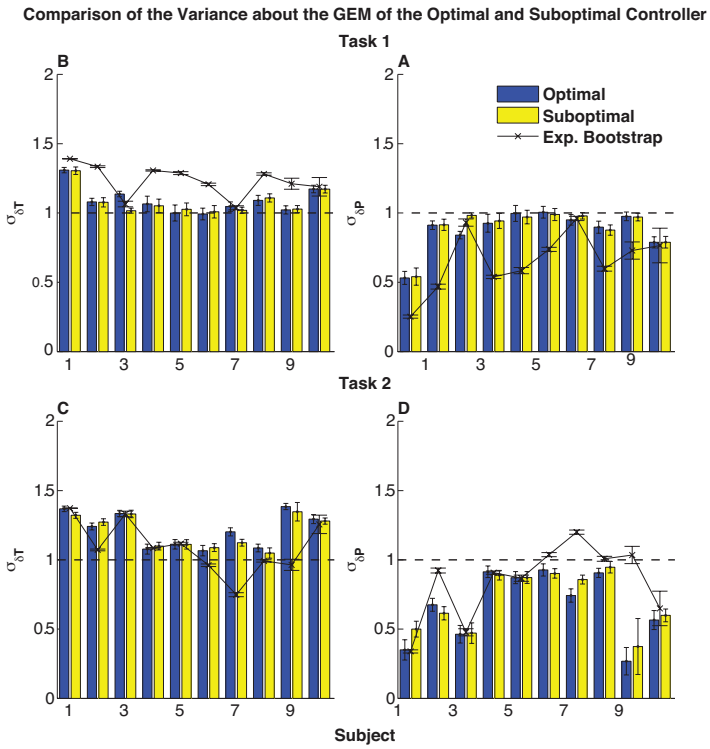

Figure 39: Comparison of the variance using the optimal and suboptimal controller versus the experimental data set for (A) Task 1 and (B) Task 2.

Figure 39 the fluctuation in the deviation in the tangential and perpendicular direction about the GEM during the performance of Task 1 (A-B) and Task 2 (C-D). The results indicated that there were no significantly differences between the optimal and suboptimal control for both tasks. Since we did not expect the model to *replicate* the time series of the reaching distance and reaching time exactly, but only estimate the dynamics, we did not expect the fluctuation to be closely matched. On average, we expected the model to accurately predict the average reaching distance and reaching time, the fluctuations along and perpendicular to the GEM were more difficult for the model to enforce. However, for most subjects, the model did a pretty good job of estimating the variance with respect to 1. For example, for Task 1 σ_{δ_T} was greater than one and σ_{δ_P} was less than 1 for the output from both controllers and the experimental data (Figure 39

A-B). Both controllers captured that subjects were more variable along the direction tangential to the GEM and less variable in direction perpendicular to the GEM.

Similarly for Task 2, both controllers also captured the general dynamics along and the perpendicular to the GEM. In general, most subjects were more variable in direction tangential to the GEM and less variable in the direction perpendicular to the GEM. For Task 2, the fluctuation of subject 7 and 9 were more difficult to capture than other subjects. For subject 9, both controllers predicted the subject would be significantly less variable ($p<0.005$) (Figure 39 D). However, the overall results demonstrate that these controllers were capable of estimating the general deviation along the GEM.

While the standard deviation of δ_P and δ_T showed the variability of subjects in the direction tangential and perpendicular to the GEM, it did not provide any detail on the movement to movement dynamics. Therefore, the λ's in the δ_P and δ_T direction were calculated to provide insights on the correlation from movement to movement.

The bootstrapping results of the λ_{δ_P} and λ_{δ_T} for both tasks are shown in Figure 40. In general, the data set were consistently structured across the 400 reaching movements for Task 1 and Task 2. During Task 2, the experimental data show that subject 7 displayed correlations that were significantly different than other subject. Similar to subject 7, subject 9 correlations about the perpendicular direction were close to zero.

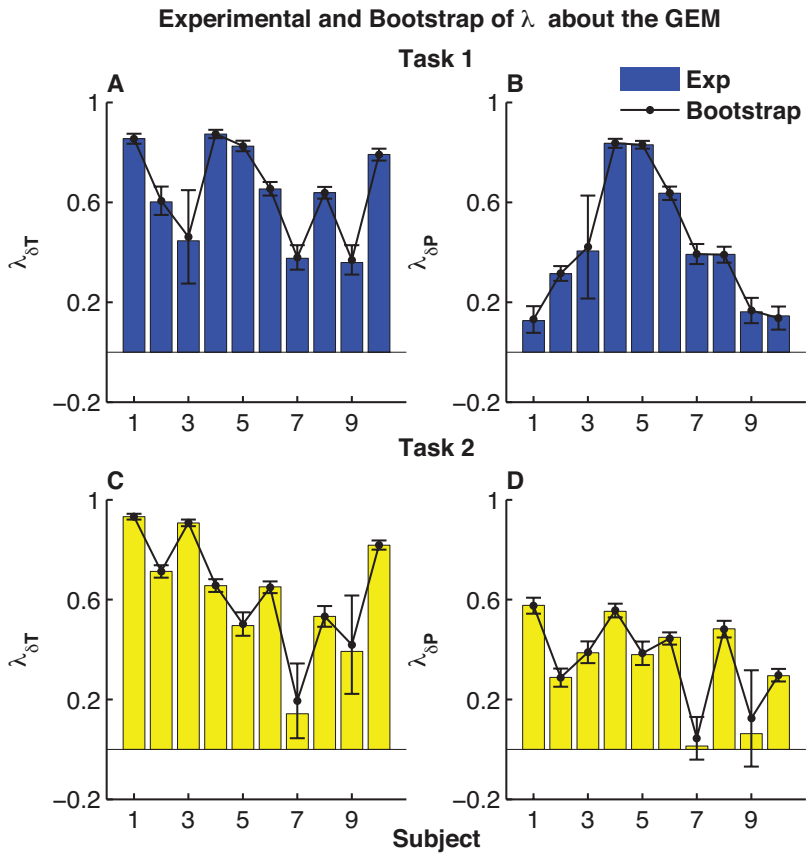

Figure 40: The comparison of the lambdas of the tangential $\left(\lambda_{\delta_T}\right)$ and perpendicular $\left(\lambda_{\delta_P}\right)$ direction to the goal manifold for (A) Task 1 and (B) Task 2.

Figure 41 shows the estimation of the optimal and suboptimal controllers of the movement to movement correlation for Task 1 and Task 2. The results showed that, in general, there were no significant differences between the optimal and suboptimal controllers. These two controllers, on average, captured the movement to movement correlation for most subjects. These trends were consistent for all subjects during Task 1 and Task 2.

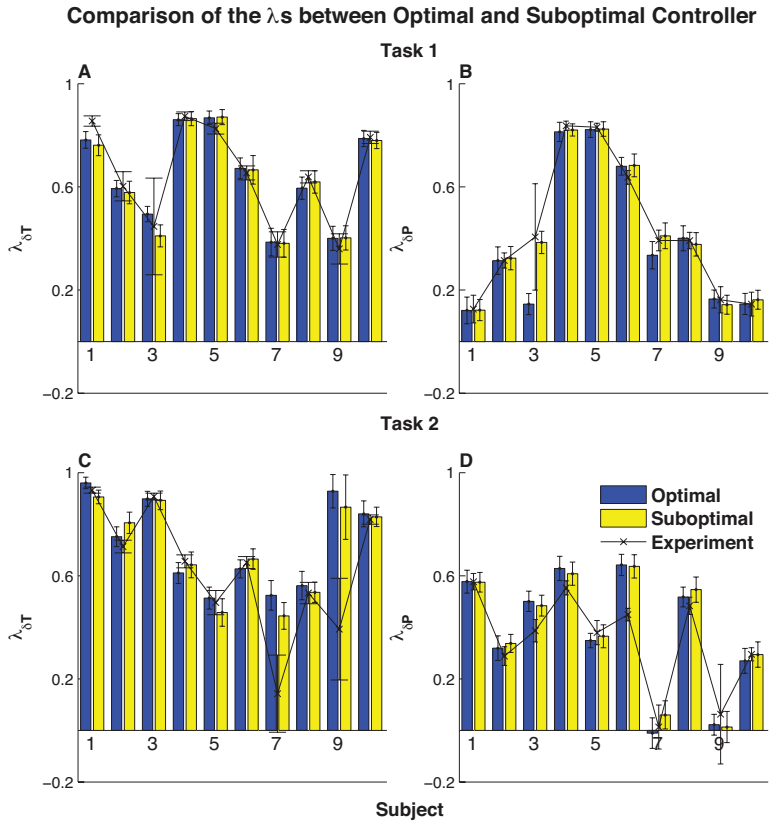

Figure 41: Comparison of the linear correlation in the tangential (λ_{δ_T}) and perpendicular (λ_{δ_T}) direction for (A) Task 1 and (B) Task 2 between the optimal and suboptimal inter-trial controller.

Overall, the optimal and suboptimal controller performed well against the experimental data. While they did not replicate the experimentally data on every calculated outputs; these two controllers did captured the distinct behaviors exhibited by the experiment.

DISCUSSION

Redundancy is inherent in every task (Bernstein 1976). Everyday, people execute these tasks almost flawlessly and briskly; yet never exactly. Yet, seldom do they consider the complex control mechanisms that allow them to perform these tasks with repeated accuracy. Redundancy is not a problem, but rather an opportunity for multiple control mechanisms embedded in the human system to work harmoniously to exploit the redundancy in the task. Yet, the architecture that lays out these control mechanisms still remains relatively unknown. Even for a simple task such as reaching, extensive research has been done on how the central nervous system regulates and executes this task (Karniel and Inbar 1997; Nishikawa, Murray et al. 1999; Olivier 2006; Wininger, Kim et al. 2009; Mistry, Theodorou et al. 2013). While experimental and mathematical approaches have been proposed to understand how the redundancy *problem* is solved (Yang, Scholz et al. 2007; Abe and Sternad 2013); here we propose an approach that might explain how people *exploit* the redundancy in the task to execute the task.

For example, when reaching at a constant frequency (Gates and Dingwell 2008), there is an infinite combination of reaching speeds (S) and distances (D) that will achieve this goal, so long as D/S =T. Subject can make fast and long reaching movement or short and slow reach movement, both scenarios would maintain the same movement time. As the nervous system finds the desired speed and distance, the variability in the direction of the task-relevant space was minimized while the task–irrelevant variability was not. Variation in the direction of the task-irrelevant space has no effect on the goal of the task. The results show strong tendency for subjects to align themselves with the GEM. The study suggested that controlling for the GEM could be a strategy subjects used to counter fatigue during task. Therefore, there is implication that resolving redundancy is not solely about solving the problem, but how to use redundant to improve performance.

Furthermore, experimental results (Latash, Scholz et al. 2001; Cusumano and Cesari 2006; Dingwell, Smallwood et al. 2013) have shown that people are able to learn and exploit the redundancy within the task (see Chapter 4) to find the goal manifold and

increase performance (Muller and Sternad 2009). People were more variable in the direction along the task (indicate *less* control) and less variable in the direction perpendicular to the task (indicate *more* control) (Todorov 2004). However, the experimental results alone do not provide insight on the specific possible control strategy that individual employ to exploit the inherent redundancy within the task to increase their performance. In this study, a mathematical model of the inter-trial controller was extended to provide further insight on the strategy adopted by each subject. Here the results from the experimental data were used to evaluate whether this architecture of the inter-trial control can estimate the dynamics exhibited by the subjects experimentally.

The inter-trial control estimates the movement to movement dynamics during the task. The structure of the inter-trial controller was designed to accommodate certain features observed in redundant reaching task (Dingwell, John et al. 2010). First, people could perform the task by finding a point on the goal manifold and *stay* there for the duration of the trial. Second, subject could exploit the redundancy inherent in the task and display solution along the goal manifold. Third, subject could ignore the GEM and perform the task in a different but effective manner with respect to the goal of the task. However, even in the last case, there is flexibility in the inter-trial controller to account for other strategies adopted by subject.

Strategic Differences

Task 1

The results from our simulation showed that the inter-trial controllers (both optimal and suboptimal) captured the general dynamics exhibited by each subject from movement to movement. However, it is still unclear what insights can we extract about the subject's strategy during the performance of the task. Does the structure of the controller derived from the optimization process tell us any thing about the strategy adopted by each subject? Experimental data have demonstrated that subjects learned and exploited the redundancy in the task (Dingwell, Smallwood et al. 2013). Here, we

summarize the results from a few select subjects to hypothesize the possible control strategy adopted by each subject.

The figure below shows the experimental reaching distance and reaching time for three selected subjects during the performance of Task 1.

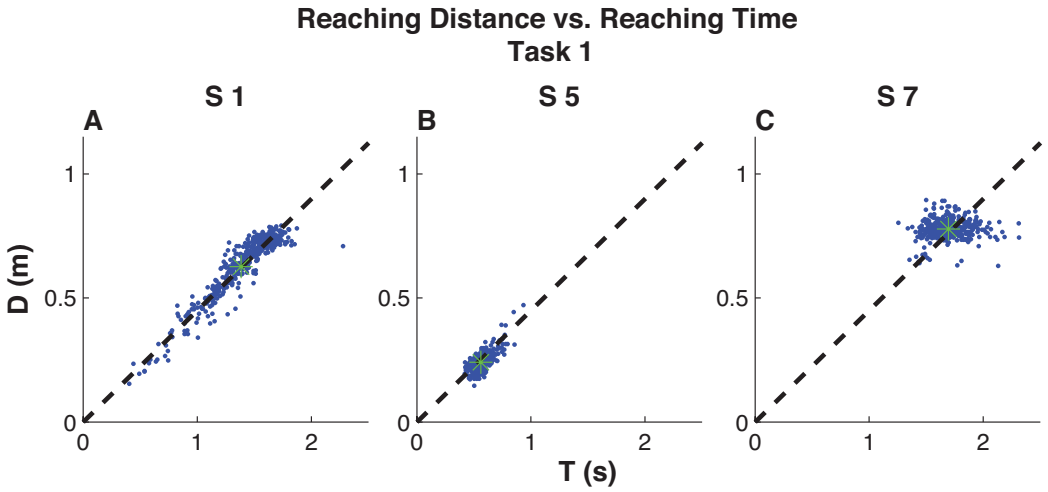

Figure 42: Experimental reaching distance (D) vs. reaching time (T) for three selected subject. Each subject displayed unique behavior during the performance of the reaching task.

From the spread of the data set, we can see that subject 1 (S1) was significantly more variable than subject 5 (S5) and subject 7 (S7). S1 was clearly finding other solutions on or around the goal manifold. S5 data spread showed a more concentrate reaching solution. While S5 solutions were still along with the GEM; the solutions were less variable in the direction along the GEM. It is difficult from observation of the data set alone of S7 to determine the possible strategy employ by this subject during the performance of the task. While the objective of the task was achieved (movements combination on or near the solution manifold), the subject's reaching solutions clearly did not align along the GEM, indicating possibly that S7 ignored the GEM or did not exploit the inherent redundancy in the task. These were some of the features we can identify by looking at the experimental data. How do these data translate to the parameter of the optimal and suboptimal controller?

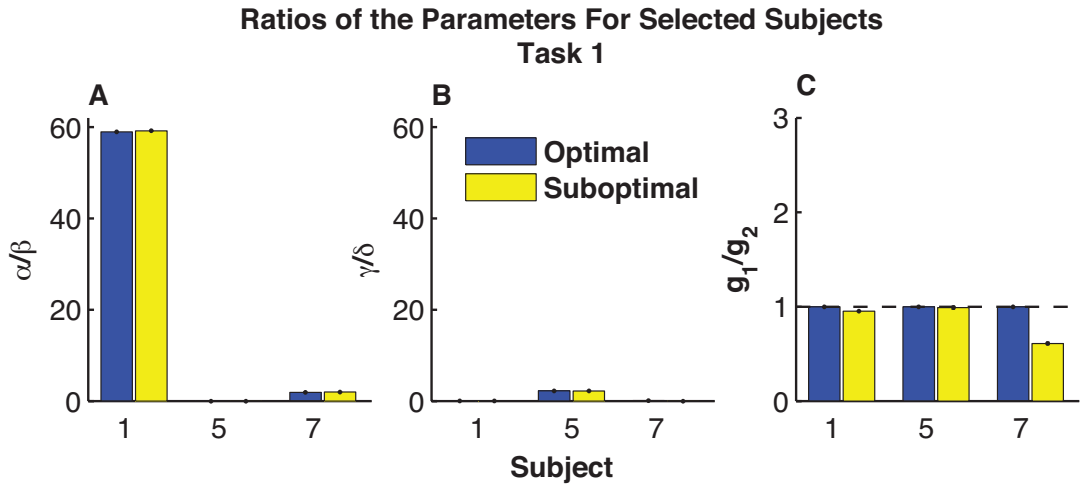

Figure 43: The ratios of the parameters for three selected subject for Task 1 from both the optimal and suboptimal controller. The raw values of the gains were close to 1. By definition, the optimal gains ≡1.

The ratio of the gain indicated that these subjects were operating at or near optimal with respect to the cost function of the controller $\left(g_1 / g_2 \approx 1\right)$. The controller for S1 indicated a larger α/β $\left(\overline{\alpha}_1 = 17.862 \pm 2.833, \overline{\beta}_1 = 0.303 \pm 0.048\right)$ and a smaller γ/δ $\left(\overline{\gamma}_1 = 0.521 \pm 0.083, \overline{\delta}_1 = 12.552 \pm 1.986\right)$ ratio. This was possibly achieved by strongly adjusting the reaching time and weakly adjusting the reaching distance. This was evident when examining the values of the A matrix which correlated the movement to movement fluctuation about the preferred operating point. For S1, the fluctuation $\left(\varepsilon_k\right)$ was strongly correlated by the current reaching time $\left(T_k\right)$ when comparing with other elements in the matrix. Furthermore, if we calculate the normalized standard deviation ratio in the direction along and perpendicular to the GEM for S1 $\left(\sigma_{1,\delta_T} / \sigma_{1,\delta_P} = 5.510\right)$, it was higher than for S5 $\left(\sigma_{5,\delta_T} / \sigma_{5,\delta_P} = 2.202\right)$ and S7 $\left(\sigma_{7,\delta_T} / \sigma_{7,\delta_P} = 1.080\right)$. From these data, we can conclude that S1 clearly learned and performed the task well. S1 also exploited the redundancy in the task and was adept to finding other solutions on the manifold. The ratio of the variance also indicated a clear structured variance along the GEM.

Experimental approach such as UCM, has long argued that these structured variances indicate the controlling mechanism during the performance of the Task (Scholz, Schoner et al. 2000; Black, Smith et al. 2007; Yang, Scholz et al. 2007).

$$A_1 \approx \begin{bmatrix} -0.746 & 0.013 \\ 0.063 & -0.236 \end{bmatrix}, \quad A_5 = \begin{bmatrix} -0.111 & 0.000 \\ 0.000 & -0.219 \end{bmatrix}, A_7 = \begin{bmatrix} -0.613 & 0.014 \\ 0.000 & -0.332 \end{bmatrix} \tag{50}$$

However, these controllers provided a significantly different control structures for S5 $\alpha/\beta = 0$ $\left(\bar{\alpha}_5 = 0.000 \pm 0.000, \bar{\beta}_5 = 2.526. \pm 0.760\right)$ and a relatively larger γ/δ $\left(\bar{\gamma}_5 = 18.680 \pm 6.250, \bar{\delta}_5 = 8.341 \pm 2.800\right)$ ratio. From the spread of the data for S5, the data suggested that S5 was aligning their reaching distance and reaching time along the GEM and the relative larger variance indicates some control in the direction perpendicular to the GEM. However, the estimations from the controllers suggested that subjects were not actively correcting for deviation about the GEM and mildly favoring a preferred operating point. S5, exhibited similar structured data like S1; however, the controllers did not capture similar dynamics. Such discrepancies between the structured data and the model structure emphasized the value tool of using mathematical model to provide further insights on the true dynamics of the system and cautious on using variance to identify control. Furthermore, examining the A matrix for S5, it showed an uncoupling between the reaching distance and reaching time because the off diagonal element was approximately zero. In addition, there were relatively weak correlations between reaching distance and reaching time. The optimal and suboptimal controller should have captured the same control architecture as S1 if S5 was performing the task with similar movement to movement dynamics as S1.

The data from S7 was more skewed about the GEM. S7 had a variance ratio of approximately 1, which meant that variation along the GEM was similar to variation perpendicular to the GEM. However, the data set did lie near or on the GEM (Figure 42). The controllers estimate an $\alpha/\beta \approx 1.965$ $\left(\bar{\alpha}_7 = 4.023 \pm 2.382, \bar{\beta}_7 = 2.055 \pm 1.218\right)$ and a relatively smaller γ/δ (≈ 0.068) values $\left(\bar{\gamma}_7 = 0.729 \pm 0.433, \bar{\delta}_7 = 10.763 \pm 6.398\right)$. The α

and β value indicated that the subject was not aware of the goal manifold, but the subject was not strongly exploiting the redundancy in the task. The subject could be exploiting these task spaces by randomly moving randomly near or on the GEM. The A matrix provided further evidence that the subject was not compensating for the reaching distance and reaching in a way that demonstrate the exploitation of the redundancy inherent in the task. The larger δ showed that there was very weak coupling in the reaching distance and time with the fluctuation in the deviation about the preferred operating point. The off diagonal matrix was approximately zero, while the diagonal matrix was relative strong. This indicated an independent correction for the reaching distance and reach time. Subjects could be correcting for error by adjusting reaching time and reaching distance from movement to movement but seldom in conjunction to find the solution about the manifold.

Task 2

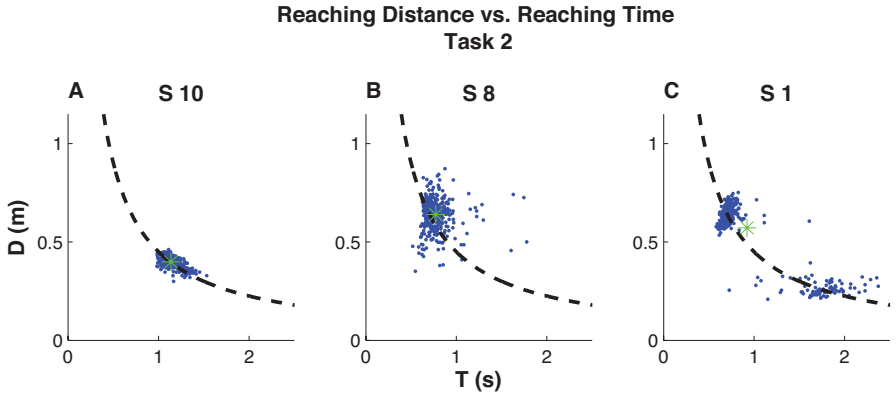

Figure 44: Reaching distance and time of three selected subjects. These subject displayed different data distribution during the performance of Task 2.

Similar to Task 1, we examined three subjects who exhibited different behavior during the performance of the task and analyze how the structure of the controller could provide more insights on how subjects resolved the redundancy in the task. Figure 44 shows the reaching distance and reaching time for these selected subjects. While Task 2 was less intuitive than Task 1, analysis of the experimental data showed that subjects

were able to learn and perform the task well. For all three subjects, when the parameters of the controller were found by allowing all six parameters to change, all three subjects trended toward suboptimal. While the task might have influenced these subjects to perform in the task in a different way, their calculated outputs from the optimal and suboptimal controller were similar.

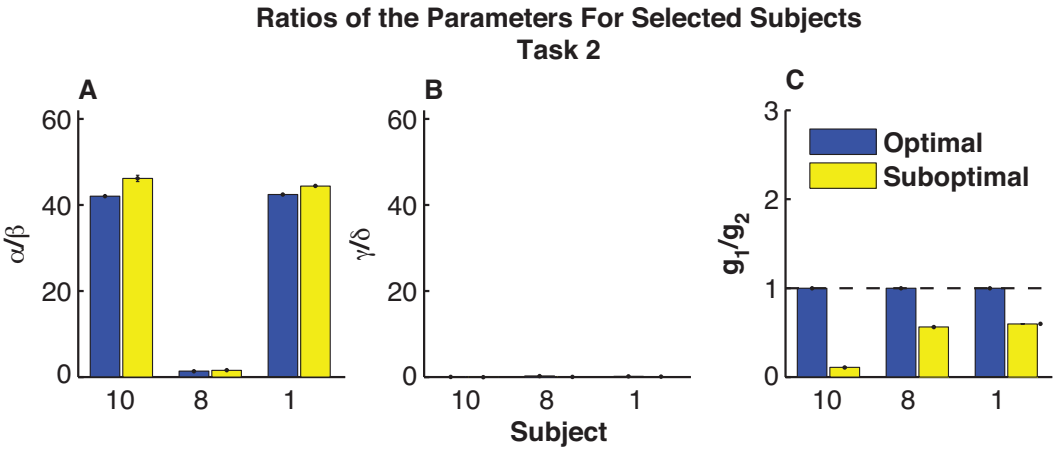

Figure 45: Ratios of the parameters of the optimal and suboptimal controller for selected subjects during the performance of Task 2.

From the data distribution (Figure 44a), S10 reaching distance and reaching time aligned along the GEM. The ratio of the variance along the tangential and perpendicular was slightly larger than 1 $\left(\sigma_{10,\delta_T} / \sigma_{10,\delta_P} = 1.554\right)$. Both controllers (Figure 45A) generated a control structure that indicated that the subject was aware of the GEM and performed the task with respect to the GEM $\alpha = \left(\bar{\alpha}_{10} = 11.638 \pm 2.698\right)$ and $\beta = \left(\bar{\beta}_{10} = 0.269 \pm 0.0625\right)$. These controllers suggested that the subject was correcting in the direction perpendicular to the GEM. Therefore, S10 was more variable in the direction along the GEM and less variable in the direction perpendicular to the GEM. Furthermore, these controllers suggested a very small γ/δ ratio $\left(\bar{\gamma}_{10} = 1.444 \pm 0.551, \bar{\delta}_{10} = 9.709 \pm 2.255\right)$. Eq. 51 shows the average A matrix from the suboptimal controller. For S10, there were coupling between the reaching distance and

reaching time. The distance fluctuation was positively correlated to reaching time and negatively correlated to reaching distance.

$$A_{10} = \begin{bmatrix} -0.409 & 0.014 \\ 0.128 & -0.380 \end{bmatrix}, \quad A_8 = \begin{bmatrix} -0.473 & 0.008 \\ 0.009 & -0.312 \end{bmatrix}, A_1 = \begin{bmatrix} -0.613 & 0.014 \\ 0.000 & -0.332 \end{bmatrix} \tag{51}$$

The ratio of the variance in the direction tangential and perpendicular direction for S8 was relatively larger than for S10 $\left(\sigma_{8,\delta_T} / \sigma_{8,\delta_P} = 2.172\right)$ but the data set was not as aligned along the GEM as S1. Based on the variance, it would suggest that S8 was controlling for fluctuations the direction perpendicular to the GEM and loosely controlling for deviations about the GEM. However, the structure of the suboptimal and optimal controllers suggested a slightly different control strategy.

Figure 45 shows the α/β $\left(\bar{\alpha} / \bar{\beta} = 1.485 \pm 0.006\right)$ for S8 was significantly smaller than S10 $\left(\bar{\alpha}_8 = 3.689 \pm 1.948, \bar{\beta}_8 = 2.4765 \pm 1.305\right)$. Furthermore, there were no significant differences between the α's and β's for S8. This indicated that while the S8 was correcting for deviation perpendicular to the GEM; the subject was also gravitating toward a preferred operating point and find the solution near or around this point. Furthermore, based on the γ/δ $\left(\bar{\gamma} / \bar{\delta} = 0.138 \pm 0.000\right)$ ratios, the A matrix indicated no coupling between the fluctuation about the POP and the reaching distance and reaching time (Eq. 51). The correlation matrix indicated that S8 was adjusting for the variation from movement to movement by manipulating the reaching distance and reaching time independently. This demonstrated that while the variance in the tangential and perpendicular direction could give some indications of what was controlled during the task; the structure of the control and the correlation matrix provided further insight on how the subjects generated the structured variance.

While most subjects demonstrated a cloud of data distribution, S1 showed the most peculiar data distribution attributing to the double clouds of data along or near the (Figure 44 C). The ratio of the variance in the direction tangential and perpendicular to

the GEM $\left(\sigma_{1,\delta_T} / \sigma_{1,\delta_P} = 5.517\right)$ was relatively larger than S8 and S10. Based on the variance, it would strongly suggest that the subject was correcting for deviation along the perpendicular to the GEM while loosely correct for deviation along the GEM. Furthermore, it indicated that this subject adeptly exploited the solution manifold during the performance of the task. Both the optimal and suboptimal controller generated a control structure with larger α/β $\left(\overline{\alpha} / \overline{\beta} = 44.120 \pm 0.367\right)$ and smaller γ/δ ratio $\left(\overline{\gamma} / \overline{\delta} = 0.024 \pm 0.000\right)$. Similar to S8, there were no coupling between the reaching distance and reaching time Eq. 51.

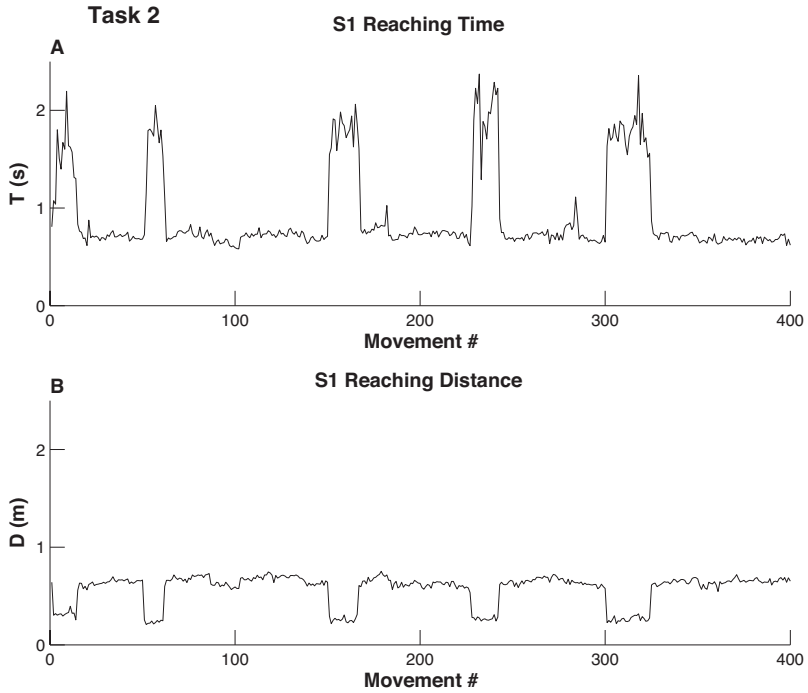

Figure 46: Time series of the reaching distance and reaching time for S1 during the performance of Task 2.

While both controllers hypothesized the subject was exploiting the inherent redundancy in the task; however, the controllers and the variance could not capture how the subjects manipulate his/her reaching distance and reaching time. Figure 46 shows the time series for the reaching distance and reaching time. From the time series, it was clear

that this subject was jumping between the two different points on the goal manifold to improve his/her performance of the task.

Optimal vs. Suboptimal

Based on the dynamics metrics and the calculate outputs there were no significantly differences between the optimal and suboptimal controller across all subjects for both Task 1 and Task 2. In general, both controllers perform well in estimating the experimental data, except for estimation the σ's. However, across the 10 subjects modeled, only subject 3 (S3) demonstrated that the estimation from the suboptimal controller was significantly better than the estimation from the optimal controller during the performance of Task 1. Given the flatness of the solution space and subject were assume to be "optimal" during the initial search; it is possible that the model was not able to find *better* solutions.

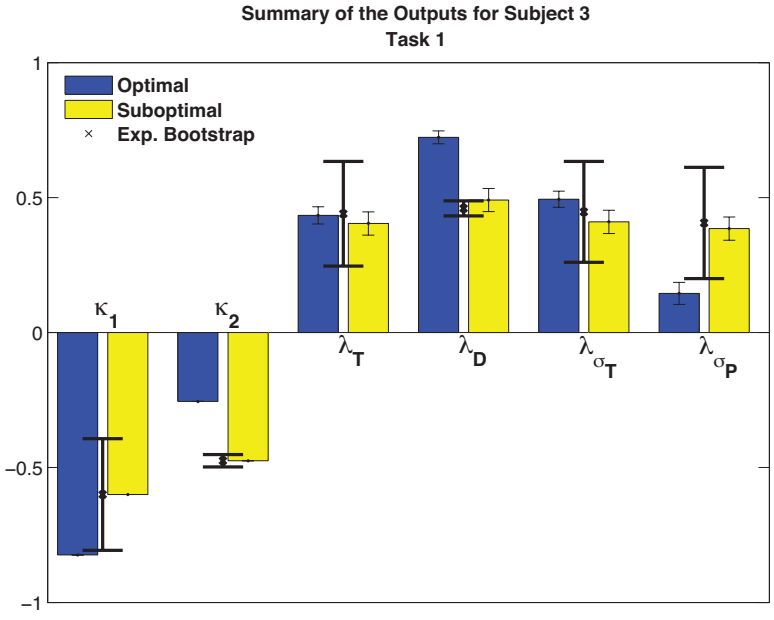

Figure 47: Summary of the calculated outputs from the optimal and the suboptimal controller as compared to the experimental data for Task 1.

Figure 47 shows the summary of the out for S3 from the optimal and suboptimal controller as compared to the experimental data. There were instances where the

suboptimal controller did a better job of fitting estimating the experimental data $\left(\kappa_2, \lambda_D \ \lambda_{\sigma_P}\right)$ while showing no significant differences for other metrics. It is possible that S3 was performing suboptimal with respect to the cost function while still achieving the objective of the task. There was no a priori notion that the subject would perform the task optimally with respect to the cost function. Since no specific information was given to the subjects on what was the task; these subject were free to experiment with different reaching strategy as long as the objective of the task was achieved.

CONCLUSION

From the experimental data, we know that subjects can learn and exploit the inherent redundancy in the task. Given a task, whether intuitive (Task 1) or not (Task 2) subjects were able to find solution on the goal manifold; however, it did not reveal how each individual subject found these solutions. Our results demonstrated that strictly looking at how the variance or other experimental measurements are structured could provide a false interpretation of the actual dynamics that are active during the task. Furthermore, such experimental approach would not be sufficient to capture the movement to movement fluctuation. While the model the controller presented here does not represent all possible mechanisms that might be active during the reaching task, it sufficient to provides deeper insights on what each subject might be doing during the performance of the task. All our results indicated that these models were able to estimate the movement dynamics that were happening during the performance of the task.

Under ideal experimental condition, we expect the model to accurate predict the movement to movement dynamics during the task; however, given that subject were not instructed to do anything other than improve their reaching performance, it is possible that subject were doing something that could be accounted for by this model. However, looking across the totality of many calculated measures, these models could confidently estimate the general subjects adopted to learn or resolve the redundancy inherent in the task.

The results demonstrate the strength in using the inter-trial controller to estimate the dynamic of subject performing redundant reaching task. In this study, the models only optimizes the correlation matrix of experimental data; therefore, there were no constrains on the outputs. However, the controllers show extreme consistency in predicting the calculated outputs. From these results, we believe that the structure of the inter-trial control provide us with an important tool in understand how people perform redundant task from one movement to the next.

Chapter 6: General Discussion and implications

These studies have provided important insights on the effect of noise and control on the redundant task. In the first study, the premise was to understand how simple control minimizes the effect of noise during a redundant task. In this case, understand where to apply control could provide guidance on how rehabilitation process could be designed to minimize energy cost while increasing performance. In the second study the objective was to determine how might the nervous system controls and regulates movement in the presence of noise during a redundant task. Noise is inherent in motor control system; therefore, minimizing noise alone is wasteful and counterproductive task. The nervous system constantly demonstrate its perfection around us by silently exploiting and using noise to solve the redundancy that are presence in our daily world. Therefore, how movements are coordinated and regulated can provide tremendous insight on how rehabilitation devices and process could be designed and develop to slowly assimilated people back to daily living activities.

According to the World Health Report(2002), stroke is the leading cause of serious, long term disability in the United State as well as in Europe. With the increase in life expectancy and obesity rate, stroke occurrence is predicted to increase by 25% by 2025(Heidenreich, Trogdon et al. 2011). Stroke survivors suffer long-term physical and cognitive impairment as a consequence of stroke. With the residual disability experienced by stroke survivors, neuro-rehabilitation is critical in reducing the need for dependent care and minimizing the long-term effect of stroke by promoting independence in activities of daily living (ADL). One of the goals of neuro-rehabilitation is the recovery of motor impairment and reintegration of survivors into ADL. Traditionally, survivors undergo hours of physical therapeutic exercise with physical assistant to regain lost motor function; however, such intensive process can be financially costly. Since 1980, robotic-assisted rehabilitation has been promoted as a cheaper and more effective approach to traditional rehabilitation. Current studies (Picelli, Melotti et al. 2012; Vaney,

Gattlen et al. 2012; Wu, Yang et al. 2012; Moreno, Barroso et al. 2013; Zhang, Davies et al. 2013) have shown that robotic-assisted rehabilitation do not provide significantly advantages over traditional approach; however, advances in motor control could provide more effective robotic-assisted devices for clinical application. While the advances of robotic has far exceeded the current technology employed for rehabilitation; the technological bottle neck is not in the technology, but in the deployment of these technologies. Without the neural roadmap, current clinical design cannot provide the technological leap beyond traditional and tested approach.

Beyond the emotional and cognitive impairments suffered by stroke survivors, physical impairments such as: reduced muscle power, reduced joint stability and or mobility, balance impairment and altered gait pattern. Many advances have been made in motor control and rehabilitation to precipitate motor recovery. Numerous studies on gait pattern during rehabilitation(Sale, De Pandis et al. 2013; Zhang, Davies et al. 2013) (Hasan, Park et al. 2009; van Swigchem, Weerdesteyn et al. 2011; Wang, van Asseldonk et al. 2011; Galli, Cimolin et al. 2012; Luu, Low et al. 2013) have provided critical information about neuropathy gaits and normal gaits. Experimentally and clinical, robotic-assisted treadmill such as Lokomat ® provides direct functional exercise for lower extremity. However, Lokomat ® has been demonstrated to not perform significantly better than traditional over-ground rehabilitation(Norouzi-Gheidari, Archambault et al. 2012; Vaney, Gattlen et al. 2012); therefore a better understanding of motor control could guide the development of more effect human-robotic interaction that could result in more effective rehabilitation design and devices. Motor control researches examining the peripheral neuropathy on gaits(Dingwell, Ulbrecht et al. 1999; Neptune 2000; Dingwell and Cavanagh 2001; Gates and Dingwell 2007) demonstrate the potential of developing more efficient clinical system for rehabilitation as well as novel metric for measuring performance and progress.

Significantly more researches have been done on upper extremity (Hesse, Schulte-Tigges et al. 2003; Norouzi-Gheidari, Archambault et al. 2012; Ladenheim,

Altenburger et al. 2013; Loureiro, Harwin et al. 2013; Mazzoleni, Sale et al. 2013). While early developments of robotic rehabilitation like the MIT-MANUS have been exercise-focused; new rehabilitation designs have focused on more functional tasks (e.g. turn a door knob, using a screw drive). Functional and goal targeted training that are relevant to ADL have been demonstrated to be more effective in functional recovery than traditional exercise (Kwakkel, Kollen et al. 2008; Murphy and Corbett 2009). However, currently there are no significant financial and performance benefit of using robotic-assisted technology; therefore, there are opportunity for innovation for robotic rehabilitation. High-level of motor control such as stochastic optimal control could be implemented to penetrate the motor recovery at the neural level. Such implementation could accelerate function adaption of lost motor connection and neural network plasticity would enable new pathways to be created to regain normal motor mobility.

New motor control approach not only can change the traditional control schematic, but also provides new and more accurate metric for measuring rehabilitation progress. Besides traditional kinematic measures, new measuring techniques could involve movement to movement variability and dynamics stability measurement. Dynamics stability measurements are more enriched by its correlation to motor learning and motor exploitation. Such measurements would provide more information on cognitive recovery that are not possible by traditional kinematics metrics.

Although there are ample evidences to suggest that robot-assisted rehabilitation could potentially replace traditional approach by reducing the cost and increase efficient. However, current technologies are still lagging behind by our understanding of motor control and the slow adaptation of these technologies into clinical setting. Therefore, new motor control approach such as GEM provides a new avenue to redesign and reshape clinical rehabilitation setting. Understand motor control could spur new technology that would provide a clear financial and performance benefits over traditional rehabilitation process. Increases in efficiency could reduce assistant supervision and reduce healthcare

cost while allowing for more immediate therapeutic treatment to increase the successful outcome.

Appendix General Coding

SIMULATION CODING

```
%-Modify:  8/20/2012
    %-Adaptive to individual subject
    %-Starting position is proportional to the variance in DP and DT
    %-Incorporate bootstrapping
    %-Using raw data
    %-Create "big" Matrix to Output both data type

%-Number of subject
    NumSub = 10;

for r=1:NumSub
    %-LOAD EXPERIMENTAL DATA
        %-FileName for VGEM
        if (r<10)
            FileName = ['S0' int2str(r) 'V2Testing.txt'];
        else
            FileName = ['S' int2str(r)  'V2Testing.txt'];
        end

        %-Raw Data
        EData = load(FileName);

        RT = EData(:,2);
        RD = 0.01*EData(:,1);
        V=0.45;

        %-Raw data Output
        DataMean(:,2*r-1:2*r) = [ mean(RT) mean(RD);
                                  std(RT) std(RD)];
        %-Find Operating Point on GEM that is closest to mean [T,D]:
        MeanRT = mean(RT);          MeanRD = mean(RD);
        TStar = (MeanRT+V.*MeanRD) ./ ((V.^2)+1);
        DStar = V.*TStar;

        %- Shift coord to align axes with Operating point on the GEM:
        RTShift = RT - TStar;
        RDShift = RD - DStar;

        %- Calculate DeltaT, DeltaP, & DeltaR:
        DeltaT = (1./sqrt(1+(V.^2))) .* (RTShift + (V.*RDShift));
        DeltaP = (1./sqrt(1+(V.^2))) .* ((-V.*RTShift) + RDShift);
        DeltaR = sqrt( (RT-TStar).^2 + (RD-TStar).^2);

        %-Compute Stability Multiplier (Lambda) for each measure:
        N = length(RT);
        PRD = polyfit(RD(1:(N-1),1), RD(2:N,1), 1);   LambdaRD =
        PRD(1);
                PRT = polyfit(RT(1:(N-1),1), RT(2:N,1), 1);   LambdaRT
```

```
= PRT(1);

PDT = polyfit(DeltaT(1:(N-1),1), DeltaT(2:N,1), 1); LambdaDT =
PDT(1);
PDP = polyfit(DeltaP(1:(N-1),1), DeltaP(2:N,1), 1); LambdaDP =
PDP(1);
PDR = polyfit(DeltaR(1:(N-1),1), DeltaR(2:N,1), 1); LambdaDR =
PDR(1);

%-Lambda Outputs
ExpDataLam(r,:) = [ LambdaRT LambdaRD LambdaDT LambdaDP
LambdaDR];

%-Shift data to DStar & TStar
RT=RT - TStar;
RD=RD - DStar;

%-Building the k and k+1 matrix
RTDCur =[RT(1:N-1), RD(1:N-1)];
RTDNxt =[RT(2:N),   RD(2:N)];

%-Calculate the difference before calculating A matrix
ERTD =[RTDNxt-RTDCur];

%-Find A Matrix of the difference between deviation between Nxt
& Cur
A=transpose(RTDCur\ERTD);

%-Calculate A Matrix using mvregres
[BetaT, SigmaT, ResidT] = mvregress(RTDCur, ERTD(:,1));
[BetaD, SigmaD, ResidD] = mvregress(RTDCur, ERTD(:,2));

%-Calculate error from the residual matrix
TDErrorMean(r,:)= [mean(ResidT), mean(ResidD)];
TDErrorstd(r,:)=  [std(ResidT), std(ResidD)];

%-Root Mean Estimation of the noise
SSresidT(:,r)=sum(ResidT(:).^2);
RMST(r)=sqrt(SSresidT(:,r)/length(ResidT));

SSresidD(:,r)=sum(ResidD(:).^2);
RMSD(r)=sqrt(SSresidD(:,r)/length(ResidD));

ExpAMatrix(:,2*r-1:2*r) = A;

%-Calculate the experiment Eigven Vector and Eigven Value of
the AMod
[Vec, Val]=eig(A);

%-Output EigenValue and Eigenvector matrix
ExpVec(:,2*r-1:2*r) = Vec;
```

```
    ExpVal(r, 1:2)=[Val(1,1), Val(2,2)];

%-OPTIMIZATION PROCEDURE

    %-Optimization Parameters
    options.MaxFunEvals = 1000;
    options= optimset('Algorithm','sqp','TolX',1e-6);

    %-Number of Trial
    Trial=30;

    for w=1:Trial
        %-OPTIMAL SEARCH WITH FOUR PARAMETERS
            %- x(1) = alpha; x(2)=beta; x(3)= gamma; x(4)=delta

            %-Constrained Optimization (Optimal)
            a= [-1  0  0  0;
                 0 -1  0  0;
                 0  0 -1  0;
                 0  0  0 -1];

            b=[0;0;0;0];

            %-Initialize Iterate Search Parameters
                fvalG = 100;
                p=1;
                q=1;
                MaxS =10;

            while (p<=MaxS)
                %-Initial condition for 4 parameter search
                LR=ExpDataLam(r,3)/ExpDataLam(r,4);

                x01(1)=1+floor(10*rand());     %-alpha
                x01(2)=x01(1)/LR;              %-beta

                x01(3)=1+floor(10*rand());     %-gamma
                x01(4)=x01(3);                 %-delta

                [x1Temp,fval1]=fmincon(@(x)
                MinParamFour(x,A,V),x01,a,b,[],[],[],[],[],options)
                ;

                %-Global optimal
                if (fval1<fvalG)
                    x1=x1Temp;      %-one
                    OptMatrix(q,5*r-4:5*r) = [x1 fval1];
                    fvalG=fval1;
                    q=q+1;
                end
```

```
        p=p+1;
    end

    %-Optimal parameters Output
    ParamFour(w, 6*r-5:6*r)=[x1 1 1];

    %-Calculate optimal A Matrix
    OptATemp = CalAMatrixOpt(x1,V);

    %-Calculate the eigen Vector and eigen Value of the
    AMod
    [VecM, ValM]=eig(OptATemp);

    %-Output EigenValue and Eigenvector matrix
    OptVecM(2*w-1:2*w, 2*r-1:2*r) = VecM;
    OptValM(w, 2*r-1:2*r)=[ValM(1,1), ValM(2,2)];

    OptAMod(2*r-1:2*r,2*w-1:2*w)=OptATemp;

 %-SUBOPTIMAL SEARCH WITH SIX PARAMETERS
    a= [-1  0  0  0  0  0;
         0 -1  0  0  0  0;
         0  0 -1  0  0  0;
         0  0  0 -1  0  0;
         0  0  0  0 -1  0;
         0  0  0  0  0 -1];
    b=[0;0;0;0;0;0];

    %-Iterate Search Parameters
    fvalG = 100;
    p=1;
    q=1;

    while (p<=MaxS)
        %-Constrained Suboptimal search (six Parameters)
      x02=[x1 rand() rand()];

        %-Suboptimal parameters Search

[x2Temp,fval2]=fmincon(@(x),MinParam(x,A,V),x02,a,b,[],[],[
],[],[],options);

        %-Global optimal
        if (fval2 < fvalG)
            x2=x2Temp;
            SubOptMatrix(q,7*r-6:7*r) = [x2 fval2];
            fvalG=fval2;
            q=q+1;
        end
        p=p+1;
    end
```

```
    %-Suboptimal parameters Output
    ParamSix(w,6*r-5:6*r)=x2;

    %-Calculate optimal A Matrix
    SubOptATemp = CalAMatrixSubOpt(x2,V);

    clear VecM ValM
    %-Calculate the Eigven Vector and Eigven Value of the
     AMod
    [VecM, ValM]=eig(SubOptATemp);

    %-Output EigenValue and Eigenvector matrix
    SubOptVecM(2*w-1:2*w, 2*r-1:2*r) = VecM;
    SubOptValM(w, 2*r-1:2*r)=[ValM(1,1), ValM(2,2)];

    SubOptAMod(2*r-1:2*r,2*w-1:2*w)=SubOptATemp;

%-SUBOPTIMAL SEARCH WITH 2 OPTIMAL PARAMETER
    a = [-1  0;
         0 -1];

    b = [0;0];

     %-initialize Iterate Search Parameters
        fvalG = 100;
        p=1;
        q=1;

    while (p<=MaxS)
        %-Constrained Suboptimal search (six Parameters)
        x03=[rand(), rand()];

        %-Suboptimal parameters Search
                              [x3Temp,fval3]=fmincon(@(x)
        MinParamg(x,A,V,x1),x03,a,b,[],[],[],[],[],options)
        ;

        %-Global optimal
        if (fval3 < fvalG)
            x3=x3Temp;      %-one
            SubOptMatrix2(q,7*r-6:7*r) = [x1 x3 fval3];
            fvalG=fval3;
            q=q+1;
        end
        p=p+1;
    end

    x3g = [x1 x3];

    %-Suboptimal parameters Output
    ParamSix2(w,6*r-5:6*r)=x3g;
```

```
                %-Calculate optimal A Matrix
                SubOptATemp = CalAMatrixSubOpt(x3g,V);

                clear VecM ValM
                %-Calculate the Eigven Vector and Eigven Value of the
                AMod
                [VecM, ValM]=eig(SubOptATemp);

                %-Output EigenValue and Eigenvector matrix
                SubOptVecM2(2*w-1:2*w, 2*r-1:2*r) = VecM;
                SubOptValM2(w, 2*r-1:2*r)=[ValM(1,1), ValM(2,2)];

                SubOptAMod2(2*r-1:2*r,2*w-1:2*w)=SubOptATemp;
        end
end
```

BOOTSTRAP CODE

```
%---------------------Bootstrap Code-----------------------------------
Bootstrap code to calculate the parameters in the system (reaching
distance, reaching time, λ, A matrix, and the parameters from the
optimization of the optimal and suboptimal controller)
%----------------------------------------------------------------------
%-Initialize Matrix Size
  ExpDataMean = ones(10,4);
  ExpDataLam  = ones(10,5);

%-BOOTSTRAP OF EXPERIMETNAL DATA
    NumSub = 10;    %- # Of subject

    for r=1:NumSub
        %-LOAD IN EXPERIMENTAL DATA
            %-FileName for VGEM
            if (r<10)
                FileName = ['S0' int2str(r) 'V2Testing.txt'];
            else
                FileName = ['S' int2str(r)  'V2Testing.txt'];
            end

            %-Raw Data
            EData = load(FileName);
            RTRaw = EData(:,2);
            RDRaw = 0.01*EData(:,1);

            %-Normalize Data
            RT = RTRaw;
            RD = RDRaw;
            V  = 0.45;

            %-Raw data Ouput
            ExpDataMean(r,:)= [ mean(RT) mean(RD) std(RT) std(RD)];

            %-Compensating for DStar and TStar
            MeanRT = mean(RT);          MeanRD = mean(RD);
            TStar = (MeanRT+V.*MeanRD) ./ ((V.^2)+1);
            DStar = V.*TStar;

        %-CALCULATING LAMBAS (LINEAR FLUCTUATION)
          %- Shift coordinates to align axes with 0perating point on
          the GEM:
            RTShift = RT - TStar;
            RDShift = RD - DStar;

            %- Calculate DeltaT, DeltaP, & DeltaR:
            DeltaT = (1./sqrt(1+(V.^2))) .* (RTShift + (V.*RDShift));
            DeltaP = (1./sqrt(1+(V.^2))) .* ((-V.*RTShift) + RDShift);
            DeltaR = sqrt( (RT-TStar).^2 + (RD-TStar).^2);
```

```
    %-Compute Stability Multiplier (Lambda) for each measure:
    N = length(RT);
    PRT = polyfit(RT(1:(N-1),1), RT(2:N,1), 1);
    LambdaRT = PRT(1);
    PRD = polyfit(RD(1:(N-1),1), RD(2:N,1), 1);
    LambdaRD = PRD(1);


    PDT = polyfit(DeltaT(1:(N-1),1), DeltaT(2:N,1), 1);
    LambdaDT = PDT(1);
    PDP = polyfit(DeltaP(1:(N-1),1), DeltaP(2:N,1), 1);
    LambdaDP = PDP(1);
    PDR = polyfit(DeltaR(1:(N-1),1), DeltaR(2:N,1), 1);
    LambdaDR = PDR(1);

    %-Lambda Outputs
    ExpDataLam(r,:) = [ LambdaRT LambdaRD LambdaDT LambdaDP
    LambdaDR];

%-CALCULATE REGRESSION MATRIX A
    %-Move it to the mean ( assuming RTshift and RDShift)
    RT=RTShift;
    RD=RDShift;

    %-Building the k and k+1 matrix
    oneMat=ones(length(RD)-1,1);

    %-Current and next reaching matrix
    RTDCur =[RT(1:N-1), RD(1:N-1)];
    RTDNxt =[RT(2:N), RD(2:N)];

    %-Calculate the difference before calculating A matrix
    ERTD =RTDNxt-RTDCur;

    %-Find A Matrix of the difference between deviation between
    Nxt & Cur
    A=transpose(RTDCur\ERTD);

%-CALCULATE THE EIGENVALUE AND EIGENVECTOR OF A MATRIX
    [Vec, Val]=eig(A);

    %-Output EigenValue and Eigenvector matrix
    ExpVec(:, 2*r-1:2*r) = Vec;
    ExpVal(r, 1:2)=[Val(1,1), Val(2,2)];

    A11(r) =A(1,1);
    A12(r) =A(1,2);
    A21(r) =A(2,1);
    A22(r) =A(2,2);

    AM(:,2*r-1:2*r) =A;
```

```
%-BOOTSTRAPPING
    Trial=2000;
    m=300;
    mmax=399;

    %-Generate 300 random counter
    for k=1:Trial
        for i=1:m
            if (i==1)
                IntMat(i,1)=randi(mmax);
            else
                iFlag=1;
                while (iFlag ~= 0)
                    iTemp = randi(mmax);
                    IntMat(i,1)=iTemp;
                    icount=0;
                    for j=1:i-1
                        if (iTemp==IntMat(j,1))
                            icount=icount +1;
                        end
                    end

                    if (icount ==0)
                        iFlag=icount;
                    end
                end
            end
        end

        %-Sampling Data From Bootstrapping Matrix
        for i=1:m
            %-Sampling Time
            B_RTCur(i) = RTRaw(IntMat(i));
            B_RTNxt(i) = RTRaw(IntMat(i)+1);

            %-Sampling Distance
            B_RDCur(i) = RDRaw(IntMat(i));
            B_RDNxt(i) = RDRaw(IntMat(i)+1);
        end

        %-Bootstrap Mean and Standard Data Output
        B_DataMean(r,:)= [ mean(B_RTCur) mean(B_RDCur)
         std(B_RTCur) std(B_RDCur)];

        %-CACULATING BOOTSTRAP LAMBDAS

            %-Compensating for DStar and TStar for Current and
         Next Data Set
            B_MeanRTCur = mean(B_RTCur);
            B_MeanRDCur = mean(B_RDCur);
```

```
B_MeanRTNxt = mean(B_RTNxt);
B_MeanRDNxt = mean(B_RDNxt);

%-Compensate for DStar and TStar
B_TStarCur = (B_MeanRTCur+V.*B_MeanRDCur) ./
((V.^2)+1);
B_DStarCur = V.*B_TStarCur;

B_TStarNxt = (B_MeanRTNxt+V.*B_MeanRDNxt) ./
((V.^2)+1);
B_DStarNxt =  V.*B_TStarNxt;

%-Shift Data Points to Center
B_RTShiftCur = B_RTCur - B_TStarCur;
B_RDShiftCur = B_RDCur - B_DStarCur;

B_RTShiftNxt = B_RTNxt - B_TStarNxt;
B_RDShiftNxt = B_RDNxt - B_DStarNxt;

%-Calculating DeltaT and DeltaP and Delta R
B_DeltaTCur = (1./sqrt(1+(V.^2))) .* (B_RTShiftCur
+ (V.*B_RDShiftCur));
B_DeltaPCur = (1./sqrt(1+(V.^2))) .* ((-
V.*B_RTShiftCur) + B_RDShiftCur);
B_DeltaRCur = sqrt( (B_RTShiftCur).^2 +
(B_RDShiftCur).^2);

B_DeltaTNxt = (1./sqrt(1+(V.^2))) .* (B_RTShiftNxt
+ (V.*B_RDShiftNxt));
B_DeltaPNxt = (1./sqrt(1+(V.^2))) .* ((-
V.*B_RTShiftNxt) + B_RDShiftNxt);
B_DeltaRNxt = sqrt( (B_RTShiftNxt).^2 +
(B_RDShiftNxt).^2);

%-Compute Stability Multiplier (Lambda) for each
measure:
N = length(B_RTCur);
B_PRT = polyfit(B_RTCur, B_RTNxt, 1);
B_LambdaRT = B_PRT(1);
B_PRD = polyfit(B_RDCur, B_RDNxt, 1);
B_LambdaRD = B_PRD(1);

B_PDT = polyfit(B_DeltaTCur, B_DeltaTNxt, 1);
B_LambdaDT = B_PDT(1);
B_PDP = polyfit(B_DeltaPCur, B_DeltaPNxt, 1);
B_LambdaDP = B_PDP(1);
B_PDR = polyfit(B_DeltaRCur, B_DeltaRNxt, 1);
B_LambdaDR = B_PDR(1);

%-Lambda Outputs
B_DataLam(k,5*r-4:5*r) = [ B_LambdaRT B_LambdaRD
 B_LambdaDT B_LambdaDP B_LambdaDR];
```

```
%-BOOTSTRAP FOR CALCULATING EIGENVECTOR/VALUE

    %-Bootstrapping matrix for Calculating
 Eigenvector/value
        %-Find the A matrix
    for i=1:m
        B_RTDCur(i,:) = [RTRaw(IntMat(i)) ,
 RDRaw(IntMat(i))];
        B_RTDNxt(i,:) =
 [RTRaw(IntMat(i)+1),RDRaw(IntMat(i)+1)];
    end

    %-Calculate the difference before calculating A
matrix
    B_ERTD =B_RTDNxt-B_RTDCur;

    %-Find the bootstrap A matrix
    B_A = transpose(B_RTDCur\B_ERTD);

    %-Calculate the eigvenValue and EigenVector
    [B_Vec, B_Val]= eig(B_A);

    %-Save Bootstrap Output EigenValue and Eigenvector
   matrix
    B_ExpVec(2*k-1:2*k,2*r-1:2*r) = B_Vec;
    B_ExpVal(k,2*r-1:2*r)=[B_Val(1,1), B_Val(2,2)];

%-BOOTSTRAP FOR CALCULING THE OPTIMAL PARAMETERS

    %-calculate A using mvregression
    [B_BetaT, B_SigmaT, B_ResidT] = mvregress(B_RTDCur,
    B_ERTD(:,1));
    [B_BetaD, B_SigmaD, B_ResidD] = mvregress(B_RTDCur,
    B_ERTD(:,2));

    %-Root Mean Estimation of the noise
    B_SSresidT = sum(B_ResidT.^2);
    B_RMST     = sqrt(B_SSresidT./length(B_ResidT));

    B_SSresidD = sum(B_ResidD.^2);
    B_RMSD     = sqrt(B_SSresidD./length(B_ResidD));

    %-Store residual Matrix for all trial
    B_ResidTMat(k,2*r-1:2*r) = B_RMST;
    B_ResdiDMat(k,2*r-1:2*r) = B_RMSD;

    %-Individual bootstrap A element
    B_A11(k,r)=B_A(1,1);
    B_A12(k,r)=B_A(1,2);
    B_A21(k,r)=B_A(2,1);
    B_A22(k,r)=B_A(2,2);
```

```
%-OPTIMIZATION PROCEDURE

    %-Optimization Setting
    options.MaxFunEvals = 1000;
    options= optimset('Algorithm','sqp','TolX',1e-
    5);

    %-OPTIMAL SEARCH WITH FOUR PARAMETERS

        %-Constrained Optimization (Optimal)
        a = [-1  0  0  0;
              0 -1  0  0;
              0  0 -1  0;
              0  0  0 -1];

        b =[0;0;0;0];

        %-Initialize Iterate Search Parameters
        fvalG = 1E5;
        p=1;
        q=1;
        MaxS =100;

        while(p<MaxS)
            %-Initial condition for 4 parameter
        search
            LR=ExpDataLam(r,3)/ExpDataLam(r,4);

            x01(1)=1+floor(10*rand());     %-alpha
            x01(2)=x01(1)/LR;              %-beta

            x01(3)=1+floor(10*rand());     %-gamma
            x01(4)=x01(3);                 %-delta

            [x1Temp,fval1]=fmincon(@(x)
        MinParamFour(x,A,V),x01,a,b,[],[],[],[],[],o
        ptions);

            %-Global optimal
            if (fval1<fvalG)
                x1=x1Temp;
                OptMatrix(q,5*r-4:5*r) = [x1
        fval1];
                fvalG=fval1;
                q=q+1;
            end
            p=p+1;
        end

        %-Optimal parameters Output
        ParamFour(k, 6*r-5:6*r)=[x1 1 1];
```

```
    %-Calculate optimal A Matrix
    OptATemp = CalAMatrixOpt(x1,V);

    clear VecM ValM

    %-Calculate the Eigven Vector and Eigven
    Value of the AMod
    [VecM, ValM]=eig(OptATemp);

    %-Output EigenValue and Eigenvector matrix
    OptVecM(2*k-1:2*k, 2*r-1:2*r) = VecM;
    OptValM(k, 2*r-1:2*r)=[ValM(1,1),
     ValM(2,2)];

    OptAMod(2*r-1:2*r,2*k-1:2*k)=OptATemp;

%-SUBPTIMAL SEARCH WITH SIX PARAMETERS

    %-Constrained Optimization
    a= [-1  0  0  0  0  0;
         0 -1  0  0  0  0;
         0  0 -1  0  0  0;
         0  0  0 -1  0  0;
         0  0  0  0 -1  0;
         0  0  0  0  0 -1];

    b=[0;0;0;0;0;0];

    %-Initialize Iterate Search Parameters
    fvalG = 1E5;
    p=1;
    q=1;

    while(p<MaxS)

        %-Constrained Suboptimal search (six
    Parameters)
        x02=[x1 rand() rand()];

        [x2Temp,fval2]=fmincon(@(x)
    MinParam(x,A,V),x02,a,b,[],[],[],[],[],optio
    ns);


        %-Global optimal
        if (fval2<fvalG)
            x2=x2Temp;
            SubOptMatrix(q,7*r-6:7*r) = [x2
    fval2];
            fvalG=fval2;
```

```
                q=q+1;
            end
            p=p+1;
        end

        %-Suboptimal parameters Output
        ParamSix(k,6*r-5:6*r)=x2;

        %-Calculate optimal A Matrix
        SubOptATemp = CalAMatrixSubOpt(x2,V);

        clear VecM ValM
        %-Calculate the Eigven Vector and Eigven
        Value of the AMod
        [VecM, ValM]=eig(SubOptATemp);

        %-Output EigenValue and Eigenvector matrix
        SubOptVecM(2*k-1:2*k, 2*r-1:2*r) = VecM;
        SubOptValM(k, 2*r-1:2*r)=[ValM(1,1),
        ValM(2,2)];

        SubOptAMod(2*r-1:2*r,2*k-
        1:2*k)=SubOptATemp;

%-SUBOPTIMAL SEARCH WITH 2 OPTIMAL PARAMETER
    %-Constrained Optimization
    a = [-1  0;
          0 -1];

    b = [0;0];

    %-Initialize Iterate Search Parameters
    fvalG = 1E5;
    p=1;
    q=1;

    while (p<=MaxS)
        %-Constrained suboptimal search (six
    Parameters)
        x03=[rand(), rand()];

        %-Suboptimal parameters Search
        [x3Temp,fval3]=fmincon(@(x)
       MinParamg(x,A,V,x1),x03,a,b,[],[],[],[],[],o
       ptions);

        %-Global optimal
        if (fval3 < fvalG)
            x3=x3Temp;
            SubOptMatrix2(q,7*r-6:7*r) = [x1 x3
         fval3];
            fvalG=fval3;
```

```
                    q=q+1;
                end
            p=p+1;
        end

        x3g = [x1 x3];

        %-Suboptimal parameters Output
        ParamSix2(k,6*r-5:6*r)=x3g;

        %-Calculate optimal A Matrix
        SubOptATemp = CalAMatrixSubOpt(x3g,V);

        clear VecM ValM

        %-Calculate the Eigven Vector and Eigven Value of
        the AMod
        [VecM, ValM]=eig(SubOptATemp);

        %-Output EigenValue and Eigenvector matrix
        SubOptVecM2(2*k-1:2*k, 2*r-1:2*r) = VecM;
        SubOptValM2(k, 2*r-1:2*r)=[ValM(1,1), ValM(2,2)];

        SubOptAMod2(2*r-1:2*r,2*k-1:2*k)=SubOptATemp;
    end
end
```

References

(2002). "The World Health Report 2002 - Reducing Risks, Promoting Healty Life." Retrieved 2013, from http://www.who.int/whr/2002/en/.

Abe, M. O. and D. Sternad (2013). "Directionality in distribution and temporal structure of variability in skill acquisition." Front Hum Neurosci **7**: 225.

Alexander, R. M. (1997). "A Minimum Energy Cost Hypothesis for Human Arm Trajectories." Biological Cybernetics **76**(2): 97-105.

Bays, P. M. and D. M. Wolpert (2007). "Computational principles of sensorimotor control that minimize uncertainty and variability." The Journal of Physiology **578**(2): 387-396.

Bernstein, N. (1976). The problem of interrelation of coordination and localization. In: the Coordination and Regulation of Movements. New York, Pergamon.

Bizzi, E., N. Accornero, et al. (1984). "Posture control and trajectory formation during arm movement." J Neurosci **4**(11): 2738-2744.

Black, D. P., B. A. Smith, et al. (2007). "Uncontrolled manifold analysis of segmental angle variability during walking: preadolescents with and without Down syndrome." Exp Brain Res **183**(4): 511-521.

Braun, D. A., A. Aertsen, et al. (2009). "Learning optimal adaptation strategies in unpredictable motor tasks." Journal of Neuroscience **29**(20): 6472-6478.

Braun, D. A. and D. M. Wolpert (2007). "Optimal control: when redundancy matters." Curr Biol **17**(22): R973-975.

Campolo, D., F. Widjaja, et al. (2013). "Analysis of accuracy in pointing with redundant hand-held tools: a geometric approach to the uncontrolled manifold method." PLoS Comput Biol **9**(4): e1002978.

Chu, V. W., D. Sternad, et al. (2013). "Healthy and dystonic children compensate for changes in motor variability." J Neurophysiol.

Cohen, R. and D. Sternad (2009). "Variability in motor learning: relocating, channeling and reducing noise." Experimental Brain Research **193**(1): 69-83.

Cohen, R. G. and D. Sternad (2012). "State space analysis of timing: exploiting task redundancy to reduce sensitivity to timing." J Neurophysiol **107**(2): 618-627.

Collins, J. J. (1995). "The Redundant Nature of Locomotor Optimization Laws." Journal of Biomechanics **28**(3): 251-267.

Cusumano, J. P. and P. Cesari (2006). "Body-goal variability mapping in an aiming task." Biol Cybern **94**(5): 367-379.

Cusumano, J. P. and J. B. Dingwell (2013). "Movement Variability Near Goal Equivalent Manifolds: Fluctuations, Control, and Model-Based Analysis." Human Movement Science **In Press**.

Dingwell, J. B. and P. R. Cavanagh (2001). "Increased variability of continuous overground walking in neuropathic patients is only indirectly related to sensory loss." Gait Posture **14**(1): 1-10.

Dingwell, J. B. and J. P. Cusumano (2000). "Nonlinear time series analysis of normal and pathological human walking." Chaos **10**(4): 848-863.

Dingwell, J. B. and J. P. Cusumano (2010). "Re-interpreting detrended fluctuation analyses of stride-to-stride variability in human walking." Gait Posture **32**(3): 348-353.

Dingwell, J. B., J. John, et al. (2010). "Do humans optimally exploit redundancy to control step variability in walking?" PLoS computational biology **6**(7): e1000856.

Dingwell, J. B., H. G. Kang, et al. (2007). "The effects of sensory loss and walking speed on the orbital dynamic stability of human walking." J Biomech **40**(8): 1723-1730.

Dingwell, J. B., R. F. Smallwood, et al. (2013). "Trial-to-trial dynamics and learning in a generalized, redundant reaching task." J Neurophysiol **109**(1): 225-237.

Dingwell, J. B., J. S. Ulbrecht, et al. (1999). "Neuropathic gait shows only trends towards increased variability of sagittal plane kinematics during treadmill locomotion." Gait Posture **10**(1): 21-29.

Domkin, D., J. Laczko, et al. (2005). "Joint angle variability in 3D bimanual pointing: uncontrolled manifold analysis." Exp Brain Res **163**(1): 44-57.

Domkin, D., J. Laczko, et al. (2002). "Structure of joint variability in bimanual pointing tasks." Exp Brain Res **143**(1): 11-23.

Dornay, M., A. T. R. H. I. P. R. L. K. J. R. S. M. K. Kawato, et al. (1996). "Minimum Muscle-Tension Change Trajectories Predicted by Using a 17-Muscle Model of the Monkey's Arm." J Mot Behav **28**(2): 83-100.

Dounskaia, N. (2005). "The internal model and the leading joint hypothesis: implications for control of multi-joint movements." Experimental Brain Research **166**(1): 1-16.

Dounskaia, N., J. A. Goble, et al. (2011). "The role of intrinsic factors in control of arm movement direction: implications from directional preferences." Journal of neurophysiology **105**(3): 999-1010.

Engelbrecht, S. E. (2001). "Minimum Principles in Motor Control." Journal of Mathematical Psychology **45**(3): 497-542.

Faisal, A. A., L. P. Selen, et al. (2008). "Noise in the nervous system." Nat Rev Neurosci **9**(4): 292-303.

Flash, T. (1987). "The control of hand equilibrium trajectories in multi-joint arm movements." Biol Cybern **57**(4-5): 257-274.

Flash, T. and N. Hogan (1985). "The Coordination of Arm Movements: An Experimentally Confirmed Mathematical Model." Journal of Neuroscience **5**(7): 1688-1703.

Franklin, G., D. Powell, et al. (2002). Feedback Control of Dynamic Systems. Upper Saddle River, New Jersey, Prentice Hall.

Furuya, S. and H. Kinoshita (2007). "Roles of proximal-to-distal sequential organization of the upper limb segments in striking the keys by expert pianists." Neurosci Lett **421**(3): 264-269.

Galli, M., V. Cimolin, et al. (2012). "Gait pattern in myotonic dystrophy (Steinert disease): a kinematic, kinetic and EMG evaluation using 3D gait analysis." J Neurol Sci **314**(1-2): 83-87.

Galloway, J. C. and G. F. Koshland (2002). "General coordination of shoulder, elbow and wrist dynamics during multijoint arm movements." Experimental brain research. Experimentelle Hirnforschung. Experimentation cerebrale **142**(2): 163-180.

Galna, B. and W. A. Sparrow (2006). "Learning to minimize energy costs and maximize mechanical work in a bimanual coordination task." J Mot Behav **38**(6): 411-422.

Gates, D. H. and J. B. Dingwell (2007). "Peripheral neuropathy does not alter the fractal dynamics of stride intervals of gait." J Appl Physiol **102**(3): 965-971.

Gates, D. H. and J. B. Dingwell (2008). "The effects of neuromuscular fatigue on task performance during repetitive goal-directed movements." Exp Brain Res **187**(4): 573-585.

Gerus, P., G. Rao, et al. (2010). "A clinically applicable model to estimate the opposing muscle groups contributions to isometric and dynamic tasks." Annals of biomedical engineering **38**(7): 2406-2417.

Goble, J. A., Y. Zhang, et al. (2007). "Directional biases reveal utilization of arm's biomechanical properties for optimization of motor behavior." Journal of neurophysiology **98**(3): 1240-1252.

Gribble, P. L., L. I. Mullin, et al. (2003). "Role of cocontraction in arm movement accuracy." J Neurophysiol **89**(5): 2396-2405.

Gribble, P. L. and D. J. Ostry (1999). "Compensation for interaction torques during single- and multijoint limb movement." Journal of Neurophysiology **82**(5): 2310-2326.

Gribble, P. L., D. J. Ostry, et al. (1998). "Are complex control signals required for human arm movement?" Journal of Neurophysiology **79**(3): 1409-1424.

Guigon, E., P. Baraduc, et al. (2008). "Optimality, stochasticity, and variability in motor behavior." Journal of Computational Neuroscience **24**(1): 57-68.

Hamilton, A. F., K. E. Jones, et al. (2004). "The scaling of motor noise with muscle strength and motor unit number in humans." Exp Brain Res **157**(4): 417-430.

Harris, C. M. and D. M. Wolpert (1998). "Signal-Dependent Noise Determines Motor Planning." Nature **394**(6695): 780-784.

Hasan, M. K., J. H. Park, et al. (2009). "Patient-specific walking pattern simulation in a gait trajectory guiding device." Conf Proc IEEE Eng Med Biol Soc **2009**: 7126-7130.

Heidenreich, P. A., J. G. Trogdon, et al. (2011). "Forecasting the future of cardiovascular disease in the United States: a policy statement from the American Heart Association." Circulation **123**(8): 933-944.

Hesse, S., G. Schulte-Tigges, et al. (2003). "Robot-assisted arm trainer for the passive and active practice of bilateral forearm and wrist movements in hemiparetic subjects." Archives of Physical Medicine and Rehabilitation **84**(6): 915-920.

Hogan, N. (1984). "An organizing principle for a class of voluntary movements." Journal of Neuroscience **4**(11): 2745-2754.

Jagodnik, K. M. and A. J. van den Bogert (2010). "Optimization and evaluation of a proportional derivative controller for planar arm movement." J Biomech.

John, J. and J. P. Cusumano (2007). Inter-Trial Dynamics of Repeated Skilled Movements. ASME 2007 International Design Engineering, Las Vegas.

John, J. and J. P. Cusumano (2007). Inter-Trial Dynamics of Repeated Skilled Movements. ASME Conference Proceedings: ASME 2007 International Design Engineering Technical Conferences and Computers and Information in Engineering Conference (IDETC/CIE2007). September 4–7, 2007 , Las Vegas, Nevada, USA, ASME. **2007 (48027):** 707-716 (Paper no. DETC2007-35380).

Karniel, A. and G. F. Inbar (1997). "A model for learning human reaching movements." Biol Cybern **77**(3): 173-183.

Kawato, M., Y. Maeda, et al. (1990). "Trajectory formation of arm movement by cascade neural network model based on minimum torque-change criterion." Biol Cybern **62**(4): 275-288.

Ketcham, C. J., N. V. Dounskaia, et al. (2004). "Multijoint movement control: the importance of interactive torques." Progress in brain research **143**: 207-218.

Kistemaker, D. A., J. D. Wong, et al. (2010). "The central nervous system does not minimize energy cost in arm movements." Journal of neurophysiology **104**(6): 2985-2994.

Konczak, J., H. vander Velden, et al. (2009). "Learning to Play the Violin: Motor Control by Freezing, Not Freeing Degrees of Freedom." Journal of Motor Behavior **41**(3): 243-252.

Körding, K. P. and D. M. Wolpert (2004). "Bayesian integration in sensorimotor learning." Nature **427**(6971): 244-247.

Kuo, A. D. (1995). "An optimal control model for analyzing human postural balance." IEEE Trans Biomed Eng **42**(1): 87-101.

Kutch, J. J., A. D. Kuo, et al. (2008). "Endpoint force fluctuations reveal flexible rather than synergistic patterns of muscle cooperation." J Neurophysiol **100**(5): 2455-2471.

Kwakkel, G., B. J. Kollen, et al. (2008). "Effects of robot-assisted therapy on upper limb recovery after stroke: a systematic review." Neurorehabil Neural Repair **22**(2): 111-121.

Ladenheim, B., P. Altenburger, et al. (2013). "The effect of random or sequential presentation of targets during robot-assisted therapy on children." NeuroRehabilitation **33**(1): 25-31.

Latash, M. L., J. F. Scholz, et al. (2001). "Structure of motor variability in marginally redundant multifinger force production tasks." Exp Brain Res **141**(2): 153-165.

Latash, M. L., J. P. Scholz, et al. (2002). "Motor control strategies revealed in the structure of motor variability." Exerc Sport Sci Rev **30**(1): 26-31.

Laursen, B., B. R. Jensen, et al. (1998). "Effect of speed and precision demands on human shoulder muscle electromyography during a repetitive task." European Journal of Applied Physiology and Occupational Physiology **78**(6): 544-548.

Levin, O., A. Forner-Cordero, et al. (2008). "Evidence for adaptive shoulder-elbow control in cyclical movements with different amplitudes, frequencies, and orientations." Journal of Motor Behavior **40**(6): 499-515.

Loeb, G. E., W. S. Levine, et al. (1990). "Understanding sensorimotor feedback through optimal control." Cold Spring Harb Symp Quant Biol **55**: 791-803.

Loureiro, R., W. Harwin, et al. (2013). "Evaluation of Reach and Grasp Robot-Assisted Therapy Suggests Similar Functional Recovery Patterns on Proximal and Distal Arm Segments in Sub-Acute Hemiplegia." IEEE Trans Neural Syst Rehabil Eng.

Luu, T. P., K. H. Low, et al. (2013). "An individual-specific gait pattern prediction model based on generalized regression neural networks." Gait Posture.

Mazzoleni, S., P. Sale, et al. (2013). "Effects of proximal and distal robot-assisted upper limb rehabilitation on chronic stroke recovery." NeuroRehabilitation **33**(1): 33-39.

McDonald, P. V., R. E. A. Vanemmerik, et al. (1989). "The Effects of Practice on Limb Kinematics in a Throwing Task." Journal of Motor Behavior **21**(3): 245-264.

McDonnell, M. D. and L. M. Ward (2011). "The benefits of noise in neural systems: bridging theory and experiment." Nature Reviews Neuroscience **12**(7): 415-426.

Mistry, M., E. Theodorou, et al. (2013). "Optimal control of reaching includes kinematic constraints." J Neurophysiol **110**(1): 1-11.

Moreno, J. C., F. Barroso, et al. (2013). "Effects of robotic guidance on the coordination of locomotion." J Neuroeng Rehabil **10**: 79.

Muller, H., T. D. Frank, et al. (2007). "Variability, covariation, and invariance with respect to coordinate systems in motor control: reply to Smeets and Louw (2007)." J Exp Psychol Hum Percept Perform **33**(1): 250-255.

Muller, H. and D. Sternad (2009). "Motor learning: changes in the structure of variability in a redundant task." Adv Exp Med Biol **629**: 439-456.

Murphy, T. H. and D. Corbett (2009). "Plasticity during stroke recovery: from synapse to behaviour." Nat Rev Neurosci **10**(12): 861-872.

Neptune, R. R. (2000). "Computer modeling and simulation of human movement. Applications in sport and rehabilitation." Phys Med Rehabil Clin N Am **11**(2): 417-434, viii.

Nguyen, H. P. and J. B. Dingwell (2012). "Proximal versus distal control of two-joint planar reaching movements in the presence of neuromuscular noise." J Biomech Eng **134**(6): 061007.

Nishii, J. and Y. Taniai (2009). "Evaluation of Trajectory Planning Models for Arm-Reaching Movements Based on Energy Cost." Neural Computation **21**(9): 2634-2647.

Nishikawa, K. C., S. T. Murray, et al. (1999). "Do arm postures vary with the speed of reaching?" J Neurophysiol **81**(5): 2582-2586.

Norouzi-Gheidari, N., P. S. Archambault, et al. (2012). "Effects of robot-assisted therapy on stroke rehabilitation in upper limbs: systematic review and meta-analysis of the literature." J Rehabil Res Dev **49**(4): 479-496.

Ohta, K., M. M. Svinin, et al. (2004). "Optimal trajectory formation of constrained human arm reaching movements." Biol Cybern **91**(1): 23-36.

Olivier, G. (2006). "Visuomotor priming of a manual reaching movement during a perceptual decision task." Brain Res **1124**(1): 81-85.

Osu, R., N. Kamimura, et al. (2004). "Optimal impedance control for task achievement in the presence of signal-dependent noise." Journal of Neurophysiology **92**(2): 1199-1215.

Osu, R., K. Morishige, et al. (2009). "Feedforward impedance control efficiently reduce motor variability." Neurosci Res **65**(1): 6-10.

Peterka, R. J. (2003). "Simplifying the complexities of maintaining balance." IEEE Engineering in Medicine and Biology Magazine **22**(2): 63-68.

Picelli, A., C. Melotti, et al. (2012). "Does robotic gait training improve balance in Parkinson's disease? A randomized controlled trial." Parkinsonism Relat Disord **18**(8): 990-993.

Sale, P., M. F. De Pandis, et al. (2013). "Robot-assisted walking training for individuals with Parkinson's disease: a pilot randomized controlled trial." BMC Neurol **13**(1): 50.

Scheidt, R. A., J. B. Dingwell, et al. (2001). "Learning to move amid uncertainty." J Neurophysiol **86**(2): 971-985.

Scheidt, R. A. and C. Ghez (2007). "Separate adaptive mechanisms for controlling trajectory and final position in reaching." J Neurophysiol **98**(6): 3600-3613.

Scheidt, R. A., D. J. Reinkensmeyer, et al. (2000). "Persistence of motor adaptation during constrained, multi-joint, arm movements." J Neurophysiol **84**(2): 853-862.

Scholz, J. P., N. Kang, et al. (2003). "Uncontrolled manifold analysis of single trials during multi-finger force production by persons with and without Down syndrome." Exp Brain Res **153**(1): 45-58.

Scholz, J. P. and G. Schöner (1999). "The uncontrolled manifold concept: Identifying control variables for a functional task." Experimental Brain Research **126**(3): 289-306.

Scholz, J. P., G. Schoner, et al. (2000). "Identifying the control structure of multijoint coordination during pistol shooting." Exp Brain Res **135**(3): 382-404.

Schouten, A. C., E. de Vlugt, et al. (2001). "Optimal posture control of a musculo-skeletal arm model." Biol Cybern **84**(2): 143-152.

Scott, S. H. (2004). "Optimal feedback control and the neural basis of volitional motor control." Nat Rev Neurosci **5**(7): 532-546.

Secco, E. L., L. Valandro, et al. (2005). "Optimization of two-joint arm movements: a model technique or a result of natural selection?" Biol Cybern **93**(4): 288-306.

Selen, L. P., D. W. Franklin, et al. (2009). "Impedance control reduces instability that arises from motor noise." J Neurosci **29**(40): 12606-12616.

Sohn, M. H., J. L. McKay, et al. (2013). "Defining feasible bounds on muscle activation in a redundant biomechanical task: practical implications of redundancy." J Biomech **46**(7): 1363-1368.

Sparrow, W. A. and K. M. Newell (1998). "Metabolic energy expenditure and the regulation of movement econonmy." Psychonomic Bulletin & Review **5**(2): 171-196.

Sternad, D., M. O. Abe, et al. (2011). "Neuromotor noise, error tolerance and velocity-dependent costs in skilled performance." PLoS Comput Biol **7**(9): e1002159.

Stroeve, S. (1998). "Neuromuscular control model of the arm including feedback and feedforward components." Acta Psychol (Amst) **100**(1-2): 117-131.

Stroeve, S. (1999). "Impedance characteristics of a neuromusculoskeletal model of the human arm I. Posture control." Biol Cybern **81**(5-6): 475-494.

Takahashi, C. D., D. Nemet, et al. (2003). "Neuromotor noise limits motor performance, but not motor adaptation, in children." J Neurophysiol **90**(2): 703-711.

Tee, K. P., E. Burdet, et al. (2004). "A model of force and impedance in human arm movements." Biol Cybern **90**(5): 368-375.

Todorov, E. (2004). "Optimality principles in sensorimotor control." Nature Neuroscience **7**(9): 907-915.

Todorov, E. (2005). "Stochastic optimal control and estimation methods adapted to the noise characteristics of the sensorimotor system." Neural Comput **17**(5): 1084-1108.

Todorov, E. and M. I. Jordan (1998). "Smoothness maximization along a predefined path accurately predicts the speed profiles of complex arm movements." J Neurophysiol **80**(2): 696-714.

Todorov, E. and M. I. Jordan (2002). "Optimal feedback control as a theory of motor coordination." Nature Neuroscience **5**(11): 1226-1235.

Todorov, E., W. Li, et al. (2005). "From task parameters to motor synergies: A hierarchical framework for approximately-optimal control of redundant manipulators." J Robot Syst **22**(11): 691-710.

Tolhurst, D. J., J. A. Movshon, et al. (1983). "The statistical reliability of signals in single neurons in cat and monkey visual cortex." Vision Res **23**(8): 775-785.

Uno, Y., M. Kawato, et al. (1989). "Formation and Control of Optimal Trajectory in Human Multijoint Arm Movement: Minimum Torque-Change Model." Biological Cybernetics **61**(2): 89-101.

Valero-Cuevas, F. J., M. Venkadesan, et al. (2009). "Structured variability of muscle activations supports the minimal intervention principle of motor control." Journal of Neurophysiology **102**(1): 59-68.

van Beers, R. J., P. Haggard, et al. (2004). "The role of execution noise in movement variability." J Neurophysiol **91**(2): 1050-1063.

van Swigchem, R., V. Weerdesteyn, et al. (2011). "Near-normal gait pattern with peroneal electrical stimulation as a neuroprosthesis in the chronic phase of stroke: a case report." Arch Phys Med Rehabil **92**(2): 320-324.

Vaney, C., B. Gattlen, et al. (2012). "Robotic-assisted step training (lokomat) not superior to equal intensity of over-ground rehabilitation in patients with multiple sclerosis." Neurorehabil Neural Repair **26**(3): 212-221.

Wang, L., E. H. van Asseldonk, et al. (2011). "Model Predictive Control-based gait pattern generation for wearable exoskeletons." IEEE Int Conf Rehabil Robot **2011**: 5975442.

Wininger, M., N. H. Kim, et al. (2009). "Spatial resolution of spontaneous accelerations in reaching tasks." J Biomech **42**(1): 29-34.

Winter, D. A. (2005). Biomechanics and Motor Control of Human Movement, 3rd Ed. New York, NY, John Wiley & Sons, Inc.

Wu, C. Y., C. L. Yang, et al. (2012). "Effect of therapist-based versus robot-assisted bilateral arm training on motor control, functional performance, and quality of life after chronic stroke: a clinical trial." Phys Ther **92**(8): 1006-1016.

Wu, Y. H., N. Pazin, et al. (2013). "Improving finger coordination in young and elderly persons." Exp Brain Res.

Yang, J. F., J. P. Scholz, et al. (2007). "The role of kinematic redundancy in adaptation of reaching." Exp Brain Res **176**(1): 54-69.

Zajac, F. E. (2002). "Understanding muscle coordination of the human leg with dynamical simulations." J Biomech **35**(8): 1011-1018.

Zhang, M., T. C. Davies, et al. (2013). "Effectiveness of robot-assisted therapy on ankle rehabilitation--a systematic review." J Neuroeng Rehabil **10**: 30.